Mass loss of stars on the asymptotic giant branch: Mechanisms, models and measurements

Astron Astrophys Rev (2018) 26:1
https://doi.org/10.1007/s00159-017-0106-5

REVIEW ARTICLE

Mass loss of stars on the asymptotic giant branch

Mechanisms, models and measurements

Susanne Höfner[1] · **Hans Olofsson**[2]

Received: 30 June 2017

Abstract As low- and intermediate-mass stars reach the asymptotic giant branch (AGB), they have developed into intriguing and complex objects that are major players in the cosmic gas/dust cycle. At this stage, their appearance and evolution are strongly affected by a range of dynamical processes. Large-scale convective flows bring newly-formed chemical elements to the stellar surface and, together with pulsations, they trigger shock waves in the extended stellar atmosphere. There, massive outflows of gas and dust have their origin, which enrich the interstellar medium and, eventually, lead to a transformation of the cool luminous giants into white dwarfs. Dust grains forming in the upper atmospheric layers play a critical role in the wind acceleration process, by scattering and absorbing stellar photons and transferring their outward-directed momentum to the surrounding gas through collisions. Recent progress in high-angular-resolution instrumentation, from the visual to the radio regime, is leading to valuable new insights into the complex dynamical atmospheres of AGB stars and their wind-forming regions. Observations are revealing asymmetries and inhomogeneities in the photospheric and dust-forming layers which vary on time-scales of months, as well as more long-lived large-scale structures in the circumstellar envelopes. High-angular-resolution observations indicate at what distances from the stars dust condensation occurs, and they give information on the chemical composition and sizes of dust grains in the close vicinity of cool giants. These are essential constraints for building

✉ Susanne Höfner
susanne.hoefner@physics.uu.se

Hans Olofsson
hans.olofsson@chalmers.se

[1] Division of Astronomy and Space Physics, Department of Physics and Astronomy, Uppsala University, Box 516, 75120 Uppsala, Sweden

[2] Department of Space, Earth and Environment, Chalmers University of Technology, Onsala Space Observatory, 43992 Onsala, Sweden

Published online: 09 January 2018

realistic models of wind acceleration and developing a predictive theory of mass loss for AGB stars, which is a crucial ingredient of stellar and galactic chemical evolution models. At present, it is still not fully possible to model all these phenomena from first principles, and to predict the mass-loss rate based on fundamental stellar parameters only. However, much progress has been made in recent years, which is described in this review. We complement this by discussing how observations of emission from circumstellar molecules and dust can be used to estimate the characteristics of the mass loss along the AGB, and in different environments. We also briefly touch upon the issue of binarity.

Keywords Stars: AGB and post-AGB · Stars: atmospheres · Stars: evolution · Stars: mass loss · Stars: winds, outflows · Circumstellar matter

1 Setting the stage

Studies of pre-solar dust grains found in meteorites reveal that the material from which our solar system formed has its origin in stars with a wide range of fundamental properties (see, e.g., Nittler and Ciesla 2016). The isotopic composition of individual dust grains makes it possible to trace them back to either massive stars which exploded in core-collapse supernova events, or to less massive stars which lost a significant part of their mass through stellar winds during their late stages of evolution. This review takes a closer look at the latter process, focusing on the phase when low- and intermediate-mass stars ascend the asymptotic giant branch (AGB). The massive winds of these cool luminous giants play a decisive role in determining their observable properties, their further evolution and their final fate (e.g., Herwig 2005; Lattanzio and Karakas 2016), as well as providing the building blocks for new generations of stars and planets (e.g., Tielens 2005). Therefore, it is of fundamental importance for a wide range of astrophysical problems to understand the mechanisms which cause these outflows, and to measure their properties.

The structure of this review reflects the development of our knowledge about mass loss on the AGB, from a purely descriptive to an increasingly predictive nature. After an introductory part, which describes fundamental properties of AGB stars and basic concepts, we discuss the methods which are used to measure mass-loss rates and other wind properties, and we give a broad overview of the results. Then, we turn to the mechanisms which cause the outflows, giving a description of modelling approaches as well as key theoretical results, before comparing the current generation of wind models to observations. In this context, a special emphasis is put on problems in establishing the dependence of the mass-loss rate on fundamental stellar parameters, which is essential for models of stellar and galactic chemical evolution. Finally, we discuss known challenges and open questions, and we round off with conclusions and future perspectives, regarding both theoretical and observational work. While we give some key historic references to illustrate the development of the field, the focus is on describing the current state of the art, and discussing where improvements will be necessary in the future.

Over the years, AGB stars have become a broad research topic, and not all fundamental aspects can be covered here as was attempted in Habing and Olofsson (2003). The interior structure and evolution (which will only be summarized briefly below) are discussed in the extensive review by Herwig (2005). Nucleosynthesis and stellar yields of single AGB stars are the topic of a recent review by Karakas and Lattanzio (2014), while binary evolution is discussed by De Marco and Izzard (2017). Willson (2000) gives a detailed analysis of problems in deriving a "mass-loss formula", i.e., a quantitative description of how the mass-loss rate depends on fundamental stellar parameters, as used in evolution models. The textbook by Gail and Sedlmayr (2014) provides a detailed introduction to the physics and chemistry of circumstellar envelopes around AGB stars.

1.1 Stars on the asymptotic giant branch: evolution and properties

The AGB phase is a late stage in the evolution of low- and intermediate-mass stars, with an initial mass range of about 0.5–8 $M_\odot$ (the exact value of the upper limit depends on the treatment of convection). After leaving the main sequence, these stars go through a first red giant branch (RGB) phase, and come out of the subsequent central-He-burning stage with an inert carbon/oxygen core where eventually the electron-degeneracy pressure dominates. For these stars, nuclear burning in the stellar core is over. They will ascend a red giant branch for the second time, the AGB, powered by alternating burning of H and He in thin shells surrounding their inert C-O core. This will be their final evolutionary stage as stars, before they turn into white dwarfs. Taking into account the age of the Universe, the observable AGB stars correspond to an initial mass in excess of $\approx 0.8\,M_\odot$; less massive stars have not had time to reach the AGB, yet. Assuming that stellar birth follows approximately a Salpeter initial-mass function (IMF), the majority of stars that have died in our Universe have done this directly following the AGB stage.

The double-shell burning structure of AGB stars, i.e., a He-burning inner shell which is replenished by a H-burning outer shell, leads to a phenomenon called He-shell flash, or thermal pulse. In a cyclic process, phases of intense He-shell burning, which last a few hundred years, interrupt longer periods of quiescent H-shell burning with a duration of a few $\times\, 10^4$ year, depending on mass. The He-burning activates nucleosynthesis in the inter-shell region, and the outward flow of the energy released by He-burning causes extinction of the H-shell burning and leads to dredge-up of material from the inter-shell region to the surface via the convective outer envelope of the star. It is during the thermally pulsing stage (TP-AGB) that AGB stars produce a large fraction of the elements we find in the universe, and the efficiency of the third dredge-up process determines how much of this nucleo-enriched material will reach the surface (see, e.g., Karakas and Lattanzio 2014, for an overview of nucleosynthesis on the AGB, and for definitions of technical terms).

AGB stars are initially of spectral type M (with C/O $\approx$ 0.5 by number), but the gradual dredge-up of newly produced carbon may eventually lead to a situation where C/O $>$ 1 in the atmosphere, and a carbon star has formed. There is a lower limit to the initial mass ($\approx$ 1.5 $M_\odot$ for solar composition, less for lower metallicity) for

this process to work. In the transition from spectral type M to C, S-stars are formed ($0.5 \lesssim$ C/O $\lesssim 1$ covering the spectral types MS, S, and SC). The hot-bottom-burning (HBB) process prevents the formation of carbon stars when the initial mass is above a certain limit ($\approx 4\,M_\odot$ for solar composition, less at lower metallicity) since CNO-burning destroys the carbon produced by He-burning. Thus, the most massive AGB stars are likely to remain M-stars to the end.

The low effective temperatures (around 3000 K and below) and high luminosities (a few 10^3 to a few $10^4\,L_\odot$) reached during the AGB phase correspond to typical stellar radii of several hundred solar radii. In combination with current masses well below $8\,M_\odot$, the resulting surface gravities are typically 4–5 orders of magnitude below that of a sun-like star. This makes AGB stars prone to lose mass from the loosely bound surface layers if a sufficiently effective process can accelerate the atmospheric gas beyond the escape velocity. A phenomenon that presumably adds to the effects of low surface gravity is dynamical levitation of the atmospheres due to shock waves, triggered by stellar pulsation. The existence of stellar pulsations in AGB stars was earlier deduced from their pronounced photometric variability with typical periods of 100–1000 days, and later supported by observations of variable spectral line profiles, due to Doppler shifts, and changes in stellar radii, derived with interferometric methods. Classically, variable AGB stars are divided into irregular, semiregular (SRV), and Mira variables based on the regularity and amplitude of the light curve in the visible.

Mass-loss rates of AGB stars, determined with various observational methods, are typically in the range of 10^{-8}–$10^{-5}\,M_\odot\,\mathrm{year}^{-1}$, but values as high as $10^{-4}\,M_\odot\,\mathrm{year}^{-1}$, or even above, have been found for more extreme objects. Thus, it has been observationally shown that AGB stars can eventually reach mass-loss rates so high that mass loss is the process which determines the evolutionary time scales, instead of nuclear burning. Hence, a full understanding of AGB evolution, e.g., its time scales, the maximum luminosity reached, the nucleosynthesis outcome, and the yield to the interstellar medium (ISM), requires an understanding of the mass-loss process.

In line with the general opinion, we argue in this review that the most likely wind-acceleration mechanism is radiation pressure on microscopic solid-state particles (dust grains), formed in atmospheres that are levitated by pulsation. Seen from the perspective of quantitative modelling, this mass-loss mechanism is complicated, since it involves a range of interacting, time-dependent physical processes on microscopic and macroscopic scales, as well as a coupling of dynamical phenomena in the stellar interior (convection, pulsation), the atmosphere (strong radiating shocks), and the wind formation region (dust condensation, radiative acceleration), which correspond to quite different physical regimes, Fig. 1. At present, it is still not fully possible to predict the mass-loss rate from first principles, as a function of fundamental stellar parameters, only. However, much progress has been made during the last decades, and this is one of the two main topics of this review. The other one concerns the observational characterization of the mass-loss process, e.g., its magnitude, geometry, kinematics, composition, and its dependence on stellar characteristics such as mass, luminosity, and metallicity. This is done by studying the properties of the escaping material, i.e., the circumstellar envelope (CSE) of gas and dust.

An important aspect is the extent to which AGB stars contribute to the chemical evolution over cosmic time in terms of dust and element production, and to the inte-

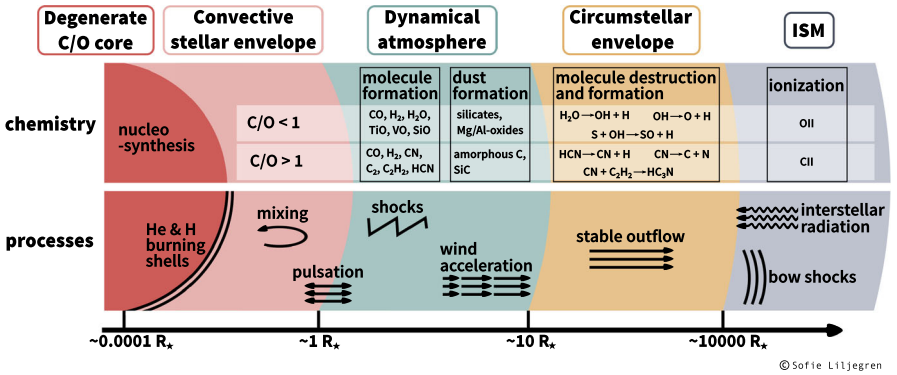

Fig. 1 A schematic figure of an AGB star and its circumstellar environment, including regions and processes of relevance to this review. The stellar radius (R_*) of a typical AGB star is of the order 1 AU (above 100 solar radii). By courtesy of S. Liljegren

grated light of galaxies. Estimates suggest that AGB stars are a major source of dust in the Milky Way (e.g., Tielens 2005), but their contribution to dust production in the early universe is still debated (Michałowski 2015, and references therein). To asses the effects of AGB stars on their host galaxies requires, among other things, an understanding of how the mass-loss process depends on stellar metallicity. This will affect the mass return, not only directly, but also through the fact that a less efficient mass loss may lead to a significant fraction of the $\approx 3-8\,M_\odot$ stars ending as supernovae of type 1.5, with consequences for the early chemical evolution. Mass loss also determines the maximum luminosity reached by an AGB star. Current estimates suggest that AGB stars dominate the mid-IR light in young to moderate-age galaxies with low amounts of diffuse dust (Villaume et al. 2015, and references therein). Any errors in our understanding of the mass loss thus propagate into errors in our understanding of the chemical evolution of the universe and the evolution of galaxies.

1.2 Early indications of mass loss

The first evidence of (substantial) post-main-sequence mass loss came through observations of the binary system α Her by Deutsch (1956). Circumstellar absorption lines were seen in the spectrum of the companion star, suggesting circumstellar gas as far away as $10^5\,R_\odot$ from the M giant. With an estimated outflow velocity of $10\,\mathrm{km\,s^{-1}}$, the gas velocity is well above the escape velocity at this point. The estimated mass-loss rate was $3\times10^{-8}\ M_\odot\,\mathrm{year}^{-1}$. In a study of similar systems, Reimers (1975) derived an empirical relation between mass-loss rate and stellar characteristics (luminosity, mass, and radius) that bears his name.

There were also indirect indications. Auer and Woolf (1965) found that the Hyades cluster contains about a dozen white dwarfs (WDs); each one must have a mass below the Chandrasekhar limit of $1.4\,M_\odot$. But, the Hyades cluster has stars with a mass of $2\,M_\odot$ that are still on the main sequence (MS). Consequently, the white dwarf progenitors must have lost at least $0.6\,M_\odot$ during their post-MS evolution.

The advent of infrared observations led to considerable progress, e.g., the 2.2 μm IRC-survey by Neugebauer and Leighton (1969) and the AFGL catalogue of Price and Walker (1976). It was shown that late-M red giants often have an excess of radiation at infrared wavelengths, an effect of dust in a CSE. In some objects, the dust optical depth is so high that most of the stellar energy are emitted at wavelengths longer than 2 μm. Gillett et al. (1968) and Woolf and Ney (1969) attributed an emission band around 10 μm to small silicate particles, and Gehrz and Woolf (1971) estimated circumstellar dust masses and mass-loss rates of M giants. Similar results were found for carbon stars (Woolf and Ney 1969). The appearance of different dust compositions around M- and C-type giants was explained by Gilman (1969) to be the consequence of the high binding energy of the CO molecule, which prevents the less abundant of the two elements from forming other molecules and solids. The launch of the space telescope IRAS in 1983, which made a full-sky survey at 12, 25, 60, and 100 μm, increased substantially the number of detected mass-losing sources.

Wickramasinghe et al. (1966) showed that light pressure on graphite grains can push both the grains and the surrounding gas out of the stellar gravitational field, as a consequence of momentum exchange between dust and gas. Circumstellar OH (in maser emission) was first detected in 1968 (Wilson and Barrett 1968), and circumstellar CO rotational lines were observed a few years later towards the carbon star IRC+10216 (aka CW Leo) (Solomon et al. 1971). The first detailed physical/chemical model of a CSE was presented by Goldreich and Scoville (1976). The OH masers were explained as due to infrared pumping of OH molecules in a shell where they formed through the dissociation of H_2O by the interstellar radiation field.

Theoretical arguments suggested that very high mass-loss rates—well in excess of what would result from an extrapolation of Reimers' law—must be reached at the end of the AGB evolution (Renzini and Voli 1981; Vassiliadis and Wood 1993). This phenomenon is often referred to as "superwind". The observational support for such a phase came with the identification of mass-loss rates reaching $10^{-4}\ M_\odot\ \mathrm{year}^{-1}$ and beyond using OH 1612 MHz maser line observations of so-called OH/IR stars (Engels et al. 1983; Baud and Habing 1983).

In the decades following these initial discoveries, considerable progress has been made thanks to both space- and ground-based instrumentation, as will be discussed in this review. These developments have given access to spectral energy distributions with a wide wavelength coverage (unaffected by terrestrial features), high spectral resolution data on circumstellar atomic/molecular lines, and structural information on CSEs via interferometry of nearby objects, complemented by large-scale surveys and photometric monitoring of large samples of stars. In recent years, high-angular resolution techniques, covering wavelengths from the visual to the radio regime, have started to give direct insights into the dynamical atmospheres and wind acceleration regions of AGB stars which is essential for understanding the mass-loss mechanism.

1.3 The onset of outflows: atmospheric conditions and forces

Considering the high luminosities of AGB stars, it is natural to assume that their winds are driven by radiation pressure. Each photon carries momentum corresponding to its

energy divided by the speed of light, and the total momentum of the photons emitted by the star per second is given by the stellar luminosity divided by the speed of light (L_*/c). This quantity is comparable to, or exceeds, the typical momentum of the gas and dust leaving the star per second, which can be expressed as mass-loss rate multiplied by terminal wind velocity ($\dot{M}\upsilon_\infty$). Assuming the so-called single-scattering limit (i.e., each stellar photon transfers momentum through one interaction, corresponding to $\dot{M}\upsilon_\infty = L_*/c$), a typical star with a luminosity of $L_* = 5000\,L_\odot$ should, in principle, be able to sustain a wind with a velocity of $10\,\mathrm{km\,s^{-1}}$ and a mass-loss rate of about $10^{-5}\,M_\odot\,\mathrm{year}^{-1}$.

This argument is, of course, based on a simple order-of-magnitude estimate, and it ignores the fact that the material leaving the star must be lifted out of the gravitational potential, not just accelerated to its final speed from a state of rest. To estimate the forces which are necessary for driving a stellar wind, they should be compared to the gravitational force of the star. Radiative acceleration, i.e, the transfer of momentum from photons to matter through absorption and scattering, depends critically on the total radiative cross section per mass of stellar material. To estimate the amount of opacity required for driving a stellar wind by radiative pressure, we consider the relative magnitude of the outwards directed radiative acceleration compared to the inwards directed gravitational acceleration acting on a layer of material, i.e.,

$$\frac{a_{\mathrm{rad}}}{a_{\mathrm{grav}}} = \frac{\langle\kappa\rangle\, L_*}{4\pi\, c\, G M_*} \tag{1}$$

where $\langle\kappa\rangle$ is the flux mean opacity (total cross section per unit mass), and M_* denotes the current mass of the star (G = gravitation constant). The possible values of this ratio fall into two distinct regimes, i.e., < 1 where gravitational attraction dominates and > 1 where the radiative acceleration exceeds gravity, separated by the special case where the two forces are equal in magnitude. The latter situation corresponds to a critical value of the flux mean opacity, given by

$$\langle\kappa\rangle_{\mathrm{crit}} = \frac{4\pi\, c\, G M_*}{L_*} \approx 2.6 \left(\frac{M_*}{M_\odot}\right)\left(\frac{L_*}{5000\,L_\odot}\right)^{-1} \left[\mathrm{cm^2\,g^{-1}}\right]. \tag{2}$$

It should be noted here that wind driving may be a cumulative process, with radiative pressure acting on material that is temporarily moving upwards on a ballistic trajectory, due to the effect of shock waves. In that case, a value of $a_{\mathrm{rad}}/a_{\mathrm{grav}}$ that is somewhat below 1 may be sufficient to lift the material out of the stellar potential well. Nevertheless, $\langle\kappa\rangle_{\mathrm{crit}}$ as given in Eq. (2) is a good order-of-magnitude estimate for the flux-mean opacity required to drive an outflow, and a starting point for a discussion of relevant opacity sources.

In the atmospheres of cool giant stars, most of the gas is in molecular form, and certain species may condense into solid particles in the upper atmospheric layers. In principle, both gas and dust opacities might contribute to radiative pressure. In practice, however, the flux mean opacity will be dominated by those species that absorb or scatter photons efficiently in the near-IR wavelength region, around the stellar flux maximum. For comparison, we note that the winds of hot luminous giants,

with typical velocities of about 1000–3000 km s^{-1}, are presumably driven by atomic line opacity, with Doppler shifts in the wind acceleration zone strongly increasing the effective line width (see, e.g., Owocki 2010; Smith 2014; Puls et al. 2015, for recent reviews on mass-loss mechanisms in massive stars). With typical velocities in AGB star winds being about a factor of 100 lower, the latter effect is much smaller, and atomic lines are not expected to contribute significantly to the radiative pressure in these cool stars, where the photospheric flux declines steeply in the visual and UV. The rich spectrum of vibration–rotation lines of abundant molecules, on the other hand, overlaps with the stellar flux maximum in the near-IR wavelength region, and their contribution to radiative pressure has been discussed in the literature (e.g., Elitzur et al. 1989; Jorgensen and Johnson 1992). While molecules clearly have a significant impact on the thermal structures of AGB star atmospheres, it seems that their total flux-mean opacity does not reach values which affect atmospheric and wind dynamics (e.g., Cherchneff et al. 1991; Bessell et al. 1996; Liljegren et al. 2016).

In contrast, dust grains are good candidates for driving winds of AGB stars, as they can be very efficient at absorbing and/or scattering the stellar photons, depending on their chemical composition and size. The optical properties of solid particles are mostly determined by electronic transitions in the visual to UV range, and lattice modes in the mid-IR region, which give rise to the characteristic spectral features observed in CSEs (see Sect. 2.1). Certain materials which are likely ingredients of circumstellar dust around AGB stars (e.g., amorphous carbon, or magnesium-iron silicates) are also efficient absorbers in the near-IR range around the stellar flux maximum. If dust particles with the right properties are abundant in the outer atmospheric layers, their collective opacity can easily exceed $\langle\kappa\rangle_{\rm crit}$ and trigger an outflow.

Dust species that are commonly associated with wind driving (i.e., amorphous carbon or silicates) will typically condense at temperatures of 1500–1000 K, or below. A rough estimate for the temperature of dust particles as a function of distance from the center of the star, $T_{\rm d}(r)$, can be obtained by assuming that (i) the grain temperature is set by radiative equilibrium, (ii) the stellar radiation field can be described with a Planck function corresponding to the effective temperature T_*, geometrically diluted with distance, and (iii) the grain absorption coefficient can be approximated with a power law $\kappa_{\rm abs} \propto \lambda^{-p}$ in the relevant wavelength region around the stellar flux maximum, where λ denotes the wavelength and p is a material-dependent constant (see, e.g., Bladh and Höfner 2012, for examples of such fits). This leads to

$$T_{\rm d}\,(r) \approx T_*\,(2r/R_*)^{-\frac{2}{4+p}} \tag{3}$$

where R_* is the stellar radius (see, e.g., Lamers and Cassinelli 1999, for a derivation of this formula). The closest distance at which grains of a given material can form (without evaporating due to radiative heating) is denoted as $R_{\rm c}$ in the following. It can be estimated by finding the point where the grain temperature is equal to the condensation temperature $T_{\rm c}$ of the material. According to Eq. (3), when setting $T_{\rm d}\,(R_{\rm c}) = T_{\rm c}$, we obtain

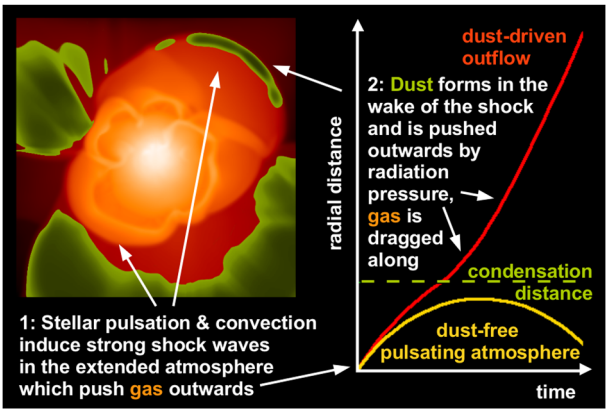

Fig. 2 An illustration of the Pulsation-Enhanced Dust-DRiven Outflow (PEDDRO) scenario. Left: a central slice through a global 3D radiation-hydrodynamical model of an AGB star (Freytag and Höfner 2008), showing effects of convection and pulsation on the gas density (orange) and dust distribution (green) in the extended atmosphere of the star (width of the box: about 4 R_*). Right: a schematic diagram showing trajectories of mass layers in the atmosphere and wind acceleration zone. From Höfner (2016)

$$R_c/R_* \approx 0.5\ (T_c/T_*)^{-\frac{4+p}{2}}\ . \tag{4}$$

As an example, we consider grains of amorphous carbon which are generally assumed to drive the winds of C-rich AGB stars: in this case, $p \approx 1$ and $T_c \approx 1500$ K, leading to $R_c \approx 2$–$3\ R_*$, which is in good agreement with detailed models and observations. The situation for silicate grains, forming in atmospheres with O-rich chemistry, is more intricate, as will be discussed in Sect. 4.2, but condensation distances are in the same range.

In the case of a hydrostatic stellar atmosphere, the gas density drops exponentially with distance from the star, and even at the low surface gravities of AGB stars practically no gas would be found at typical dust condensation distances. This problem was recognized early on, and different levitation mechanisms, as well as alternative wind driving mechanisms, have been discussed in the literature (cf. Sect. 6.2.2). Over the years, however, a broad consensus has been reached that a combination of pulsation-induced shock waves and radiation pressure on dust is the most promising mechanism to explain atmospheric levitation and wind driving, especially regarding the more evolved AGB stars with low effective temperatures, large pulsation amplitudes, and high mass-loss rates. This scenario of a pulsation-enhanced, dust-driven outflow (see Fig. 2) is supported by various observations, ranging from correlations of mass-loss indicators with pulsation properties (e.g., Whitelock et al. 1991, 2003; Glass et al. 2009; McDonald and Zijlstra 2016) to spatially resolved structures of dynamical atmospheres and dust formation regions (e.g., Tej et al. 2003; Wittkowski et al. 2007; Zhao-Geisler et al. 2012; Karovicova et al. 2013; Stewart et al. 2016b; Khouri et al. 2016a; Ohnaka et al. 2017).

1.4 Basic concepts and definitions

As outlined above, there is convincing empirical evidence for substantial mass loss during AGB evolution. A reliable quantitative determination of the mass-loss rate for individual stars, and of trends with stellar parameters, is, however, a rather complex problem, as will be discussed in detail in the following sections. Here, we introduce some basic concepts and definitions that will be used throughout the text.

Mass-loss rate Mass loss from AGB stars usually takes the form of a continuous, more or less steady, outflow of gas and dust, i.e., a stellar wind. The mass-loss rate is defined by the total mass escaping from the stellar atmosphere in all directions per unit of time, $\dot{M}$. Theoretically, it can be determined by integrating the local mass flux in the stellar wind over a closed surface around the star, e.g., a spherical shell, which is located at a suitable distance where the flow velocity exceeds the local escape velocity. In practice, this means that both the mass density and the flow velocity (in direction and magnitude) have to be known at any point of this shell, since the local mass flux is the product of these two quantities.

The standard CSE model Extracting the necessary information to determine mass-loss rates from (mostly spatially unresolved) observations requires assumptions about the structure of the CSE, to make an interpretation of the relevant spectral features possible. The standard CSE scenario, commonly used for deriving mass-loss rates, assumes a steady, spherically symmetric outflow. Regarding the radial profile of the flow velocity, different approaches may be used, (i) a purely kinematic one, directly prescribing a radial velocity profile (or a constant velocity, for large distances from the star), or (ii) a dynamical one, where the velocity profile results from solving an equation of motion, taking relevant forces into account. In the latter case, it is usually assumed that the outflow is accelerated by radiation pressure on dust grains which form instantaneously at a distance from the star where they are thermally stable. The dust grains transfer momentum to the surrounding gas through collisions, thereby accelerating it away from the star. In the following, we will refer to this set of assumptions as the Steady Circumstellar Radiative Acceleration (SCRA) scenario. When considering the large-scale structure of the CSE, averaging over time-scales far longer than the pulsation period, the assumption of a steady flow is quite natural. Also, presuming that radiation pressure and gravity are the dominant forces, an overall spherical symmetry of the outflow can be expected. Models based on the standard CSE scenario can be used to derive mass-loss rates and other wind properties by comparing the resulting synthetic spectra with corresponding observations. Different mass-loss indicators (molecular line profiles, dust features, and the overall shape of the SED), as well as more specific model assumptions, will be discussed in Sect. 2.

Predictive power of wind models While SCRA-type models allow the calculation of radial profiles of flow velocities and densities in CSEs, they require the dust properties (composition, abundance, grain size) and the mass-loss rate (or the gas density and velocity at the condensation radius) as input parameters, in order to set the starting conditions of the steady outflow. In Sects. 4 and 5, we will discuss a different type of dynamical models which predict dust properties, wind velocities and mass-loss rates for given stellar parameters and pulsation properties by following the flow

of matter from the pulsating sub-photospheric layers, through the time-dependent dynamical atmosphere, into the dust formation and wind acceleration region. In accordance with the underlying mass-loss mechanism, we will refer to these models as Pulsation-Enhanced Dust-DRiven Outflow (PEDDRO) models, to distinguish them from SCRA-type models. Finally, it should also be mentioned here that a more sophisticated type of SCRA models has been developed, where dust formation is treated as a non-equilibrium process, and grain growth in the accelerating wind is described in detail. This type of steady wind model is nowadays mostly used in combination with stellar evolution models, in order to predict dust yields and spectral energy distributions of stellar populations. Since the basic problem of the SCRA-type models remains, i.e., that the mass-loss rate is a model input, not a result, we will mention such models only briefly in this review.

2 Measurements of mass-loss rates: background

In this section, we describe various empirical methods for estimating stellar mass-loss rates on the AGB, and discuss their underlying assumptions, and their advantages and shortcomings. Since all methods for estimating mass-loss rates are based on the radiation emitted by the gas and dust in the CSE produced by the mass loss, we start with some general information on its properties.

2.1 Basic properties of circumstellar envelopes

The gas and dust particles that escape the stellar gravitational attraction form a stellar wind which is observable as an expanding CSE around the AGB star. Since the mass-loss rates and acceleration efficiencies vary substantially depending on the properties of the mass-losing star (and in some cases its surroundings), the characteristics of the CSEs also vary considerably, e.g., in terms of opaqueness, geometry, kinematics, and chemistry.

At the highest mass-loss rates, the central star will be highly obscured, i.e., essentially all of the stellar (optical) radiation is absorbed in the circumstellar dust and re-emitted at longer wavelengths. On such objects, in principle, only information from the CSE is available. In general, the mass-loss rates are lower than this, and the stellar and circumstellar characteristics can be studied simultaneously, although they are not always easy to disentangle. The winds of AGB stars are slow by astronomical standards; the large majority are found to have velocities in the range 3–30 $\mathrm{km\,s^{-1}}$, and typical values fall in the range 5–15 $\mathrm{km\,s^{-1}}$, reflecting the low escape velocities at the surfaces of these giant, moderate-mass stars.

The chemical compositions of the gas and dust in the CSE reflect the composition of the stellar atmosphere at the time when the material was ejected, although not necessarily in a straightforward way. In particular, the relative abundances of C and O are important, both for the atmosphere and CSE, due to the high binding energy of the CO molecule. CO forms deep inside the atmosphere, effectively binding up the less abundant of the two species (which therefore also determines the abundance of CO) and leaving the rest of the more abundant species to form other molecules and solids.

Consequently, the stellar spectra and wind acceleration by radiation pressure on dust are both strongly affected by the C/O ratio. In the context of the CSE and mass-loss rate determinations, the CO molecule plays a special role due to its stability against dissociation, making it a tracer of the gas density over a wide radial range. Throughout this review, we often describe separately the characteristics of O-CSEs (connected to M-type AGB stars, C/O $<$ 1 by number), C-CSEs (carbon stars, C/O $>$ 1), and S-CSEs (stars of spectral types MS, S, and SC, with C/O close to 1).

The CSE gas primarily consists of hydrogen in molecular form (H_2), efficiently produced in the cool ($\lesssim$ 2500 K) atmospheres of AGB stars, at least for sufficiently high mass-loss rates (Glassgold and Huggins 1983). The expanding hydrogen gas stays molecular until it eventually becomes photodissociated by the energetic interstellar UV field. In addition to H_2, the CSEs of AGB stars have proven to be surprisingly rich in molecular species of varying complexity; more than 90 different species (not counting isotopologues) have been detected. The molecular setups of O- and C-CSEs are markedly different (Cernicharo et al. 2000; Velilla Prieto et al. 2017), except for the fact that CO is the most abundant molecule (next to H_2) in both cases (H_2O may rival CO in O-CSEs). The S-CSEs appear to lie in between the O- and C-CSEs chemistry-wise (Schöier et al. 2011; Danilovich et al. 2014). This diversity of molecular species is the effect of a varied astrochemistry: thermal-equilibrium (TE) stellar atmosphere chemistry, non-TE chemistry induced by shocks due to pulsational motion, and circumstellar chemistry proper, often induced by photodissociation (Millar 2016). It is not clear whether chemical surface reactions on grains play an important role in the circumstellar case. In the C-CSEs, there is also evidence of very large molecules, often seen in post-AGB objects where they are believed to be excited by UV emission: features in the range 3–12 μm have been assigned to polyaromatic hydrocarbons (PAHs) or very small hydrogenated amorphous carbon grains (HACs) (Buss et al. 1993), and even fullerenes (C_{60} and C_{70}) have been detected (Cami et al. 2010; Sloan et al. 2014).

The CSE dust constitutes about one percent or less of the total circumstellar mass. Yet, the dust provides large diagnostic capacity, and it plays a major dynamic role. As for the gas, the dust composition depends on the C/O ratio. The O-CSEs are dominated by silicate dust, in amorphous form (features at 10 and 18 μm), except for the low-mass-loss-rate objects where various Si-free oxides appear prominently, in particular alumina (Al_2O_3; feature at 13 μm) (Blommaert et al. 2006; Golriz et al. 2014). Crystalline silicate dust (reaching about 10 % by mass), e.g., forsterite features at 11, 23, 28, 33, and 69 μm, is also present (Blommaert et al. 2014). This leads to sharper dust features whose characteristics are sensitive to, e.g., temperature and composition (de Vries et al. 2010). It was initially thought that the fraction of crystalline dust increased with mass-loss rate, but that has recently been questioned (Liu et al. 2017). In addition, there is amorphous and crystalline water ice ($<$ 20 % by mass) at the highest mass-loss rates (Lombaert et al. 2013). In the C-CSEs, the featureless amorphous carbon dust emission is dominating. Features due to SiC (at 11.3 μm) and possibly MgS ("the 30 μm feature") dust are present (Lombaert et al. 2012; Messenger et al. 2013), but not the sharper features seen in O-CSEs. For historic overviews on studies of dust in CSEs, see, e.g., Dorschner (2010) and Molster et al. (2010).

The CSEs are interesting in their own rights, but in the context of this review their main importance is that they provide observational possibilities for estimating stellar mass-loss rates.

2.2 The standard CSE model

Most mass-loss rate estimates are based on the assumption of a "standard" CSE around the AGB star. This is a spherical cloud of smoothly distributed gas and dust particles, formed by a constant stellar mass-loss rate and expanding with a velocity that is constant outside a limited acceleration region. Depending on the strength of collisional coupling, the gas and dust components may move at different speeds. Added to this basic picture are descriptions of important physical and chemical processes, such as heating, cooling, chemical reactions, and photodissociation. All mass-loss rate estimates are more or less dependent on the extent to which these assumptions are valid.

Velocity profiles As briefly mentioned in Sect. 1.4, the description of the flow velocity in a CSE model may be handled in different ways. The simplest approach is a kinematic one, where the radial profile of the velocity follows a prescribed parameterized shape, or is assumed to be constant (a good approximation at larger distances from the star, beyond the limited wind acceleration zone). The kinematic approach is often used in connection with the modelling of molecular line profiles since they contain information about gas velocities, making it possible to constrain free parameters in the assumed radial profiles. Alternatively, the flow velocity profile can be derived by solving an equation of motion that takes the relevant forces into account. This method is mostly used in connection with mass-loss indicators that give no direct constraints on the velocities, in particular dust continuum emission.

As discussed in this review, there are good reasons to believe that radiation pressure on dust is an essential component of the mass-loss mechanism, at least above a critical mass-loss rate. In this scenario, the momentum of stellar photons is transferred to the dust grains by absorption and scattering and, eventually, via friction, to the gas particles. In the context of the standard CSE model, wind acceleration is regarded as a steady-state situation where dust is formed instantaneously with a given gas-to-dust-mass ratio and given grain properties, at a distance from the star where the grains are thermally stable. We will use such a description (the SCRA scenario, see Sect. 1.4) as a guideline for the interpretation of observational data. A characteristic quantity is the ratio of the radiative and gravitational forces, given by

$$\Gamma = \frac{\langle \kappa_{\rm d} \rangle L_*}{4\pi c G M_*} \frac{\upsilon_{\rm g}}{r_{\rm gd} \upsilon_{\rm d}}, \tag{5}$$

where $\langle \kappa_{\rm d} \rangle$ is the flux-mean opacity per unit mass of dust, $\upsilon_{\rm g}$ the gas velocity, $\upsilon_{\rm d}$ the dust velocity, and $r_{\rm gd}$ is defined as the ratio of the gas and dust mass-loss rates ($\dot{M}/\dot{M}_{\rm d}$; note that other definitions exist, and it is not always clear which one is used). Assuming that Γ is constant (i.e., independent of r), the SCRA scenario leads to the following expression for the gas terminal velocity, i.e., the asymptotic value of $\upsilon_{\rm g}(r)$ at large r,

$$\upsilon_\infty = \sqrt{\frac{2GM_*}{r_0}\,(\Gamma - 1) + \upsilon_0^2}, \tag{6}$$

where r_0 is the radius where the acceleration starts (approximately the dust condensation radius) and υ_0 the velocity at r_0 (often assumed to be the sound speed). In general, however, Γ is not constant, e.g., due to a dependence of $\langle\kappa_\mathrm{d}\rangle$ on distance from the star caused by changes in the radiative flux (reddening due to circumstellar absorption), or effects of grain drift relative to the gas, as will be further discussed below. Therefore, it should be noted that Eq. (6) only gives a rough estimate of υ_∞.

With density decreasing outwards in the CSE, the collisional coupling between gas and dust becomes weaker, and the dust particles tend to move outwards faster than the gas particles, i.e., the former move relative to the latter with a drift velocity. An approximate expression for its terminal value can be obtained (see, e.g., Krüger and Sedlmayr 1997). It depends on the mass-loss rate, and for low mass-loss rates it may be substantial (but it is believed to be limited by grain sputtering at some velocity), meaning that the dust velocity may be substantially higher than the gas velocity. For high mass-loss rates, the difference between the two velocities is more modest.

Density distributions The gas and dust density distributions in the CSE, $\rho_\mathrm{g}(r)$ and $\rho_\mathrm{d}(r)$, are linked to the flow velocities and mass-loss rates of the gas and dust components by the continuity equation. In a steady wind, mass conservation can be expressed as $\dot{M} = 4\pi r^2 \upsilon(r)\rho(r)$. In its simplest form (assuming a constant expansion velocity), this corresponds to

$$\dot{M}_\mathrm{i} = 4\pi r^2 \upsilon_{\infty,\mathrm{i}} \rho_\mathrm{i}(r), \tag{7}$$

where $\dot{M}_\mathrm{i}$, $\upsilon_{\infty,\mathrm{i}}$, and ρ_i are the mass-loss rate, velocity, and density of component i (gas or dust), respectively. In this case, the densities decrease with distance as r^{-2}. In the wind acceleration zone, where the flow velocity increases with r, on the other hand, the density profiles are steeper, i.e., $\rho_\mathrm{i} \propto \upsilon_\mathrm{i}(r)^{-1} r^{-2}$. Also a time-varying mass-loss rate can, under certain circumstances, be accounted for in this formalism, as long as the expansion velocity is not changing. A problem arises, however, in a situation with a time-varying expansion velocity, e.g., a faster wind catching up with a slower wind. In this case, the relation between mass-loss rate (at a given time) and density (at the corresponding radius in the CSE) breaks down. In addition to variations at the base of the wind, the joint expansion of two fluids, gas and dust, may lead to flow instabilities in the CSE (Simis and Woitke 2003; Dreyer et al. 2011) and, hence, alterations in the density structure not described by Eq. (7).

Individual molecular density distributions may differ substantially from the total gas density distribution, due to chemical processes and photodissociation. The latter depends on the shielding against the interstellar UV radiation, i.e., on the outward column density of dust or of the molecules themselves in the case of photodissociation in lines and, hence, on the mass-loss rate.[1] H_2 is the molecule with the density distribution of largest spatial extent because of its high abundance combined with it being

[1] We note that a stellar chromosphere and/or a companion may contribute significant UV emission (Montez et al. 2017).

self-shielding, i.e., it is photodissociated in lines. Its particle density, $n_{H_2}(r)$, follows an r^{-2} law in a standard CSE with constant flow velocity. The density distributions of other molecules are often expressed in terms of their fractional abundance with respect to H_2, $f_X(r) = n_X(r)/n_{H_2}(r)$.

Since there is no efficient destruction process for the dust in the wind (except for sputtering by gas particles in case of high drift velocities between dust and gas, see above), it is expected to survive to large distances from the star, and hence is, in principle, an efficient mass-loss-rate-history estimator. On the other hand, the abundances and characteristics of various dust components may vary substantially in the inner CSE due to grain formation and evolution.

Radiation fields The radiation from the central star will have characteristics that depend on the stellar evolutionary state, i.e., on the fundamental stellar parameters, and the C/O ratio. In the context of empirical mass-loss-rate estimates, the stellar spectral energy distribution is often assumed to follow that of a blackbody, but also more sophisticated theoretical stellar spectra are used. The circumstellar dust contributes scattered starlight and, in particular, its own heat radiation. This component strongly depends on the mass-loss rate. The primary effect of these two sources of radiation in this context is the heating of the dust and the excitation of atoms and molecules. Excitation of low-frequency transitions is further affected by the cosmic microwave background radiation (at $\approx$ 2.7 K) in the external parts of the CSE. Finally, the interstellar radiation field leads to molecular photodissociation and hence affects the CSE chemistry, as outlined above. This radiation component may differ depending on the location of the star with respect to, e.g., the Galactic plane and OB associations.

A major complication arises due to the pronounced variability of AGB stars. The luminosity variations are limited to about a magnitude, but variations in specific wavelength ranges can be considerably larger. The dust radiation follows the luminosity variations of the star, but it has recently been shown that also circumstellar line emission can be significantly affected by this (Cernicharo et al. 2014). However, in the context of mass-loss-rate estimates from circumstellar CO lines, this can be considered only a minor problem since the lines are dominantly collisionally excited (although some caution should be exercised at lower mass-loss rates and for higher-J lines).

Thermodynamics The local kinetic energy of the gas particles (excluding that of the bulk motion due to the outflow) is determined by heating and cooling processes according to an energy-balance equation (see, e.g., Gail and Sedlmayr 2014). The dominant heating process is due to collisions with the dust grains streaming through the gas, while one of the dominant cooling terms is due to the adiabatic expansion of the gas. There is also a substantial contribution from line cooling, mainly CO and H_2O in O-CSEs, and CO and HCN in C-CSEs. Most of the heating and cooling terms used in radiative transfer codes are given in the form of analytical descriptions for which the validity in certain parameter ranges can be questioned. As a guideline, over a sizable radial range the kinetic temperature distribution can be approximated by a power law, $r^{-\epsilon}$, where ϵ lies in the range $\approx$0.6–1.2 (Teyssier et al. 2006; De Beck et al. 2010; Maercker et al. 2016a), with some indication that it is shallower ($\approx$ 0.4) in the inner CSE (Lombaert et al. 2016). The external parts of high-mass-loss-rate CSEs may become very cool if the expansion velocity of the CSE is so high that no

heating processes can counteract the adiabatic cooling. It is expected that the gas in low-mass-loss-rate CSEs is warmer than the gas in high-mass-loss-rate CSEs.

The dust temperature is locally determined by a balance between the absorption of the infalling radiation (at shorter wavelengths) and the subsequent reemission (at longer wavelengths), see Sect. 1.3. This is discussed further in Sect. 4.2. The result is a dust temperature distribution that is fairly shallow as a function of r, $\epsilon \approx 0.4$. The more optically thick the CSE becomes, the more of the stellar radiation is converted into longer-wavelength radiation close to the star, and the cooler we expect the dust envelope to be.

2.3 Mass-loss-rate estimators

The densities and velocities in the CSE are linked to the stellar mass-loss rate via the continuity equation, Eq. (7), describing the conservation of mass. Already from a theoretical point of view, one may have to separate mass-loss rates for different components because gas and dust expand at different velocities. In addition, there is an important empirical difference between mass-loss rates based on the molecular lines and those estimated from dust emission. In the case of dust, the emission only gives information on the dust optical depth (and the dust temperature). To convert this into a dust-mass-loss rate requires an assumption on the dust expansion velocity, which is not measurable.

Unfortunately, the dominant mass component is normally not accessible to observation and, hence, no direct measure of the total mass-loss rate is available. In AGB CSEs, this applies to H_2 because its rotational energy levels are not excited in the relatively cool CSEs, and (strong) electric-dipole transitions are not allowed. Instead, a far less abundant gas probe is used, and an extrapolation to the total mass-loss rate must be done. A similar situation occurs when dust-mass-loss rates are converted to total mass-loss rates by adopting a gas-to-dust-mass ratio. However, it must be emphasized that the dust-mass-loss rate is in itself a very important property, e.g., through its relation to the chemistry and physics of the ISM, interstellar extinction, and star-formation efficiency.

There are a number of criteria that should be fulfilled by a good mass-loss-rate estimator: (i) it should be applicable to CSEs of all chemistries, as well as (ii) to a wide range of mass-loss rates and objects in different stages of evolution on the AGB; (iii) the emission should be strong and, hence, allow observations of distant objects; (iv) the radiative transfer should be manageable;[2] and finally (v) in the case of lines the fractional abundance should be known or easily estimated.

Thus, conversion of observed circumstellar properties into a stellar mass-loss rate requires a careful identification of suitable mass-loss-rate estimators. This will be discussed in the following two sections.

[2] In the case of lines, this means that (iva) the energy-level diagram should be simple and the radiative transition rates and collisional cross sections are well known and (ivb) there are observable transitions of quite varying excitation energies; in the case of dust this means that (ivc) the emission properties should be well characterized over a broad wavelength range.

2.3.1 Molecular line emission

The usefulness of a molecule as a mass-loss-rate estimator depends on the extent to which the criteria given above are fulfilled. It is clear that CO is outstanding, fulfilling essentially all criteria. Therefore, mass-loss-rate estimates based on circumstellar CO line emission will be discussed at some length.

Circumstellar CO rotational line emission Circumstellar CO rotational line emission at mm/sub-mm wavelengths is an excellent mass-loss-rate estimator for several reasons: CO is, next to H_2, the most abundant species in CSEs of all chemical types; the lines are inherently relatively weak and hence do not saturate except for high mass-loss rates; the energy levels are easily collisionally excited and, combined with the high abundance, this leads to strong lines; the energy level structure is simple where rotational lines probe an extended energy range; the abundance is believed to be determined by the fact that CO is very stable against dissociation, i.e., the C and O abundances determine the CO abundance in O- and C-CSEs, respectively. The line shape carries information on the gas expansion velocity, the optical depth, and the extent of the emitting region. The distance to the object is a major source of uncertainty through its importance for the absolute line intensities (line intensity ratios would give distance-independent estimates, but that requires a very good handle on the physics/chemistry of the CSE, and very well-calibrated observational data).

The fractional CO abundance, $f_{\rm CO}$, required to convert from CO-loss rate to total mass-loss rate, warrants a discussion. A basic uncertainty is to what extent C and O are fully associated into CO in O- and C-CSEs, respectively (e.g., Papoular 2008). A definitive observational determination of the actual circumstellar CO abundance has never been done. Furthermore, in C-stars the CO abundance follows the O abundance, and here a metallicity dependence is expected. In M-stars, where the CO abundance follows the C abundance, the situation is more complicated. For lower masses, a metallicity dependence is expected (no dredge-up of C). For higher masses, the hot-bottom-burning (HBB) process may drastically lower the C abundance and, hence, lower the CO abundance. The extreme OH/IR-stars may be of this type. Solar abundances for C and O, and full association, lead to an $f_{\rm CO}$ of 5×10^{-4} and 10^{-3} in O- and C-CSEs, respectively. Values close to these are also what is normally used for stars in the solar neighbourhood. In summary, the uncertainty in a mass-loss-rate estimate due to the assumed CO abundance is likely to be limited, i.e., within a factor of a few, but likely to be larger for S-stars and more massive M-stars.

Related to this is the size of the CO envelope, which also affects the strength of the CO lines. This is determined by photodissociation and hence the strength of the interstellar UV field. Mauron et al. (2013) have shown, using dust-scattered light, that there is a steep gradient in the strength of the interstellar radiation field with Galactic radius, and the distribution of OB associations causes substantial local variations. In lower-metallicity and/or extragalactic environments, the interstellar UV field may be very different (e.g., McDonald et al. 2015). The results on the circumstellar CO chemistry of Mamon et al. (1988) are frequently used in CO line radiative transfer modelling, but recent studies suggest that these may have to be revised (Li et al. 2014, 2016).

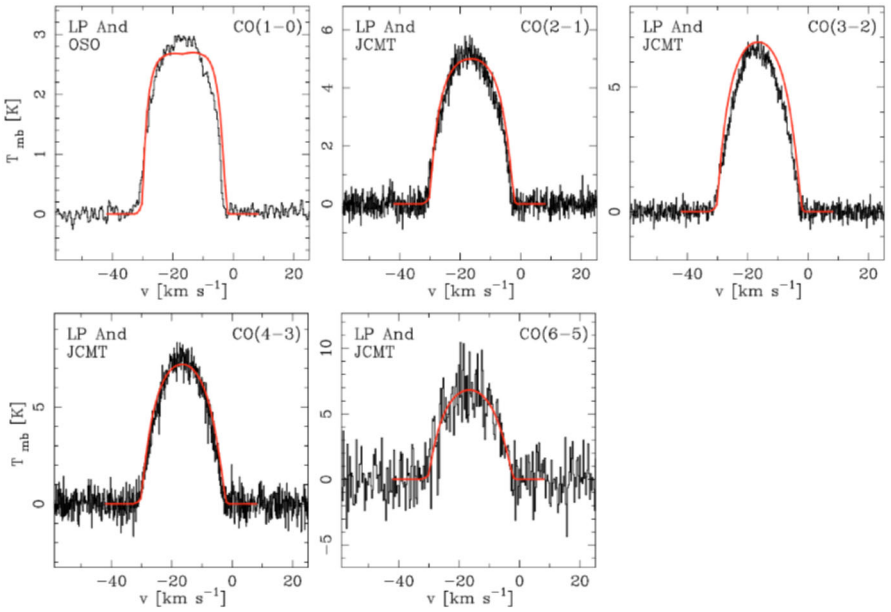

Fig. 3 Examples of observed circumstellar CO rotational lines (histogram) and the associated lines based on radiative transfer modelling (red solid line) of the carbon star LP And. The mass-loss rate is estimated to be $7 \times 10^{-6}\,M_{\odot}\,\mathrm{year}^{-1}$. Image reproduced with permission from Ramstedt et al. (2008), copyright by ESO

Descriptions of the implementation of CO line radiative transfer in numerical codes are given in, e.g., Groenewegen (1994a), Schöier and Olofsson (2001), and Decin et al. (2006). The codes include non-LTE excitation, where collisions with H_2 and/or radiative excitation through excited vibrational states are dominating, and often non-local radiative transfer. The treatment of the circumstellar thermodynamics and the dust radiation field varies though. Examples of observed and modelled CO rotational-line profiles are shown in Fig. 3. Ramstedt et al. (2008) and De Beck et al. (2010) produced mass-loss-rate estimate formulae based on observational quantities like velocity-integrated CO-line intensity and υ_{∞}, as well as on assumptions on, e.g., f_{CO} and distance to the source. The formula of Ramstedt et al. (2008) gives estimates with an uncertainty of a factor of three within the range 10^{-7} to $10^{-5}\,M_{\odot}\,\mathrm{year}^{-1}$ (and within the adopted circumstellar model), while that of De Beck et al. (2010) is more elaborate, and the mass-loss-rate range of applicability is somewhat extended.

The connection between the mass-loss rate at the retarded time t_{ret}, i.e., the time when the matter was ejected, and the density at the corresponding radius, $\approx \upsilon_{\infty} t_{\mathrm{ret}}$, makes it possible to follow mass-loss-rate variations with time, the mass-loss-rate history. Since the kinetic temperature varies with radius we expect CO lines with different excitation-energy requirements to probe different parts of the CSE. The principle is well illustrated by setting the energy of the rotational state J, $E_{\mathrm{J}} = BJ(J+1)$ (expressed in temperature unit, where $B = 2.75\,\mathrm{K}$), equal to the kinetic temperature, $T_{\mathrm{k}}(r_{\mathrm{J}})$, since most of the emission involving this energy level

will come from gas with this temperature and hence from the radius r_J. Assuming that $T_k = 250 \times (10^{15}\,\mathrm{cm}/r)^{0.7}$ K (see Sect. 2.2), we arrive at $r \approx 2 \times 10^{17}, \approx 5 \times 10^{15}$, and $\approx 10^{15}$ cm for the $J = 1$–0, 5–4, and 10–9 lines, respectively.[3] The corresponding retarded times are $\approx 6500, \approx 150$, and ≈ 30 years for $\upsilon_\infty = 10\,\mathrm{km\,s^{-1}}$. Thus, it is important to realize that lines originating from different transitions probe the mass-loss rate at different epochs in the past, and average the mass-loss rate over different time scales.

Circumstellar OH maser emission Circumstellar OH maser emission at a wavelength of 18 cm has been frequently used despite the fact that it is only seen towards O-CSEs and in maser emission, thus fulfilling few of the criteria for a good mass-loss-rate estimator. The primary reason that OH has also served as a successful mass-loss-rate estimator is that its Λ-doubling lines of the $^2\Pi_{3/2}$ ground state are strong due to the maser effect in O-CSEs, in particular the 1612 MHz line, and hence enables observations of objects at large distances. However, the maser effect causes a problem, since observed line brightnesses are not easily (and reliably) converted into quantitative measures of, e.g., the mass-loss rate. Instead OH maser emission mass-loss-rate estimates are based on the fact that the size of the emitting OH shell depends on the mass-loss rate (circumstellar OH is a photodissociation product of H_2O), and the OH luminosity for a saturated maser depends on the size of the OH shell. Hence, there is a relation between mass-loss rate and OH maser luminosity. Using this, relations between OH flux densities and mass-loss rate have been derived (e.g., Baud and Habing 1983). Mass-loss-rate estimates based on such relations are believed to provide order of magnitude estimates. OH line emission has the obvious disadvantage of not providing mass-loss-rate estimates for C-CSEs. The method has been used extensively over the years, but in this review we will only discuss it in special contexts.

The circumstellar 1612 MHz OH maser line exhibits characteristic double-peaked profiles as a consequence of the expansion of the OH shell and the maser amplification in the radial direction (Engels and Bunzel 2015). Hence, the gas expansion velocity can be determined with relatively high accuracy from the separation of the blue- and red-shifted peaks. Amplification in a shell combined with radiative excitation from the variable star provides a method for distance estimates of these objects through phase-lag measurements (Engels et al. 2015).

2.3.2 Dust emission

Dust emission can be divided into a broad continuum and sharper features ($\Delta\lambda/\lambda$ of the order $\lesssim 0.1$). The latter are due to lattice modes (the more ordered the grain structure, the sharper the features). Both properties can be used to estimate the dust optical depth of the CSE, and hence, through an assumption of the dust expansion velocity, provide a dust-mass-loss-rate estimate.

[3] Note that at low mass-loss rates the photodissociation cuts off the CO envelope such that all lines probe the entire CSE, at least for the lower-lying-J lines, see Teyssier et al. (2006).

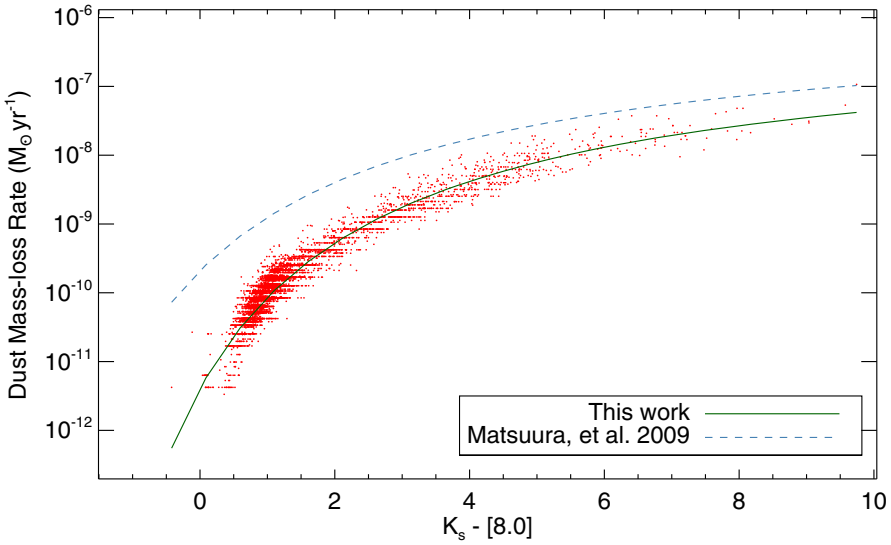

Fig. 4 Dust-mass-loss rates for a sample of carbon stars in the LMC as a function of the colour K_S–[8.0]. The dust-mass-loss rates are determined using SED fitting and assuming a dust expansion velocity of 10 km s^{-1} for all sources. The green line is a fit to the data and the dashed line is the relation derived by Matsuura et al. (2009). This illustrates not only the spread around the fit, but also the difference in relations found in different studies. Image reproduced with permission from Riebel et al. (2012), copyright by AAS

Dust features Dust features are less useful than molecular lines for estimating mass-loss rates for several reasons. They are more ambiguous and consequently an identification of the carrier is often not fool-proof. The inherent strength of a feature is less accurately known. Also, the fraction of the dust that contributes to a particular feature is difficult, if not impossible, to estimate a priori and can only be determined reliably if a full fit to the SED and all the features is produced (e.g., de Vries et al. 2010). Finally, and most importantly, at low mass-loss rates a feature is in emission and its strength increases with the mass-loss rate, but eventually the feature saturates, weakens, and finally goes into absorption with a strength that increases with the mass-loss rate (the 10 μm silicate feature provides an example; Bedijn 1987). A careful SED modelling is consequently required for an accurate estimate of the dust-mass-loss rate using dust features.

Dust continuum emission Dust continuum emission in the absence of features provides no indication of the composition of the dust, and hence caution must be taken when selecting material-dependent properties. In addition, the grain size (or, more generally, the grain-size distribution) plays an important role for the wavelength dependence of its emissivity. This applies also to the shape of the dust grains (spherical, elongated, fuzzy, etc.) and to their structure (coated, inhomogeneous, porous, etc.). Hence, dust-mass-loss rates based on fits to dust continuum emission are already from the outset affected by some considerable uncertainties. Moreover, the methods for estimating them from continuum emission can be more or less sophisticated. We will discuss four of them below.

Mono-chromatic flux density estimate In its simplest form, a "mono-chromatic" flux density is used as a dust-mass-loss-rate estimator, a method that rests on substantial simplifications. In the past, estimates based on, e.g., the IRAS 60 μm flux density were often used (e.g., Jura 1988).

Flux excess and colour estimate A considerable improvement in accuracy is obtained using a flux excess (the flux density in excess of that of the star), or using two (well-selected) flux densities and form their ratio, i.e., a colour. The relations used for estimating dust-mass-loss rate from flux excess or colour are either calibrated against other methods, or they are derived from theory for the particular dust composition in question. An example of a flux-excess estimate is provided by the work of Srinivasan et al. (2009) that is based on the Spitzer 8 μm excess (in turn estimated from SED modelling, see below). Examples of colour estimates are relations between dust-mass-loss rate and K–[12] (Whitelock et al. 2006), K–[8] and K–[24] (Matsuura et al. 2013), [6.4]–[9.3] (Groenewegen et al. 2007), and [3.6]–[8.0] (Matsuura et al. 2013; Reiter et al. 2015), where [12] is the IRAS 12 μm flux while the rest are Spitzer fluxes. A state-of-the-art example is given in Fig. 4, where dust-mass-loss rates derived from SED fits are compared to the K_S–[8.0] colour for a sample of carbon stars in the Large Magellanic Cloud (LMC).

The advantage of these methods is that the estimates are essentially distance independent, but they do not provide better than order-of-magnitude values. The obvious drawback is that they rest on the poor assumption that (for a given chemical type) the CSEs only differ by their dust optical depths. Another disadvantage is that, depending on the observational input, they are often sensitive to only a fraction of the dust components, e.g., only the warm dust, or only the emission due to small grains. Nevertheless, flux excess or colours are the most common ways of estimating dust-mass-loss rates for large samples for which data are nowadays available due to major surveys (in particular of extragalactic objects).

Spectral energy distribution (SED) estimate A safer approach is to use a coverage of the SED which is as broad as possible, and supplement this with a detailed radiative transfer model that may take into account additional complexities like multi-component dust, grain-size distribution, CSE morphology, etc. This is the most reliable of the empirical methods for obtaining dust-mass-loss-rate estimates, but it rests on a large number of assumptions; an obvious remaining problem is that the dust kinematics cannot be measured. Examples of SED fits are shown in Fig. 5. This method was applied by, e.g., Groenewegen et al. (2007) and Gullieuszik et al. (2012) to samples of stars. Because of the complex modelling it is normally not a good method for large samples, but the GRAMS grids[4] for C-rich (Srinivasan et al. 2011) and O-rich (Sargent et al. 2011) objects have been used in such contexts.

Estimate of mass-loss rate based on a dust-driven wind scenario This makes it possible to avoid explicit assumptions about the (unmeasurable) dust velocity. Instead the velocities of dust and gas are determined by the radiative pressure and the drag force between these two components. By solving the coupled problem of dynamics

[4] Extensive grids of SEDs based on COMARCS hydrostatic models for the stars (Aringer et al. 2009) and the 2Dust radiative transfer code for calculating the circumstellar parts of the SEDs (Ueta and Meixner 2003).

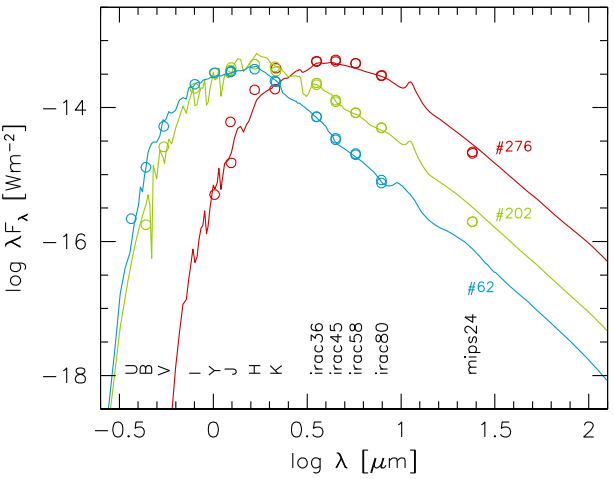

Fig. 5 Examples of SED fits to photometric data of three stars: a blue O-rich star (#62, $J - K_S = 1.2^m$), and two C-rich stars (#202, $J - K_S = 1.5^m$; #276, $J - K_S \approx 4^m$). Image reproduced with permission from Gullieuszik et al. (2012), copyright by ESO

and radiative transfer, which defines the radial structure of the outflow, SCRA-type models link the mass-loss rate to the (measurable) gas velocity and the optical depth of the CSE (which can be inferred from the observed SED). The principle can easily be illustrated for a situation where radiative pressure and gravitation are the only relevant forces, and the ratio of the corresponding accelerations, Γ, defined in Eq. (5), does not depend on the distance from the star. In that case, the equation of motion for a steady outflow can be solved explicitly. By transforming from radial distance to an optical depth scale and using the assumption that the mass-loss rate is constant, a simple relation between mass-loss rate, terminal velocity of the gas, flux-averaged optical depth of the CSE, τ_F, and stellar luminosity can be obtained, i.e.,

$$\dot{M} = \tau_F \frac{L_*}{c\upsilon_\infty} \left(1 - \frac{1}{\Gamma}\right), \tag{8}$$

(assuming that the initial velocity at the dust formation distance is negligible; for details see, e.g., Netzer and Elitzur 1993; Ivezić and Elitzur 1995). The physical interpretation is that the momentum carried away from the star per unit time by the wind, $\dot{M}\upsilon_\infty$, should equal that of the photon flow, L_*/c, times the effectiveness of the momentum transfer from photons to dust, as measured by the dust optical depth, while the parenthesis takes into account that the material must be lifted out of the stellar gravitational potential. An example of this approach is given in Groenewegen et al. (1998). Note that the formula rests on the assumption that the grains that dominate the SED are also the grains responsible for the wind acceleration.

A simple formula as the one given above will not hold for all cases, since the ratio of radiative acceleration to gravitational deceleration, Γ, in general will not be constant. It will depend on the distance from the star due to changes in the radiative flux (reddening), grain drift relative to the gas, and other processes. To derive con-

nections between wind properties and SEDs, the equations describing the dynamics and radiative transfer in the CSE, coupled by the radiative pressure, have to be solved simultaneously, using numerical methods.[5] A similarity between the general situation and the simple case of Eq. (8) is that the mass-loss rate cannot be determined from the SED (or dust optical depth), alone. For given dust properties (composition, grain size, abundance) at the starting point of the wind, the SCRA scenario will give similar SEDs for all models with the same $\dot{M}/L_*^{3/4}$ ratio (or $\dot{M}\upsilon_\infty/L_*$, which is equivalent in this context), as demonstrated by Elitzur and Ivezić (2001). Therefore, an additional quantity, e.g., the wind velocity υ_∞, has to be determined independently, to break the degeneracy between $\dot{M}$ and other parameters, regarding their effects on the SED.

A way to obtain the total mass-loss rate is to solve the equations of motion for the dust and the gas (connected via the drag force) simultaneously, using the dust optical depth (from SED modelling) and the gas terminal expansion velocity (e.g., from observed circumstellar CO lines) as constraints, and the mass-loss rate as the free parameter (Krüger et al. 1994). Ramstedt et al. (2008) used the latter approach and performed a detailed comparison between mass-loss rates estimated from circumstellar dust and from CO lines, finding that they generally agree to within a factor of three.

3 Observed mass-loss characteristics

The following overview of observational results is structured around several topics. First, we present empirical results on mass-loss rates and wind velocities for nearby stars, based primarily on CO as an indicator, which can also be used to calibrate other methods. Furthermore, resolved CSE structures make it possible to check basic assumptions of the standard CSE scenario, regarding overall spherical symmetry and steady flows, as well as giving indications about changes of mass-loss rates on evolutionary timescales. Then, we turn to larger samples of more distant, unresolved objects and the dependence of mass loss on metallicity, and we round off with a short discussion of the total mass lost by AGB stars.

3.1 Results for nearby stars

Reliable mass-loss-rate estimates are primarily based on CO rotational-line emission and are limited to nearby stars, i.e., stars within ≈ 1 kpc of the Sun, for which multi-CO-line data exist. These provide good constraints on the kinetic temperature in the CSE and hence limit uncertainties due to imperfections in the circumstellar model. The major problem for general conclusions to be drawn is sample selection, which can often be guided by the strength of the lines rather than the representativeness of the sources. Further, since these studies are dominated by stars in the solar neighbourhood the rare highest-mass-loss-rate objects may not be well represented. It must also be kept in mind that any mass-loss-rate estimate is an average over time that depends on

[5] An exception is the optically thin limit, where the two parts decouple and the dynamics may be solved analytically, if the grain properties (composition, size, abundance) at the starting point of the wind are given (see Elitzur and Ivezić 2001).

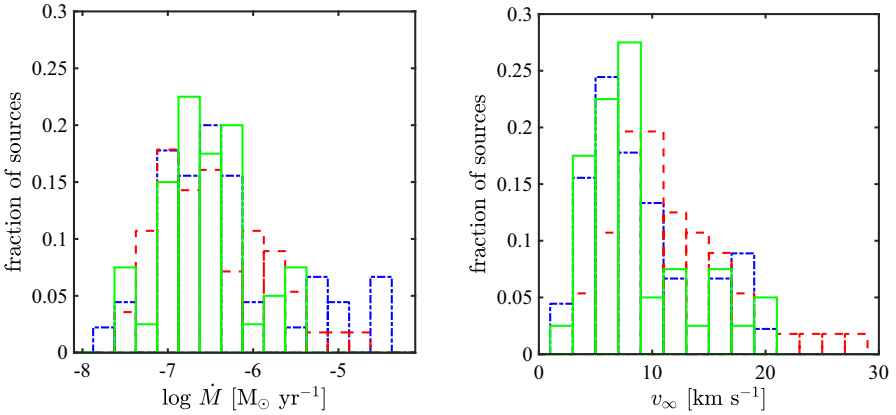

Fig. 6 Left panel: mass-loss-rate distributions for M-type (dashed-dotted, blue line), S-type (solid, green line), and carbon AGB star (dashed, red line) samples. Right panel: gas expansion velocity distributions derived from fitting the CO line widths for M-type (dashed-dotted, blue line), S-type (solid, green line), and carbon AGB star (dashed, red line) samples. Image adapted from Ramstedt et al. (2009)

the line used and the mass-loss rate itself. Using many lines probing emission from different radial ranges, it is, in principle, possible to study the mass-loss history, but such results should be regarded with some caution. We summarize here the present empirical results on mass-loss-rate and wind-velocity distributions, separated into the different chemical types of AGB stars, and discuss the current view on the temporal variations of the mass loss.

3.1.1 Mass-loss rates and kinematics

Major studies of CSEs based on CO line emission and a radiative transfer analysis have been done by, e.g., Schöier and Olofsson (2001) (C-stars), Olofsson et al. (2002) (M-stars), Ramstedt et al. (2009) (S-stars), and Teyssier et al. (2006), De Beck et al. (2010), Ramstedt and Olofsson (2014), and Danilovich et al. (2015) for samples of mixed stars. Only the results of Schöier and Olofsson (2001) and Ramstedt et al. (2009) are based on reasonably complete samples of stars. These studies provide good estimates of mass-loss rates and CSE kinematics, as well as a possibility to compare results obtained with different radiative transfer codes.

Mass-loss rates Representative results for mass-loss-rate distributions are given in Fig. 6, left panel. The major conclusions are that they are independent of the chemistry, they stretch from $\lesssim 10^{-7}$ to $\gtrsim 10^{-5}\,M_\odot\,\mathrm{year}^{-1}$, and the majority of the stars have mass-loss rates of the order a few $\times\, 10^{-7}\,M_\odot\,\mathrm{year}^{-1}$. Therefore, the total local mass-return rate is dominated by the rare high-mass-loss-rate ($\gtrsim 10^{-5}\,M_\odot\,\mathrm{year}^{-1}$) objects although they constitute only a few percent of the mass-losing objects. Extrapolating these results to the entire Milky Way suggests that the O-rich objects dominate the Galactic mass return to the ISM of AGB stars (Olofsson 2003).

The most recent study of this type is that of Danilovich et al. (2015), based on multi-line CO observations (including Herschel Space Observatory data), where mass-loss

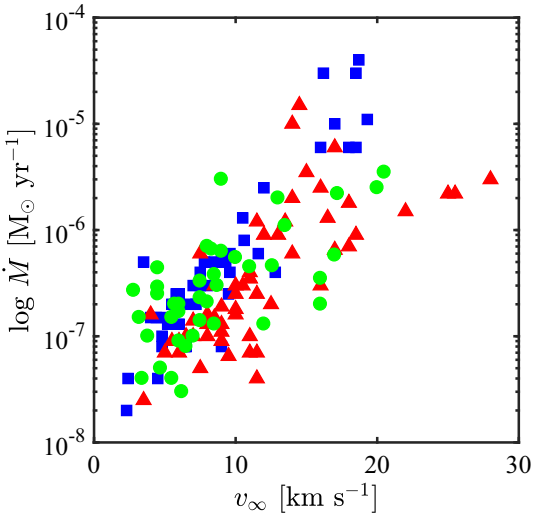

Fig. 7 Mass-loss rates plotted against the gas expansion velocities for M-type (blue squares), S-type (green dots), and carbon AGB star (red triangles) samples. Image reproduced with permission from Ramstedt et al. (2009), copyright by ESO

rates for a sample of sources covering the three chemical types are presented. They also compared their mass-loss-rate estimates to those obtained in other studies, and hence provide a comparison of results obtained using different radiative transfer codes and, to some extent, different assumptions. The conclusion is that their estimates are (on average) lower by about 40 %, but corrected for this the scatter between the different studies is modest. This reinforces the factor of three uncertainty normally attached to mass-loss-rate estimates based on CO lines (and similar model assumptions). For the majority of the stars a constant mass-loss rate, on a time scale much longer than the pulsational one and shorter than a few $\times\, 10^3$ year, gave acceptable fits to the observed data (see also Teyssier et al. 2006; De Beck et al. 2010).

Wind velocities Regarding the terminal velocity of the gas, the uncertainties of the estimates are much smaller than those of the mass-loss rates, typically $\lesssim$ 10%. Representative υ_∞ distributions are given in Fig. 6, right panel. They stretch from $\approx$ 3 to $\approx$ 30 km s^{-1}. A median velocity of $\approx$ 10 km s^{-1} applies to O- and S-CSEs, while it appears that, on average, the C-CSEs have gas expansion velocities which are a few km s^{-1} higher than those of the other two chemical types.

Figure 7 gives an important relation between the two mass-loss characteristics ($\dot{M}$ and υ_∞) which must be reproduced by any mechanism which aims at explaining stellar mass loss on the AGB. Young (1995) showed that $\dot{M} \propto \upsilon_\infty^{3.4}$ for a sample of low- to intermediate-mass-loss-rate M-stars. Similar relations have been found for samples including all chemistries, e.g., the data of Ramstedt et al. (2009) result in $\dot{M} \propto \upsilon_\infty^{3.3}$ and those of Danilovich et al. (2015) result in $\dot{M} \propto \upsilon_\infty^{2.7}$. This is broadly consistent with the scaling relation $\dot{M} \propto \upsilon_\infty^3$, resulting from the SCRA scenario according to Elitzur and Ivezić (2001) and Ivezić and Elitzur (2010), who claim that this reflects the important role of drift between gas and dust in winds of AGB stars. As will be discussed in Sect.5.1, however, alternative interpretations are possible in the context of PEDDRO models.

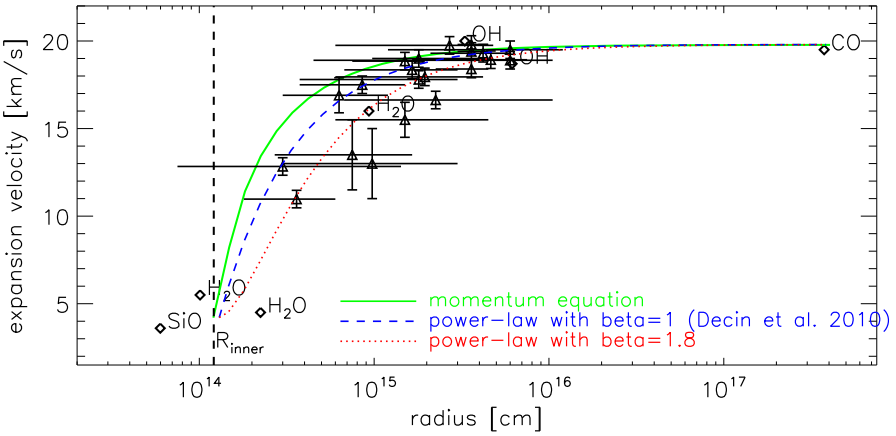

Fig. 8 The velocity profile of the M-type star IK Tau. It illustrates the different techniques used to determine the radial dependence of the gas expansion velocity (see text for details). The diamonds show the places in the CSE where the SiO, H_2O, and OH masers are located, and the terminal expansion velocity obtained from the CO($J = 1 - 0$) line. The triangles show the places in the envelope that contribute the most to the H_2O line emissions observed with the Herschel Space Observatory. The horizontal bars show the minimum and maximum radial distance of the line emission regions. The vertical bars show the uncertainty on the observed line widths. The expansion velocities obtained from solving a momentum equation (full green line), and from a power law, Eq. (9), with $\beta = 1$ (blue dashed line) and 1.8 (red dotted line) are shown. Image reproduced with permission from Decin et al. (2010), copyright by ESO

Another important constraint on the mass-loss mechanism is provided by the radial dependence of the expansion velocity, i.e., the acceleration of the gas, the velocity profile. In radiative transfer modelling of molecular lines, the velocity profile is often parameterized as:

$$\upsilon(r) = \upsilon_0 + (\upsilon_\infty - \upsilon_0)\left(1 - \frac{r_0}{r}\right)^\beta . \tag{9}$$

The expected result in a SCRA scenario is a β between $\approx$ 0.7 (low-$\dot{M}$) and $\approx$ 0.5 (high-$\dot{M}$) (Elitzur and Ivezić 2001). There are in principle two approaches to determine β for a CSE: (i) using probes that emerge from different radii (either measured or inferred from theory), or (ii) using the same probe where the excitation energy requirements of different lines act as the radial discriminator. Excepting cases where the location of the emission is actually measured, the uncertainties in the kinetic temperature law will affect the reliability of the measured velocity profile. The existing results, although fairly uncertain for individual sources, indicate that the acceleration is slower than expected, $\beta \gtrsim 1$ (Decin et al. 2010; Danilovich et al. 2015) and it may be as high as 5 (Khouri et al. 2014a), Fig. 8. Studies of H_2O maser emission also suggest acceleration over an extended region (Richards et al. 2012). There may be a chemical effect here, but as yet there is little information of this type on C-CSE winds. Indications of successive acceleration zones also exist (e.g., Decin et al. 2015; Fonfría et al. 2015).

3.1.2 Temporal variations

Mass loss is likely to be variable on time scales stretching from that of pulsations to that of the entire AGB evolution. Some of these variations can be directly observed, while others require a statistical analysis. We discuss here temporal mass-loss-rate variations that are relatively well established and that appear to be common to AGB stars, starting with significant mass-loss-rate variations on relatively short time scales and ending with the superwind phase, the final stage of mass loss after a long-term gradual increase of the average mass-loss rate in the course of the evolution on the AGB. We iterate the conclusion from above that for the majority of the well-studied objects the mass-loss-rate variations are modest over time scales $\lesssim$ few $\times$ 10^3 year (when averaged over many variability cycles), but note at the same time that there is indirect evidence that at least the non-Miras have variations in their mass-loss rates on time scales of a few hundred years (Marengo et al. 2001).

Brief episodes of enhanced mass loss The most prominent examples of short-term mass-loss-rate variations are the geometrically thin, detached gas and/or dust shells surrounding some AGB stars (about ten examples exist), suggesting that any long-term evolution of the mass loss may be (strongly) modulated on shorter time scales (few $\times$ 10^2 year). The first indications of such variations were indirect, e.g., anomalous broad-band flux ratios suggesting the presence of cold dust at large distances from the stars and a lack of warm dust close to the stars (Willems and de Jong 1988; Zijlstra et al. 1992).

Direct evidence of (highly) variable mass loss was provided by the mappings of CO line emission from geometrically thin shells around seven carbon stars (Olofsson et al. 1990; Lindqvist et al. 1999; Olofsson et al. 1996, 2000; Schöier et al. 2005), Fig. 9. The CO data were subsequently complemented with images in dust-scattered light (González Delgado et al. 2003a; Maercker et al. 2010, 2014; Olofsson et al. 2010; Ramstedt et al. 2011) and in thermal dust emission (Waters et al. 1994; Izumiura et al. 2011; Arimatsu et al. 2011; Cox et al. 2012a). Remarkably, one of the older shells, that of U Hya, has also been detected in the UV (Sanchez et al. 2015). Recently, the CO shells of the carbon stars R Scl and U Ant have been studied in detail (Olofsson et al. 2010; Maercker et al. 2012, 2016b; Olofsson et al. 2015; Kerschbaum et al. 2017). All objects with this type of detached shells are C-rich in nature. Based on the appearance of the shells, and, in particular, on their statistical properties in a relatively complete sample of carbon stars observed in CO lines (Olofsson et al. 1993), Olofsson et al. (1990) draw the conclusion that, at least for carbon stars, highly episodic mass loss is a common phenomenon during part of their final evolution on the AGB, and further suggested that the shells are connected to He-shell flashes. The magnitude of the mass-loss modulation is estimated to be of the order 10^2 for a couple of 10^2 years. Interestingly, no examples of geometrically thin gas or dust shells have been found towards M- or S-type AGB stars despite extensive observations in CO lines (e.g., Nyman et al. 1992; Kerschbaum and Olofsson 1999; Ramstedt et al. 2009) and dust emission (Cox et al. 2012a). This could be an effect of the difference in dust compositions.

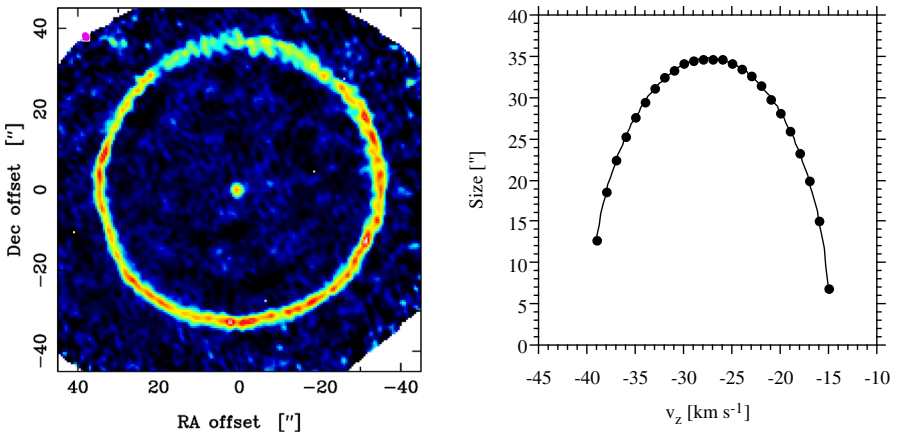

Fig. 9 Left: a ^{12}CO($J = 1$–0) image of the circumstellar environment of the carbon star TT Cyg obtained with the IRAM PdB interferometer (in a narrow velocity range centered on the systemic velocity and colour-coded in flux density per beam scale; beam shown in upper left corner). It shows a geometrically thin, detached CO shell. Its age is estimated to be $\approx$ 7000 year. Emission from the present-day wind is seen at the centre. Right: a fit of the observed sizes of the shell as a function of line-of-sight velocity to the expression $\theta(\upsilon_z) = \theta(\upsilon_{sys})\sqrt{1-[(\upsilon_{sys}-\upsilon_z)/\upsilon_\infty)]^2}$ shows the overall sphericity of the shell. Image reproduced with permission from Olofsson et al. (2000), copyright by ESO

Long-term evolution Temporal variations on long time scales ($> 10^4$ year) are not accessible by observing, e.g., CO lines (because of photodissociation), but they are, in principle, accessible through HI and dust observations. Nevertheless, studies of HI and circumstellar dust have not resulted in much further understanding of the mass-loss history of AGB stars. Therefore, most conclusions in this area are indirect.

It is very likely that the mass-loss rate of an individual star will increase systematically as it evolves along the AGB (both luminosity, size, and pulsational activity increase with time, while the mass decreases). Habing (1996) put forward a number of arguments, based on observational findings, for this. For instance, it is found that stars with "lengthened" periods must be in a later evolutionary stage than stars with the same luminosity but shorter periods (the lengthening being likely an effect of decreasing stellar mass due to mass loss). There is evidence that these "lengthened-period" stars have larger mass-loss rates, and hence their mass-loss rates have increased with time. Further, statistical studies in favor of a gradually increasing mass loss with time are based on, e.g., an OH maser luminosity function (Baud and Habing 1983; Bedijn 1988) or on the distribution of AGB-stars (and their CSEs) in a far-IR colour–colour diagram (van der Veen 1989). The main problem here is that it is difficult to discriminate between effects due to age on the AGB and, e.g., the initial mass in statistical studies (Epchtein et al. 1990).

A superwind phase A phase of very high mass loss, $\gtrsim 10^{-5}\,M_\odot\,\mathrm{year}^{-1}$, at the very end of the AGB evolution, a superwind, has been invoked for a number of reasons (see Renzini and Voli 1981; Vassiliadis and Wood 1993, and Sects. 1.2 and 5.2.3). There

is observational evidence for the existence of such a final strong wind. For instance, a number of highly evolved OH/IR-stars show CO rotational-line-intensity ratios that are not consistent with the assumption of a constant mass-loss rate (Heske et al. 1990; Lombaert et al. 2013). A reasonable explanation is a recent increase in the mass-loss rate, which has affected mainly the higher-J line emission which comes from a region smaller than that of the lower-J lines, see Sect. 2.3.1 (Groenewegen 1994b). A similar conclusion was obtained by comparing OH, CO, and dust mass-loss-rate estimates for a sample of OH/IR stars (Justtanont et al. 1996; Fong et al. 2002), although here the uncertainties in the individual estimates are considerable, and through a study of bulge M-stars (Jiménez-Esteban and Engels 2015).

However, recent studies indicate that the duration of the superwind phase may be shorter than expected. Justtanont et al. (2013) compared mass-loss rates of OH/IR stars estimated from the assumption of a dust-driven wind (Sect. 2.3.2) with those from low-J CO lines and concluded that the superwind phase is limited to $\approx$ 500 year. A source of uncertainty in the observational estimates is the CO abundance. The carbon abundance may very well be lower in these stars since they are most likely in the HBB phase (Justtanont et al. 2015), see Sect. 2.3.1. Hence, the mass-loss rates estimated from CO may be underestimated. de Vries et al. (2014) produced an independent study through analyzing crystalline silicate features, but the conclusion was the same; the superwind phase is quite limited in time. With the estimated mass-loss rates of Justtanont et al. (2013) the amount of mass lost during such a short time scale is only $\approx$ 0.1 $M_{\odot}$. On the other hand, studies of OH maser emission from OH/IR stars suggest a longer superwind phase, up to 3000 year (e.g., Engels and Jiménez-Esteban 2007). A possible explanation of this problem is that the superwind phase is repetitive, but there is presently no evidence of such large-scale structures around these stars. We must conclude that the superwind phase remains to be better observationally characterized.

3.1.3 Circumstellar morphology

One of the basic assumptions in the standard CSE model is that of sphericity and, hence, this is also the underlying assumption behind all mass-loss-rate-estimate methods. It is, therefore, important to check the validity of this assumption. Examples of deviations from sphericity on various scales and their implications are discussed further in Sect. 6.1.2.

The determination of the morphology is not a simple observational task. The conversion from a 2D brightness distribution, which in the case of line emission, also contains line-of-sight velocity information, to a 3D density distribution can be quite complicated. Radiative effects (e.g., saturation, maser action), excitation, chemistry, and observational effects (e.g., the lack of interferometer sensitivity to extended emission) may play an important role.

There is ample evidence of departures from spherical symmetry in the inner regions of CSEs (Blasius et al. 2012; Males et al. 2012; Ohnaka et al. 2016; Stewart et al. 2016a). However, these results are not necessarily attributed to a non-spherical mass loss. As outlined in Sect. 6.1.1, the stars are believed to have major convection cells, and the mass loss most likely occurs in patches in the upper atmosphere, i.e., the wind is initially most likely clumpy. If the number of clumps emitted per unit time is

limited, the number of clumps within the inner region is also limited, and there are, therefore, good reasons to expect the brightness distributions to appear asymmetric and patchy, even if the mass loss occurs isotropically when averaged over longer time scales. The clumpiness of the circumstellar medium, and its possible effects on, e.g., mass-loss-rate estimates, are further discussed in Sect. 6.1.4.

As larger regions of a CSE are studied, the effects of any clumpiness average out, and we expect to be able to infer the large-scale morphology of the CSE. The most detailed study of CO line brightness distributions in AGB CSEs, i.e., out to a few $\times$ 10^{17} cm, is provided by Castro-Carrizo et al. (2010), where interferometry data are supplemented with short-spacing information from single-dish observations. In general, the molecular CSEs are found to show a roundish shape and to a large extent isotropic expansion (a conclusion based on 11 CSEs covering the three chemical types). Nevertheless, in many of them moderate departures from overall spherical symmetry of various types are also found, e.g., elongations, more or less concentric arcs (sometimes appearing spiral-like), and kinematical evidences of aspherical winds. Another example is the (apparent) large CSE around the nearby carbon star CW Leo which shows circular symmetry in all velocity channels, when mapped in CO lines to low surface brightness, in a manner expected from spherical symmetry, Fig. 10. Some of the detached CO shells discussed in Sect. 3.1.2 have been mapped in detail, and they show a remarkable overall spherical symmetry (Olofsson et al. 2000; Maercker et al. 2016b), Fig. 9.

On even larger scales, information on the atomic CSE is obtained from observations of the HI 21 cm line. These are difficult observations to perform because of the omnipresence of this emission. Thanks to some dedicated work, however, considerable progress has been made in this area (Le Bertre and Gérard 2004; Matthews et al. 2013, 2015). In general, the data do not contradict a largely isotropic mass loss, although there is evidence of circumstellar–interstellar media interactions at large distances from the stars. These occur at radial distances much larger than the size of the CO envelopes and, hence, this has little effect on CO-based mass-loss-rate estimates. An important conclusion from these studies is that in terms of mass-loss-rate estimates the atomic CSE needs to be taken into account only at low mass-loss rates, $\lesssim 10^{-7}\,M_{\odot}\,\mathrm{year}^{-1}$ (Hoai et al. 2015).

Our knowledge of the morphology of the dust CSEs has improved significantly due to observations in dust-scattered light (e.g., Mauron et al. 2013; Sahai and Mack-Crane 2014), and through observations with the Herschel Space Observatory of thermal dust emission (e.g., Cox et al. 2012a). In particular, the latter shows that on the larger scales there are significant departures from sphericity, but these are not necessarily connected to a non-isotropic mass loss. Cox et al. (2012a) classified the morphology of dust CSEs into four groups: "fermata" (objects show bow shocks due to star and CSE moving through the ISM), "eyes" (show bow shocks and are tentatively identified with binaries), "ring" (detached, essentially spherical, thin shells, an effect of time-variable mass loss, see Sect. 3.1.2), and "irregular" (significant departures from symmetry). Some illustrative images are shown in Fig. 20. Of concern here is whether the complex morphological structures affect the dust-mass-loss-rate estimates. This is further discussed in Sect. 6.1.4.

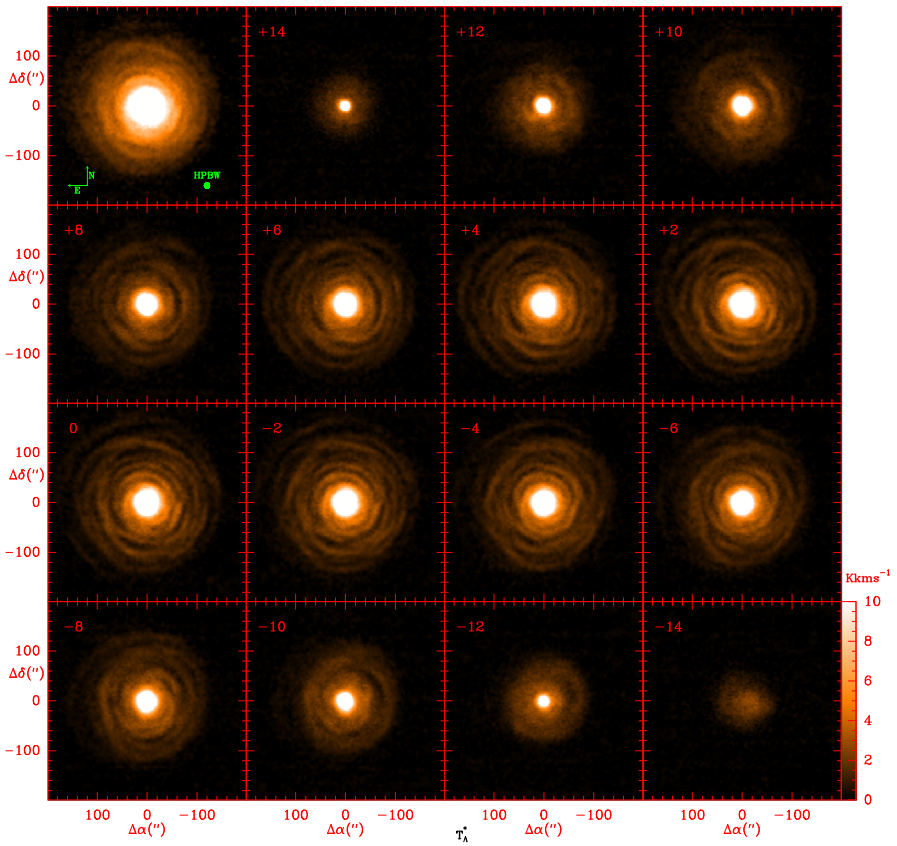

Fig. 10 Top left: velocity-integrated CO($J = 2-1$) line emission towards the carbon star CW Leo, aka IRC+10216, covering an area of $6.7' \times 6.7'$ (the $\upsilon_{\rm LSR}$ range from -41 to $-12\,{\rm km\,s^{-1}}$). The rest: velocity-channel maps (resolution $2\,{\rm km\,s^{-1}}$) where the velocities are relative to the systemic velocity ($\upsilon_{*,\rm LSR} = -26.5\,{\rm km\,s^{-1}}$). These data illustrate well both the overall spherical symmetry on large scales, and the departures from this on smaller scales. The arc structure and its implications are discussed in Sect. 6.1.3. Image reproduced with permission from Cernicharo et al. (2015), copyright by ESO

3.2 Mass loss in other environments

Studies of stars in the solar neighbourhood provide the most accurate mass-loss-rate estimates, but they are to a large extent limited in parameter space, e.g., in terms of metallicity and stellar environment, and may be heterogeneous in terms of other stellar parameters. In general, an understanding of the dependence of the mass-loss-rate characteristics on metallicity is very important for our understanding of the importance of AGB stars over the life span of the universe. This necessarily involves samples of more distant sources (in particular, including extragalactic samples), and then there are two major concerns. First, identification of the nature of the sources becomes more difficult (e.g., filter bands may not have been designed specifically for this purpose). Second, it is difficult to find suitable Galactic comparison samples. To this should be

added the increasing contamination with red supergiants (RSGs; i.e., highly evolved stars that are more massive than AGB stars) in samples of more distant objects.

For sensitivity reasons, the studies of more distant samples are hitherto almost exclusively based on circumstellar dust emission. It is natural to assume that dust plays an important role for wind-driving also in other environments, more specifically silicate dust in the case of O-rich and carbon dust in the case of C-rich objects. This introduces a systematic difference between the two chemical types since Si is not synthesized in AGB stars while C is. Thus, we can expect the dust-mass-loss rate of an M-star to depend on metallicity, while this is not necessarily the case for a carbon star (however, the atmospheric structure is also likely to be metallicity-dependent so it is difficult to estimate the extent of the mass-loss dependence on metallicity without detailed modelling). Consequently, the gas-to-dust-mass ratio to adopt when scaling to total $\dot{M}$ may differ substantially from that in the solar neighbourhood. Theoretical estimates of the metallicity dependence of stellar dust production on the AGB are given by, e.g., Nanni et al. (2013, 2014). At lower metallicity, an M-star is also more easily converted into a carbon star. Hence, we expect carbon stars to reach the highest mass-loss rates and dominate the amount of mass lost in such environments.

The CO line emission is expected to be weaker in both O- and C-CSEs of lower-metallicity because of the lower C- and O-abundances, respectively (Woods et al. 2012). Likewise, a stronger UV environment will decrease the CO envelope size for both chemical types, and hence the line strength. Both effects are likely to reduce the CO line emission from extragalactic objects. It is nevertheless encouraging that the first detection of extragalactic, mass-losing AGB stars in CO line emission has been made; four objects in the LMC were observed using the Atacama Large Millimeter/submillimeter Array (ALMA) (Groenewegen et al. 2016).

3.2.1 The Galactic Bulge and Halo

Limited studies of the AGB mass-loss characteristics of stars in the Galactic Bulge and Halo have been performed. Five inner-Bulge OH/IR stars, with a metallicity most likely somewhat higher than the solar value, have been detected in CO line emission by Winnberg et al. (2009) and Sargent et al. (2013). The estimated mass-loss rates lie on the high side, and the gas-to-dust-mass ratios center around 200. Jiménez-Esteban and Engels (2015) derived mass-loss rates (using SED fit, a dust-driven wind, and υ_∞ from OH data) for a sample of highly reddened O-rich bulge stars. Not surprisingly, the mass-loss rates are high, $(1-30)\times 10^{-5}\,M_\odot\,\mathrm{year}^{-1}$.

Lagadec et al. (2010) detected six (presumably sub-solar metallicity) carbon stars of varying origin in the Galactic Halo in CO line emission, and Lagadec et al. (2012) concluded that the estimated mass-loss rates are fairly normal when compared to nearby stars of similar characteristics, while the gas-to-dust-mass ratios lie on the high side, $\gtrsim 500$. Lagadec et al. (2010) also found that the gas expansion velocities are lower in the two Halo stars and the Sgr dSph stream star (all three well below $10\,\mathrm{km\,s}^{-1}$) than those of comparable solar neighbourhood stars. A cautionary remark though: the sample is very small.

3.2.2 The Magellanic Clouds

The metallicities of the LMC and the Small Magellanic Cloud (SMC) are $\approx 0.5\,Z_\odot$ and $\approx 0.2\,Z_\odot$, respectively, so these galaxies provide a good first step in characterising the metallicity dependence of mass loss on the AGB. The reliability and the completeness of the estimated mass-loss rates for objects in the Magellanic Clouds (MCs) have improved significantly due to the large surveys performed, e.g., MCPS (Zaritsky et al. 2004), 2MASS (Skrutskie et al. 2006), SAGE (Meixner et al. 2006), and AKARI IRC Survey (Ita et al. 2008).

Several detailed studies of limited-size samples have been performed. Groenewegen et al. (2007) presented a Spitzer-based study of 60 carbon stars in the MCs and concluded that, for a given period, the majority of the carbon stars in the MCs have mass-loss rates that are in agreement with those observed for Galactic carbon stars, and with no obvious difference between the LMC and SMC stars (based on dust-mass-loss rates from SED fits and the assumption that the objects in the MCs have υ_∞ and $r_{\rm gd}$ typical of Galactic carbon Miras). The mass-loss rates span the range 10^{-7} to a few $\times\ 10^{-5}\,M_\odot\,{\rm year}^{-1}$. Further studies of the LMC showed that only carbon stars reach very high mass-loss rates (Gullieuszik et al. 2012), and in some cases (maybe) even higher values than those of Galactic carbon stars (Gruendl et al. 2008). Yet, luminous, red, large-amplitude, long-period O-rich objects exist in the LMC (any sample of these objects is likely to contain a non-negligible fraction of RSGs). By selecting such objects it has been possible to detect 13 of them in OH 1612 MHz line emission, as summarized by Goldman et al. (2017). They found mass-loss rates in the range 10^{-5} to $10^{-4}\,M_\odot\,{\rm year}^{-1}$ and the gas-to-dust-mass ratios center around 500, substantially higher than the values (estimated in the same way) for their comparison samples of OH/IR stars in the Galactic Centre and Bulge (based on a dust-driven wind, and υ_∞ from the OH data).

Riebel et al. (2012) applied GRAMS models (see Sect. 2.3.2) to a large sample of LMC objects and concluded that carbon stars inject 2.5 times more dust than the O-rich objects. The extreme objects (almost exclusively highly reddened carbon stars) dominate, $\approx 75\,\%$ of the dust mass-return rate but $\lesssim 5\,\%$ of the population (the few RSGs, 0.1 % of the population, contribute $\approx 10\,\%$ of the dust mass-return rate). The total amount of matter contributed by the two chemistries may be more equal if the O-rich objects have higher gas-to-dust-mass ratios.

Boyer et al. (2012) analyzed SMC data and concluded that the extreme carbon stars account for almost 90 % of the dust production (the 8 μm excess was used as the dust-mass-loss-rate estimator). This conclusion is in line with the predominance of carbon stars among the extreme objects (Boyer et al. 2012; Dell'Agli et al. 2016). Nevertheless, Matsuura et al. (2013) used $\dot{M}$–colour relations and concluded that the dust mass-return rate is equally divided between O- and C-rich objects in both the LMC and SMC (the RSG contribution is negligible). They claimed that a fair fraction of the extreme objects are actually O-rich AGB stars. Such massive stars in the HBB phase were also found by Dell'Agli et al. (2015). This indicates the difficulties and the uncertainties associated with estimates like these.

Information on the kinematics of LMC AGB winds is gradually being gathered. For their LMC sample with OH 1612 MHz line emission, Goldman et al. (2017)

concluded that at similar luminosity the LMC sources have lower υ_∞ (they center around $10\,\mathrm{km\,s^{-1}}$) than those of their Galactic comparison samples. The CO line detections of four carbon stars in the LMC by Groenewegen et al. (2016) are consistent with this conclusion.

3.2.3 Other galaxies

As we proceed to more distant galaxies, the quantitative data become scarcer. The majority of the external galaxies observed are metal-poorer than the Milky Way, and the mass-losing AGB stars are most likely carbon stars. The low-mass M-stars have low dust-mass-loss rates, and the massive M-stars in the HBB phase have already left the AGB, unless there has been a recent starburst. Efficient dredge-up of C may lead to efficient dust production independent of metallicity.

In a study of eight Local Group dIrr galaxies (with metallicities around $0.1\,Z_\odot$ and below), there are objects with mass-loss rates of the order $10^{-5}\,M_\odot\,\mathrm{year}^{-1}$ in all galaxies, although there are more of them the higher the metallicity, based on $\dot{M}$–colour relations and assumed gas-to-dust-mass ratios that depend on the metallicity (Boyer et al. 2009, and references therein). Dell'Agli et al. (2016) studied in more detail one of these objects, IC1613, and concluded that carbon stars dominate among the most obscured objects, and hence also dominate the mass return. Going even lower in metallicity, about 50 dwarf galaxies have been surveyed by Boyer et al. (2015a, b). The result is that dust-producing AGB stars exist at least down to a metallicity of $\approx 0.01\,Z_\odot$, and there is no evidence of a strong link between dust production and metallicity. These results are consistent with those of other studies of extragalactic carbon stars in low-metallicity systems (Matsuura et al. 2007; Lagadec et al. 2008, 2009; Sloan et al. 2009). In a solar-metallicity environment, Jones et al. (2015) found mass-loss rates (using an $\dot{M}_\mathrm{d}$–colour relation and $r_\mathrm{gd} = 200$ for all objects) in the range 10^{-7} to a few $\times\ 10^{-5}\,M_\odot\,\mathrm{year}^{-1}$ in the dE M32.

3.3 The total mass lost by an AGB star

There is good evidence that AGB stars with masses up to 6–8 $M_\odot$ manage to end their AGB evolution with a core mass below the Chandrasekhar limit of about $1.4\,M_\odot$ (Cummings et al. 2016). Most of the mass loss occurs on the AGB, except for the lower-mass stars where mass loss on the RGB is substantial in a relative sense, of the order $\lesssim 0.25\,M_\odot$ in total (McDonald et al. 2009, 2011; Lebzelter and Wood 2011).

Initial–final mass relation Information on the total mass lost is directly coming from a comparison of white dwarf (WD) masses and their progenitor masses, the initial–final mass relation. Much progress has been made recently, and we give only a brief summary. Data have been obtained studying WDs in, e.g., wide binaries (Zhao et al. 2012) and in clusters (Kalirai et al. 2014; Cummings et al. 2015, and references therein). Cummings et al. (2016) found a tight relation between the main sequence mass M_MS and the final mass M_f, $M_\mathrm{f} = 0.154\,M_\mathrm{MS} + 0.261$, up to $\approx 4\,M_\odot$, beyond which the relation appears less steep reaching $M_\mathrm{f} \approx 1.2\,M_\odot$ at $M_\mathrm{MS} = 8\,M_\odot$, Fig. 11. The tight relation is strong evidence that mass loss is not a stochastic process

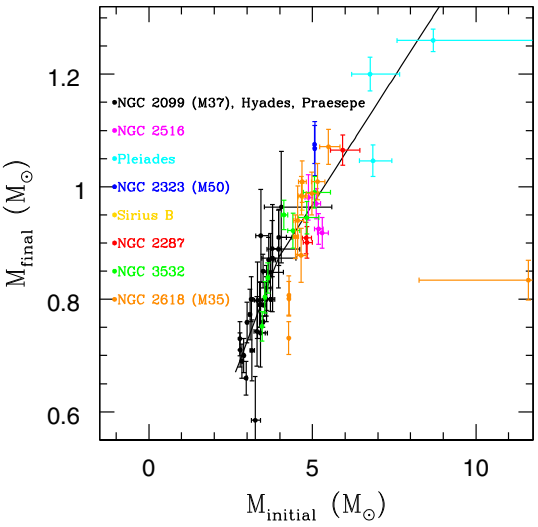

Fig. 11 The relation between initial mass and final mass for white dwarfs as derived from data for a number of open clusters. Image reproduced with permission from Cummings et al. (2016), copyright by AAS

(over long time scales), but follows an essentially predictable behavior. The results indicate that for an initial mass of 4 $M_\odot$ about 80 % of the stellar mass is lost (mainly during the AGB phase) before the WD stage is reached, while a 1 $M_\odot$ star loses $\approx$ 0.25 $M_\odot$ on the AGB.

Stellar lifetimes on the AGB Stellar lifetimes on the AGB are expected to depend on mass and metallicity and they are difficult to estimate reliably. Attempts have been made in a number of ways, often with different sensitivities to different phases of the AGB evolution. Clusters in the MCs are suitable objects for lifetime estimates, and Girardi and Marigo (2007) found AGB stellar lifetimes that peak at $\approx$ 2 Myr, and Girardi et al. (2010) found TP-AGB lifetimes between 1.2 and 1.8 Myr in a sample of metal-poor galaxies. Kalirai et al. (2014) used initial–final mass relations and found that the TP-AGB lifetime increases from 0.8 to 3 Myr in the initial mass range 1–2 $M_\odot$ and then decreases again to 0.4 Myr at 4 $M_\odot$. This is largely confirmed by Miller Bertolami (2016) who derived lifetimes from stellar evolutionary models. Thus, with AGB lifetimes in the vicinity of 1 Myr, and with typical mass-loss rates around 10^{-6} $M_\odot$ year^{-1}, and peak mass-loss rates reaching 10^{-5}–10^{-4} $M_\odot$ year^{-1} (Sect. 3.1), there is no obvious obstacle for reaching sub-Chandrasekhar core masses. Note, however, the discussion on the short duration of the high-mass-loss-rate phase in Sect. 3.1.2.

4 The pulsation-enhanced dust-driven wind scenario

The empirical estimates of wind properties discussed above are mostly based on the idealized, large-scale picture of the "standard CSE", describing a region where both the dust properties and the outflow are already established. To understand the physical processes which trigger the winds and define the mass-loss rates, however, it is necessary to study the conditions in the extended dynamical atmospheres of AGB stars

where the outflows have their origin. Until recently, these regions were only accessible with the help of models, but the ongoing progress in high-angular-resolution techniques finally makes it possible to directly test certain theoretical ideas through observations.

As outlined in Sect. 1.3, the most promising scenario for the heavy mass loss of AGB stars involves a combination of atmospheric levitation by pulsation-induced shock waves and radiative acceleration of dust grains which form in the resulting cool upper layers of the atmospheres. The dust grains transfer momentum to the surrounding gas particles through collisions, dragging them along and thereby triggering an outflow. We refer to this wind mechanism as the Pulsation-Enhanced Dust-DRiven Outflow (PEDDRO) scenario (see Fig. 2). In this section, we focus on detailed quantitative models of these processes, starting with the dynamics of the stellar interior (pulsation and convection), proceeding to atmospheric dynamics and dust formation, and, finally, discussing the development and present status of wind models that predict mass-loss rates and their dependence on fundamental stellar parameters. In Sect. 5.1, the current PEDDRO models are compared to observational results and the SCRA scenario.

4.1 Pulsation, convection, and atmospheric levitation due to shock waves

AGB stars which show signs of strong mass loss are usually semi-regular or Mira-type long-period variables (e.g., Whitelock et al. 1991, 2003; Glass et al. 2009; McDonald and Zijlstra 2016), and their pronounced variations in luminosity are generally attributed to large-amplitude pulsations. Interferometric monitoring reveals temporal variations of measured stellar diameters, as well as a strong dependence of diameters on wavelength, indicating extended, dynamical atmospheres with complex molecular layers (e.g., Burns et al. 1998; Ireland et al. 2004a, b; Woodruff et al. 2008; Lacour et al. 2009). Recent advances in high-angular-resolution techniques have made it possible to resolve the surfaces and extended atmospheres of some nearby AGB stars (e.g., Stewart et al. 2016b; Ohnaka et al. 2016; Wittkowski et al. 2017), showing temporal changes in atmospheric structures and dust properties (e.g., Haubois et al. 2015; Khouri et al. 2016a; Ohnaka et al. 2017). For the large majority of cool giants, however, dynamical processes have to be explored with indirect methods, using photometric monitoring or high-resolution spectroscopy. Light curves, in particular, are often used for studying the dynamics of distant, unresolved stars, both individually and in large photometric surveys.

Over the last 10–15 years, significant progress has been made in identifying several of the period-luminosity sequences found in survey data (e.g., MACHO, OGLE) with different pulsation modes, using linear non-adiabatic models (see, e.g., Wood 2015; Trabucchi et al. 2017, and references therein). Mira stars are probably fundamental-mode (radial) pulsators, whereas semi-regular AGB stars are interpreted as pulsating in the first or higher overtones. The improvements in the available data have also led to the discovery of substructures in the period-luminosity sequences, probably due to non-radial modes. There are, however, open problems regarding the understanding of long secondary periods (e.g., Saio et al. 2015), or concerning the pulsation modes of stars with lower luminosity (RGB stars; e.g. Soszynski et al. 2007; Mosser et al.

2013; Soszyński and Wood 2013; Takayama et al. 2013), although the latter problem may be solved by a new interpretation suggested by Trabucchi et al. (2017). Radial fundamental-mode pulsations of AGB stars have also been explored with 1D non-linear models (e.g., Ireland et al. 2008, 2011, CODEX code), including effects of pulsation-induced shocks on stellar atmospheres. Such non-linear models are probably a more appropriate tool for studying Mira variables than their linear counterparts, given the large amplitudes of the pulsations.

Global 3D radiation-hydrodynamical simulations are an alternative approach to modelling the pulsations of AGB stars, which is more direct and comprehensive, but also more computationally intensive. In this case, a parameterization of convection (e.g., in terms of mixing length theory), as used in classical linear and non-linear pulsation models, can be avoided because turbulent convective flows develop naturally as an intrinsic part of the models (see Fig. 12). An exploratory grid of such simulations for AGB stars by Freytag et al. (2017) gives first indications of how convection patterns and pulsation properties depend on stellar parameters. The 3D models demonstrate how long-lasting giant convection cells, consisting of wide upflow regions that are surrounded by turbulent downdrafts, together with short-lived smaller surface granules and radial fundamental-mode pulsations, give rise to variable surface structures and changes in luminosity. In particular, the models presented by Freytag et al. (2017) show pulsation periods that are in good agreement with the observed period-luminosity relation by Whitelock et al. (2009).

Sound waves, produced in the sub-photospheric layers by convection and pulsation, steepen into shocks when reaching the atmosphere (Fig. 12, bottom panel). There, they interact and merge, leading to a transition from a complex, small-scale network of shocks close to the surface of the convection zone to almost global, more or less radially expanding shock fronts in the outer atmospheric layers (see Fig. 12, middle). These large-scale, outwards-propagating shock fronts probably create local conditions which are comparable to those induced by spherical shock waves resulting from purely radial pulsation (for a discussion see, e.g., Wittkowski et al. 2016; Freytag et al. 2017). This may explain why spherical dust-driven wind models give mass-loss rates, spectra and photometric variations that agree well with observations, as will be discussed in Sect. 5.1.

The time-dependent dynamics of the atmosphere and wind formation region can be studied observationally with high-resolution spectroscopy since Doppler shifts reflecting the gas velocities are imprinted on spectral line profiles (e.g., Hinkle et al. 1982, 1997; Alvarez et al. 2000; Lebzelter et al. 2005a, b; Nowotny et al. 2010). One of the most prominent examples are vibration–rotation lines of CO in the near-IR wavelength region, which are formed at different depths in the atmosphere and wind, according to their excitation potential. Fundamental mode lines probe the fully established outflow, showing more or less pronounced P-Cygni profiles with little temporal variation. First overtone lines form in the dust formation and wind acceleration zone resulting in a complex time-dependent behavior of the line profiles. Second overtone lines probe the inner atmosphere where shock waves dominate the dynamics. They show systematically varying line profiles and periodic line splitting around the luminosity maximum in Mira variables as a pulsation-induced shock wave is passing through the line formation region. Since the IR spectra of C-type AGB stars tend to be strongly

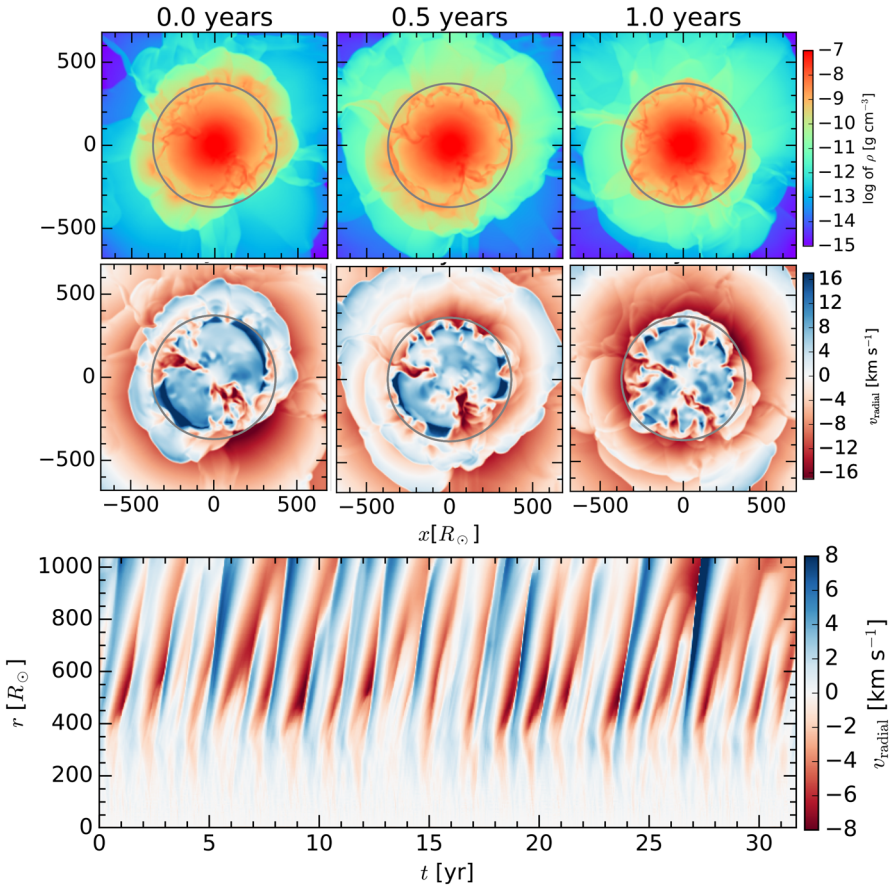

Fig. 12 Properties of a global 3D radiation-hydrodynamical model of an AGB star by Freytag et al. (2017): Top: a time series of snapshots showing the gas density for a slice through the center of the star (the grey circles indicate the average stellar radius). Middle: a time series of snapshots showing the radial component of the gas velocity for a slice through the center of the star, illustrating the size scales of convective flows. Bottom: radial gas velocity averaged over spherical shells, plotted as a function of depth and time. Radial pulsations, not obvious from looking at the sequence of radial velocity slices, are clearly visible as alternating expansions (blue) and contractions (red). The stellar interior (below about 400 $R_\odot$) shows a velocity pattern similar to standing waves. They trigger propagating shock waves in the atmosphere, which move upwards as time proceeds. Image courtesy of S. Liljegren

affected by circumstellar dust, vibration–rotation lines of CO are mostly used to study the dynamics in M- and S-type AGB stars. A recent detection of variability in the CO($J = 3 - 2$) rotational line in the first vibrationally excited state (Khouri et al. 2016b), however, is a promising step forward to probe atmospheric dynamics in C-rich objects.

Dynamic model atmospheres have been used to derive shock amplitudes (i.e., differences in pre- and post-shock gas velocities) from observations of line splitting (e.g., Willson et al. 1982; Scholz and Wood 2000; Nowotny et al. 2010). The velocity of the outwards-moving gas in the post-shock region, inferred from the Doppler shifts,

can be used to estimate a levitation distance (highest point of a ballistic trajectory for gravitationally bound gas layers), when assuming a complete conversion of kinetic into potential energy (see, e.g., the discussion in Bladh and Höfner 2012). The results indicate that, typically, the shock waves push parts of the upper atmospheric layers out to a few stellar radii, creating temporary reservoirs of cool dense gas where complex molecules and dust grains may form. This is in line with the interferometric observations and high-angular-resolution imaging results mentioned above.

4.2 Conditions for dust formation and properties of wind-driving grains

Dust grains forming in the extended atmospheres of AGB stars condense under non-equilibrium conditions, with temperature acting as a threshold, and prevailing densities and chemical abundances determining the efficiency of grain growth. At distances from the stellar photosphere where temperatures are low enough to allow for dust condensation, low gas densities lead to slow grain growth, on timescales which are comparable to those of stellar pulsation and ballistic atmospheric motions. Consequently, the grains do not adjust instantaneously to the local conditions, as in thermal and chemical equilibrium, but their properties are dependent on the evolution of the layers in which they are embedded, and a substantial fraction of the condensible material may remain in the gas phase in the atmosphere and inner wind region.

Furthermore, the temperatures of dust grains in the close vicinity of an AGB star are set by radiative processes (heating by absorption of stellar photons and cooling by thermal emission) rather than by collisions with gas particles (see, e.g., Gauger et al. 1990; Bladh et al. 2015). This leads to a strong dependence of the temperature on the composition and the corresponding optical properties of the dust particles, creating a bias against species subject to strong radiative heating, since low temperatures are a key factor for condensation.

With dust playing a critical role in the atmospheres and winds of AGB stars, models need to include appropriate descriptions of these chemical and radiative processes. A time-dependent gas-kinetic treatment of grain growth (often based on methods developed by Gail and Sedlmayr 1988, 1999, 2014; Gauger et al. 1990) has become a standard ingredient in quantitative dust-driven wind models (discussed in Sects. 4.3 and 5.1) and in studies of dust yields from AGB stars (e.g., Ferrarotti and Gail 2006; Zhukovska and Henning 2013; Nanni et al. 2013, 2014; Schneider et al. 2014). The dust grains are assumed to grow by the addition of abundant atoms and molecules from the gas phase to the surface of the solid particles. In contrast to other environments (e.g., proto-planetary discs), grain–grain collisions and coagulation can be neglected due to a combination of low densities and short dynamical timescales. The grain growth rate is determined by the slowest reaction which contributes to forming complete monomers (i.e., the basic building blocks of the solid). Usually, this bottleneck will be created by the reaction adding the least abundant chemical element. The dust decomposition rate, on the other hand, will be set by thermal evaporation or chemical sputtering. The evolution of grain size with time is determined by the competition between these processes.

Current dynamic atmosphere and wind models, based on such a description of grain growth and destruction, mostly give wind properties that are in good agreement with observations, as will be discussed in Sect. 5.1. However, some open questions remain concerning nucleation, i.e., the formation of the first solid seed particles from the gas phase. For the case of a C-rich atmospheric chemistry (C/O $>$ 1), where amorphous carbon (amC) grains most likely drive the observed outflows, many models have used classical nucleation theory to describe the formation of homogeneous amC grains directly out of the gas. For stars with less carbon than oxygen in their atmospheres (C/O $<$ 1) the nature of the first condensates is still much debated. Detailed chemical models are currently giving contradictory results about the onset of dust formation in these stars (e.g., Gail et al. 2016; Gobrecht et al. 2016, and references therein). Wind models for stars with C/O $<$ 1 therefore usually circumvent the problem of nucleation by assuming the existence of tiny seed nuclei (e.g., parameterized by an abundance relative to hydrogen), and they describe the subsequent growth of dust grains with gas-kinetic methods as outlined above.

In view of the overall complexity of the dynamics and radiative transfer, as well as a certain lack of reliable micro-physical and chemical data, the description of the dust component in present PEDDRO models tends to focus on species that are assumed to be directly or indirectly related to the wind mechanism. A dust species has to fulfill two basic criteria, in order to be considered a potential wind driver: (i) its condensation distance has to fall within the shock-levitated atmosphere (extending, typically, to a few stellar radii; cf. Sect. 4.1), and (ii) its flux-integrated opacity has to be comparable to, or exceed, the critical value of Eq. (2). In the context of the SCRA scenario, the focus is on the second criterion, which early-on lead to an identification of carbon dust as the most probable wind driver in C-rich AGB stars. Likewise, dust grains consisting of magnesium-iron-silicates (olivine- and pyroxene-type materials) have long been considered good candidates for driving the winds of AGB stars with C/O $<$ 1, based on the comparatively high abundances of the constituent chemical elements, and the prominence of corresponding mid-IR features in observed spectra (see Sects. 1.2 and 2.1).

The introduction of PEDDRO models which combine frequency-dependent radiative transfer with a detailed description of grain growth, however, leads to a re-evaluation of this latter scenario. The visual and near-IR optical properties of olivine- and pyroxene-type silicates (i.e., $Mg_{2x}Fe_{2(1-x)}SiO_4$ and $Mg_xFe_{(1-x)}SiO_3$, respectively, with $0 < x < 1$) depend critically on their Fe-content (i.e., the value of x). Materials at the Fe-free end of the range (Mg_2SiO_4 or $MgSiO_3$) are extremely transparent at visual and near-IR wavelengths, around the stellar flux maximum, in strong contrast to grains that contain even small amounts of Fe, which makes them opaque in this spectral range (see, e.g., Zeidler et al. 2011, for a detailed discussion of the effects of metal ions on optical properties of solids). The mid-IR optical properties of silicates, on the other hand, are much less dependent on the Fe-content. At a given distance from the star (i.e., when exposed to the same radiative flux), Fe-free silicates with their very low absorption coefficients in the near-IR region will be much cooler than Fe-bearing grains, which are subject to significant radiative heating. In other words, Fe-free silicates can form and survive closer to the star.

The magnitude of the effect can be estimated using Eq. (4), together with typical values of T_c and p for silicate grains. The near-IR absorption of olivine-type silicates with about equal amounts of Fe and Mg (i.e., $x \approx 0.5$, as favored by purely kinetical considerations due to similar abundances of Fe and Mg in a solar mixture) can be approximated by $p \approx +2$, whereas the corresponding Fe-free material (Mg_2SiO_4) leads to $p \approx -1$ (see Bladh and Höfner 2012, for power-law fits of dust opacities). Combining these values with a typical condensation temperature for silicates, $T_c \approx 1000$ K, results in condensation distances of $R_c \approx 9\,R_*$ and $R_c \approx 2\,R_*$, respectively. This simple estimate indicates that condensation of Fe-free silicates should easily be possible in the extended atmosphere of a pulsating AGB star, while it seems unlikely that significant amounts of Fe will be included in the dust grains within the shock-levitated layers where the outflow is triggered. Detailed models give similar results (Woitke 2006; Höfner 2008; Bladh et al. 2015), leading to the conclusion that photon absorption by Fe-rich silicates is probably not a viable mechanism for driving the outflows of typical M-type AGB stars.

An alternative mechanism which has been explored with detailed PEDDRO-type models (Höfner 2008; Bladh et al. 2015; Höfner et al. 2016) is radiation pressure due to scattering of stellar photons on Fe-free silicate grains. This requires grain sizes of about 0.1–1 μm, in order to make the dust particles efficient at scattering radiation in the near-IR wavelength region where the stellar flux peaks. Recent detections of dust grains with sizes of 0.1–0.5 μm in the close vicinity of several AGB stars (e.g., Norris et al. 2012; Ohnaka et al. 2016, 2017) lend strong support to this scenario. Furthermore, the dynamical models based on this mechanism are in good agreement with observations regarding mass-loss rates and wind velocities, as well as visual and near-IR colours, and their variation with pulsation phase (Bladh et al. 2013, 2015).

As the silicate grains start moving away from the star in the accelerating outflow, and are exposed to decreasing levels of stellar radiation, they probably become gradually enriched with small amounts of Fe and turn more opaque at near-IR wavelengths. Throughout the grain growth region, the Mg/Fe ratio is controlled by a self-regulating feedback between Fe-inclusion and resulting radiative heating (Woitke 2006). This keeps the silicate grains below the sublimation temperature, but considerably warmer than completely Fe-free grains, which is essential for the formation of their characteristic mid-IR emission features (e.g., Bladh et al. 2015, 2017). According to spectro-interferometric observations, the first traces of these features appear at around 2 stellar radii, where the grains have to be virtually Fe-free, and they become pronounced around 4–5 stellar radii, where the grains probably have accumulated a certain amount of Fe (e.g., Sacuto et al. 2013; Karovicova et al. 2013).

Spectro-interferometric observations also show that Al_2O_3 (corundum) may condense at distances of about 2 R_* or less, prior to silicate formation (e.g., Wittkowski et al. 2007; Zhao-Geisler et al. 2012; Karovicova et al. 2013). Al_2O_3 has been discussed as a possible alternative to silicates as a source of the scattered light observed close to several AGB stars (e.g., Ireland et al. 2005; Norris et al. 2012; Ohnaka et al. 2016), and as potentially forming seed particles for the condensation of silicates further out in the atmosphere where lower temperatures prevail (e.g., Kozasa and Sogawa 1997a, b). The radiation pressure resulting from such Al_2O_3 grains is too low to drive a wind for typical stellar parameters (e.g., Höfner et al. 2016), which is consistent with

the scenario of Al_2O_3 forming a dense, gravitationally bound dust shell at less than 2 R_* (see Ireland et al. 2005; Khouri et al. 2015, 2016a). However, (Höfner et al. 2016) found that the formation of composite grains with an Al_2O_3 core and a silicate mantle can speed up grain growth to sizes required for efficient photon scattering significantly, increasing both mass-loss rates and wind velocities compared to outflows driven by pure Fe-free silicate grains. Furthermore, variations of visual and near-IR colours during a pulsation cycle resulting from these models show even better agreement with observations (see Fig. 13).

4.3 Ingredients and general properties of PEDDRO models

Following the discovery of characteristic mid-IR dust features in CSEs of AGB stars, wind acceleration by radiative pressure on dust particles was first explored with simple, time-independent radial flow models (see Sects. 1.2, 2.2 and 2.3.2). This approach, however, cannot do justice to the complex time-dependent processes in the atmo-

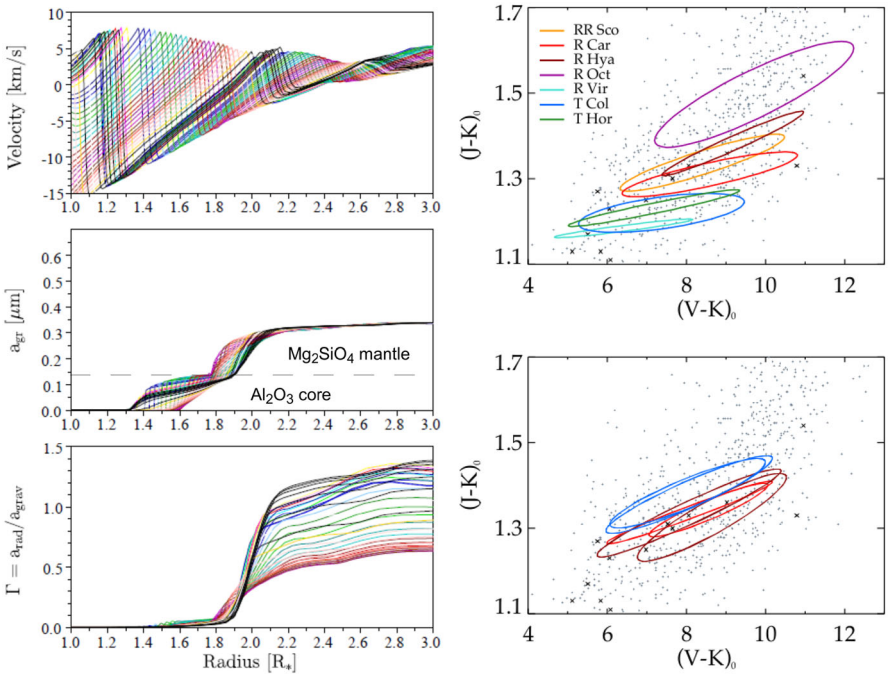

Fig. 13 Left: time-dependent radial structure of a DARWIN model for an M-type AGB star, featuring a wind driven by photon scattering on dust grains with an Al_2O_3 core and an Mg_2SiO_4 mantle (snapshots of 40 pulsation phases, zoomed in on the dust formation region). Top to bottom: gas velocity, radius of dust grains, and ratio of radiative to gravitational acceleration (the large variation of the latter quantity over a pulsation cycle in the region where grain sizes are almost constant is mostly due to changing luminosity). Right: observed and synthetic photometric variations of M-type AGB stars. Upper panel: a sample of well-observed stars with regular light curves. Lower panel: DARWIN models with core-mantle grains, as shown in the left part of this figure. Image reproduced with permission from Höfner et al. (2016), copyright by ESO

spheres of pulsating cool giant stars, as discussed in Sect. 4.1. Over the years, more advanced types of dynamical atmosphere and wind models have been developed, delivering predictions of mass-loss rates, synthetic spectra and other observables.

The beginnings of quantitative PEDDRO models can be traced back to numerical simulations studying the impact of pulsation-induced shock waves on atmospheric structure and wind generation (cf. Willson and Hill 1979; Hill and Willson 1979; Wood 1979). The efficiency of radiative cooling in the shocks affects atmospheric levitation, and consequently the resulting mass-loss rates. More efficient cooling leads to less levitation and lower mass-loss rates, since more thermal energy resulting from compression in the shock front is radiated away. In the extreme case of adiabatic shocks (i.e., no radiative cooling), on the other hand, levitation is so efficient that the models show mass-loss rates exceeding observations by orders of magnitude (cf. Wood 1979).

Early models of the PEDDRO scenario were based on a simple parameterized description of the dust component, assuming that dust condensation can be described as a function of temperature only (cf. Bowen 1988). While this method captures the role of temperature as a threshold for dust formation, it ignores that grain growth rates depend on the ambient gas densities. Models of the next generation (e.g., Fleischer et al. 1992; Höfner and Dorfi 1997; Winters et al. 2000; Jeong et al. 2003) introduced a detailed, time-dependent treatment of dust formation, as outlined in Sect. 4.2 (Gail and Sedlmayr 1988, 1999; Gauger et al. 1990), taking into account that grain growth proceeds far from equilibrium under the conditions prevailing in atmospheres and winds of AGB stars. The comparatively low densities in the dust formation region lead to timescales of grain growth that are comparable to the dynamical timescales of shock-induced ballistic motions, turning the PEDDRO scenario into a race against time: an outflow will form only if condensation is fast and efficient enough that radiation pressure can prevent the shock-levitated layers from falling back towards the star. Furthermore, if an outflow is triggered, rapidly decreasing densities in the wind will quickly quench additional grain growth, usually leading to condensation degrees of key elements (e.g., C or Si) distinctly below unity, in good agreement with recent observational studies (e.g., Khouri et al. 2014b; Lombaert et al. 2016). This implies that the presence of condensible elements in the gas phase and the existence of a corresponding dust species in the same region are not mutually exclusive.

In summary, the second-generation PEDDRO models played a critical role in demonstrating the intricate interplay of shock waves, dust formation, and wind acceleration, as well as reproducing basic observed properties of heavily dust-enshrouded C-rich AGB stars ($\dot{M}$, υ_∞, SED). Due to their simplistic (grey) treatment of radiative transfer, however, they failed to capture essential features of both C-rich AGB stars with less opaque dust-driven winds (lower mass-loss rates), and of AGB stars with C/O $<$ 1, which tend to have more transparent CSEs. Since both temperature and density are critical parameters for the onset and efficiency of grain growth, a correct treatment of energy transport in the atmosphere and wind is an essential ingredient of realistic models.

The current, third, generation of PEDDRO models, therefore features frequency-dependent radiative transfer, solved simultaneously with time-dependent gas dynamics and dust formation, taking into account both molecular and dust opacities (e.g., Höfner et al. 2003; Höfner 2008; Mattsson et al. 2010; Eriksson et al. 2014; Bladh et al. 2015;

Höfner et al. 2016). These models produce mass-loss rates, wind velocities, and spectra which are in good agreement with observations for a wide range of stellar parameters (i.e., very different conditions in the CSEs), as will be discussed in some detail in Sect. 5.1.

A remaining issue of the present PEDDRO models is how the effects of pulsation and convection are introduced. At this point, it should be noted that the stellar atmosphere and wind, where radiative processes play a crucial role for the thermal structure and dynamics, correspond to a physical regime that is very different from the stellar interior, where convection is the main energy transport mechanism. This has practical consequences for numerical simulations, and models tend to focus on one or the other region, i.e., on pulsation and convection, as described in Sect. 4.1, or the wind mechanism. In current wind models, the inner boundary of the computational domain is typically located below the stellar photosphere but above the driving zone of the pulsations, and the effects of interior dynamics on the atmosphere and wind are usually simulated by prescribing temporal variations of luminosity and gas velocity at the inner boundary. The most widely used form of this so-called piston boundary (cf. Bowen 1988) is based on a sinusoidal variation of the gas velocity, with period and amplitude as parameters, simulating the radial expansion and contraction of the stellar interior. Over the years, different recipes have been tried to bring the accompanying light curves into agreement with observations, with varying success (see, e.g., Nowotny et al. 2010; Eriksson et al. 2014; Liljegren et al. 2016).

An alternative approach to study the effects of pulsation on atmospheric dynamics and spectra of Mira stars was chosen by Bessell et al. (1996) who extracted boundary conditions from self-excited radial pulsation models. Later, CODEX models were based on a similar strategy (e.g., Ireland et al. 2008, 2011); however, none of these models produced dust-driven outflows. Freytag and Höfner (2008) tested non-sinusoidal variations of sub-photospheric velocities, derived from global 3D radiation-hydrodynamical simulations, and concluded that the critical parameter for triggering a dust-driven wind is the amplitude of the variation, not the shape of the chosen function, since this information gets lost in the transformation of pulsation-induced sound waves into shocks (see Fig. 14). In contrast, the shape of the luminosity variation, or a phase shift between the luminosity and velocity variations (which affects the timing of shock propagation through the atmosphere relative to variations in the atmospheric temperatures, set by the luminosity), may have an effect on the efficiency of dust formation and radiative acceleration, and thereby on the wind properties. Liljegren et al. (2016) estimated that the uncertainties in the mass-loss rate due to this effect may be up to $\pm 40\,\%$ for a model with typical stellar parameters. This is roughly comparable to the estimated observational uncertainties in mass-loss rates based on rotational CO lines in the radio regime (e.g., Ramstedt et al. 2008; Danilovich et al. 2015).

5 Towards a comprehensive view on AGB mass loss

A central goal of stellar wind research is to derive a quantitative description of how the mass-loss rate depends on fundamental stellar parameters, i.e., a so-called mass-

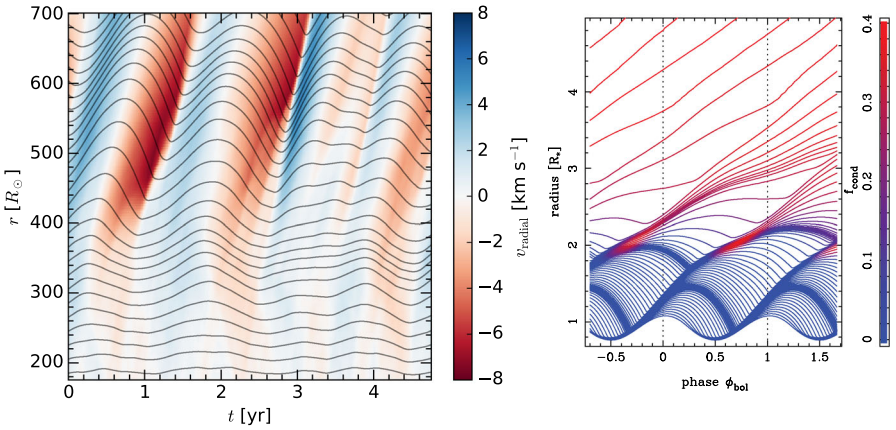

Fig. 14 Dynamics of the shock-levitated atmosphere and wind acceleration region, illustrated by tracking the radial motions of mass layers in detailed radiation-hydrodynamical models. Left panel: radial gas velocity in a 3D model by Freytag et al (2017, see also Fig. 12), averaged over spherical shells and plotted as a function of depth and time (blue = expansion, red = contraction); radial range (y-axis, in solar radii): about 0.5 to 1.8 stellar radii (black lines trace average gas motions); right panel: a spherically symmetric PEDDRO-type model for a typical C-rich mira variable, showing the region where periodic dust formation events in the wake of shocks (red zones at about 2 stellar radii) trigger an outflow (model M in Nowotny et al. 2010, fraction of carbon condensed into dust indicated in colour, with the highest values shown in red; see colour scale on the right); blue lines represent the dust-free atmosphere, roughly corresponding to the region shown in the left panel. Images reproduced with permission from Freytag et al. (2017) and Nowotny et al. (2010), copyright by ESO

loss formula. This is a key ingredient for models of stellar evolution and population synthesis. It is therefore not surprising that a lot of effort has been spent on establishing a mass-loss formula for AGB stars, both with empirical and theoretical approaches. The results of stellar evolution models which are based on such mass loss prescriptions, however, indicate that there is ample room for improvements (see, e.g., Lattanzio and Karakas 2016).

Empirical methods to derive a mass-loss formula suffer from difficulties in determining the fundamental parameters of AGB stars, and disentangling their effects on mass loss. Different stellar properties of individual stars are linked to each other and evolve together as stars ascend the AGB, which makes it difficult to isolate the dependence of the mass-loss rate on a single property. For instance, luminosity depends on both initial mass and age on the AGB, and it increases with time, while effective temperature and current mass decrease. To this should be added that studies of metallicity dependence are often based on stars in different environments (Galactic Bulge and Halo, MCs, other galaxies, see Sect. 3.2) which may differ from each other in more respects than just chemical composition. Furthermore, as will be discussed below, there may be systematic selection effects in observed samples that make them an insufficient basis for deriving a mass-loss formula.

In contrast to the empirical case, the dependence of theoretical mass-loss rates on individual stellar parameters is well known, since these are also the basic input param-

eters of PEDDRO-type wind models. The theoretical mass-loss rates can, therefore, in principle, be applied quite easily in stellar evolution models and in the construction of synthetic stellar populations. As discussed in Sect. 4, however, the predictive power of current PEDDRO models is restricted by uncertainties on the micro-physical level (e.g., regarding seed particles of dust grains, or missing chemical and optical data), and the treatment of sub-photospheric dynamics (convection, pulsation), introducing extra parameters which need to be constrained. Before discussing the dependence of mass-loss rates on stellar parameters from both an observational and a theoretical point of view, we will therefore compare various properties of current PEDDRO models to a range of observations.

5.1 State-of-the-art PEDDRO models and observations

As discussed in Sects. 4.2 and 4.3, dynamical models for the PEDDRO scenario need to combine a detailed time-dependent description of dust formation with a frequency-dependent treatment of radiative transfer, in order to capture essential physical properties of the wind-formation region. Mattsson et al. (2010) and Eriksson et al. (2014) presented the to-date most substantial grid of such models for C-rich AGB stars (based on the DARWIN code; Höfner et al. 2003, 2016). These models give two types of results, (i) mass-loss rates and other wind properties, and (ii) time series of snapshots of dynamical structures. The latter can be used to compute detailed spectra and other observable properties (as in the case of classical hydrostatic model atmospheres or SCRA-type models), allowing for a detailed comparison with observations. Eriksson et al. (2014) produced synthetic low-resolution spectra and photometry for a sub-sample of the Mattsson et al. (2010) grid with stellar parameters representative of solar-metallicity C-rich AGB stars. Furthermore, the study of photometric variability was extended by adding new dynamical models to the grid, with a higher luminosity amplitude but otherwise similar parameters, following up on the exploratory results of Nowotny et al. (2011, 2013).

A straight-forward way to test grids of PEDDRO models against observations is a comparison of the resulting combinations of mass-loss rates and wind velocities with the corresponding observed values, derived simultaneously from molecular lines in the radio regime (see Sect. 3.1). As can be seen in Fig. 15 (lower panel), models with different carbon excess (denoted as C-O and colour-coded) fall into distinct regions of the $\dot{M}$–υ_∞ diagram, and the average wind velocity increases with increasing C-O, due to a more efficient formation of wind-driving carbon dust. The group of models with the lowest C-O results in wind properties that have no counterparts in the observed stellar samples (low velocity and substantial mass-loss rates), while the other two groups of models fall within the region covered by observed wind characteristics (Fig. 15, upper panel). The absence of models with $\dot{M} > 10^{-5}\,M_\odot\,\mathrm{year}^{-1}$ can probably be attributed to the chosen range of stellar parameters (which may not cover the most evolved stars). The scarcity of outflows with low mass-loss rates relative to the observed stars may have several reasons, as will be discussed below. Figure 16 demonstrates that the models show good agreement with observations in the $\dot{M}$ vs. (J–K) diagram and the K-magnitude vs. mean (J–K) diagram. In both cases, the lack of models at

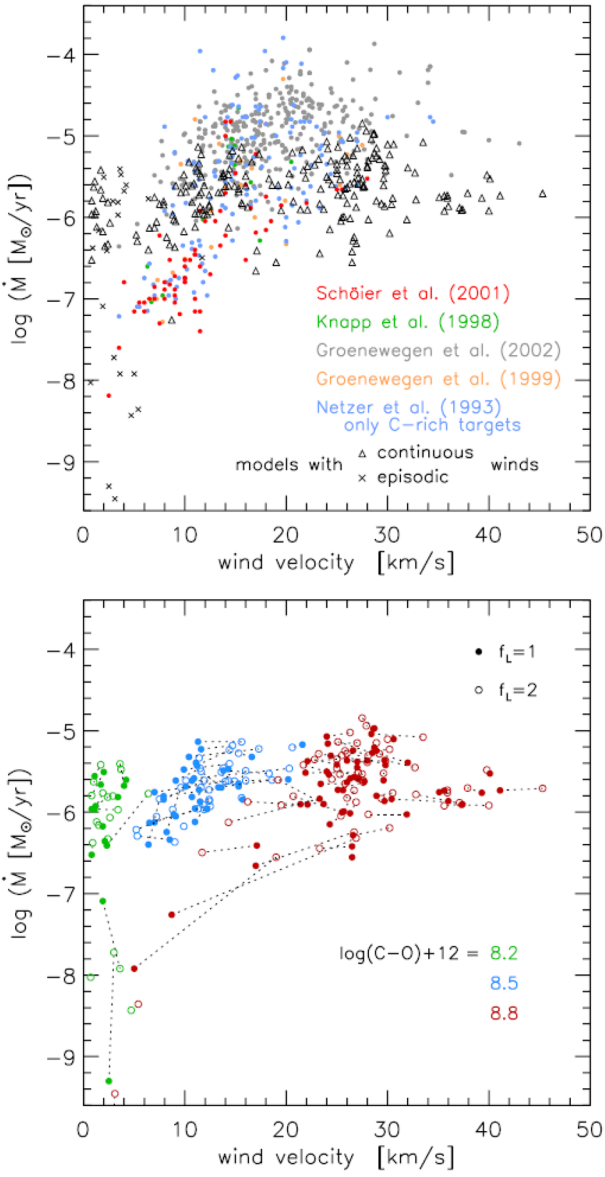

Fig. 15 Mass loss rates vs. wind velocities of PEDDRO-type wind models for C-rich AGB stars (Mattsson et al. 2010; Eriksson et al. 2014) and corresponding observational data. In the upper panel the black triangles mark models with steady winds while the black crosses denote models with episodic winds. The other symbols with different colours show values based on observations of various C-rich giants, adopted from different sources as given by the legend. The lower panel shows the model results colour-coded by carbon excess (increasing from green to blue to red, see legend). Image reproduced with permission from Eriksson et al. (2014), copyright by ESO

the reddest observed (J–K) values is probably due to the absence of models with $\dot{M} > 10^{-5}\,M_{\odot}\,\mathrm{year}^{-1}$ in the present grid.

The development of wind models for M-type AGB stars (C/O $<$ 1) based on the PEDDRO scenario proceeded much slower than for their C-rich counterparts, mostly due to uncertainties regarding the nature of the wind-driving dust grains (see Sects. 4.2 and 4.3). Recently, however, Bladh et al. (2015) presented a grid of frequency-dependent models with a detailed description of dust formation, spanning a range of typical luminosities and effective temperatures. In these models, the outflows are driven by scattering of stellar photons on Fe-free silicate grains with radii in the range of 0.1–1 μm, building on the results of Höfner (2008).

In Figs. 17 and 18, the grid of DARWIN models by Bladh et al. (2015) is compared to observations regarding resulting photometric colours, i.e., (J–K) vs. (V–K), and wind properties ($\dot{M}$ vs. υ_{∞}), respectively. The colours resulting from the models fall nicely within the observed ranges of typical M-type Mira stars, and (J–K) shows a clear correlation with stellar effective temperature, in accordance with expectations (Fig. 17). In comparison to C-rich AGB stars, the range of (J–K) values is much more narrow, due to the higher transparency of the silicate dust (less circumstellar reddening). Concerning mass-loss rate vs. wind velocity, the models with the two highest values of the seed particle abundance (shown in blue and yellow in the bottom panel of Fig. 18) give results that fit best with the observational data. As in the C-rich case discussed above, the absence of models with $\dot{M} > 10^{-5}\,M_{\odot}\,\mathrm{year}^{-1}$ is probably due to the selected range of fundamental stellar parameters.

We also note, again, a lack of models corresponding to the lowest empirical mass-loss rates. For the C-rich grid, Eriksson et al. (2014) mentioned the use of small-particle-limit dust opacities as one of the possible causes. However, this cannot explain the results of the M-type models by Bladh et al. (2015), since they take the effects of grain size on opacities into account. An alternative explanation could be of a morphological nature: In the current PEDDRO models, the outflows consist of complete, spherical layers of gas and dust. Recent observations of some nearby stars show clumpy dust and gas clouds with variable morphology in the extended stellar atmospheres (e.g., Ohnaka et al. 2017; Khouri et al. 2016a), probably due to the effects of convection or non-radial pulsations (see Sect. 4.1). This situation may lead to less material being accelerated away from the star, i.e., a wind being built up of a sequence of partial (instead of complete spherical) atmospheric layers, ejected in different directions over time (see Sect. 6.2.1). The spherical PEDDRO models have been primarily developed to describe the mass loss of Mira variables, i.e., large-amplitude radial pulsators, while the objects with the lowest mass-loss rates tend to be semi-regular variables, where non-spherical effects are probably more pronounced. In this context, it should also be kept in mind that the empirical mass-loss rates are derived based on the assumption of a smooth, spherically symmetric distribution of circumstellar matter. If the outflows are clumpy, the empirically derived values may (seriously) underestimate the true mass-loss rates (see Sect. 6.1.4).

A point that should also be taken into consideration in the discussion of Figs. 15, 16, 17 and 18 is that they give equal weight to all models, whereas different combinations of fundamental parameters will not occur with the same likelihood in observed samples, due to the influence of the initial-mass function, differences in lifetimes, and various

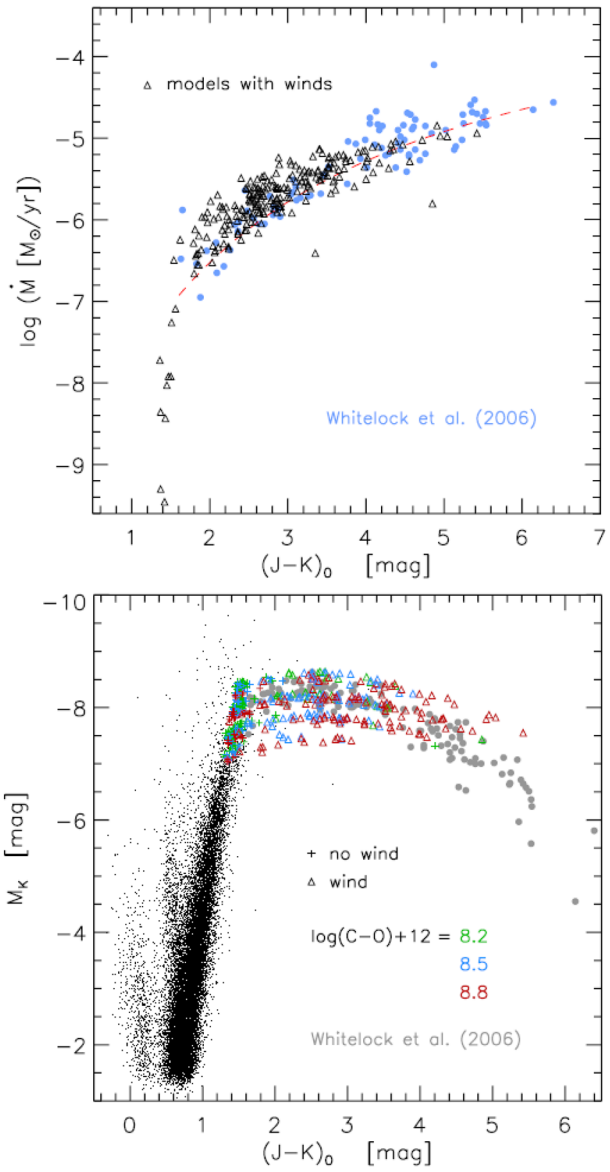

Fig. 16 Properties of PEDDRO-type wind models for C-rich AGB stars (Mattsson et al. 2010; Eriksson et al. 2014) and corresponding observational data. Upper panel: mass loss rate vs. mean (J–K) colour. The dashed line is a fit from Gullieuszik et al. (2012) for LMC carbon stars, the values derived by Whitelock et al. (2006) are plotted as blue dots. Lower panel: colour-magnitude diagram showing K-magnitudes vs. mean (J–K). The models are colour-coded according to carbon excess, the grey dots represent observations by Whitelock et al. (2006). Image reproduced with permission from Eriksson et al. (2014), copyright by ESO

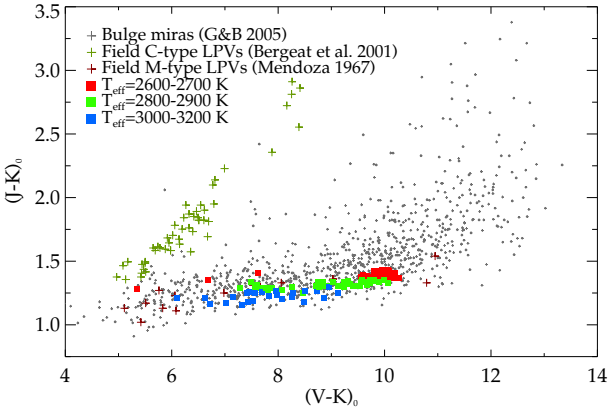

Fig. 17 Photometric properties of PEDDRO-type wind models for M-type AGB stars by Bladh et al (2015, filled squares), compared to observations compiled from various sources (plus signs). The models are colour-coded by effective temperature (see legend). Observational data: Galactic Bulge miras (Groenewegen and Blommaert 2005, grey), field M-type LPVs (Mendoza 1967, red) and C-rich giants (Bergeat et al. 2001, green; demonstrating the marked differences between M- and C-type stars). Most of the observational data are single-epoch measurements, whereas the synthetic colours are means over the pulsation cycle. Image reproduced with permission from Bladh et al. (2015), copyright by ESO

observational selection effects. Therefore, a comparison of the distributions of model results and observed data points should be made with caution. The models should be able to cover the observed values of wind properties, photometric colours, etc., but not all regions of a diagram populated by models will necessarily have counterparts in specific observed samples, even for reasonable combinations of stellar parameters.

Finally, as mentioned in Sect. 3.1, SCRA-type models by Elitzur and Ivezić (2001) predict an (exact) relation of $\dot{M} \propto \upsilon_\infty^3$ for fixed dust properties (composition, abundance and size of grains) in the case of optically thin CSEs. In their models, this relation is due to a correlation of wind acceleration efficiency with mass-loss rate (which is an input parameter of these models), caused by grain drift. Empirical data sets, based on CO lines in the radio regime, show slopes that are roughly consistent with this relation, and the correlation between $\dot{M}$ and υ_∞ seems to be tighter for M-type than for C-type AGB stars (cf. Fig. 7). It is worth noting that both C-rich PEDDRO models, for a fixed carbon excess (see Fig. 15, lower panel), and M-type PEDRRO models, for a fixed seed particle abundance (see Fig. 18, bottom panel), can reproduce the observed trends, without including grain drift.[6] A probable explanation is that the time-dependent grain growth process in the PEDDRO models, leading to diverse grain sizes (and grain abundances, in the case of C-rich models), produces a similar self-regulating effect on wind acceleration as grain drift does in SCRA-type models with fixed dust properties (which ignore the time-dependent grain growth pro-

[6] The drift of dust grains relative to the gas by which they are surrounded probably has only modest effects on PEDDRO-type models, since efficient dust formation and radiative acceleration are concentrated to the regions of high gas densities behind the propagating shock waves where drift velocities are low (see, e.g., Sandin and Höfner 2003, 2004). As grain drift introduces a number of extra computational difficulties, it is usually neglected.

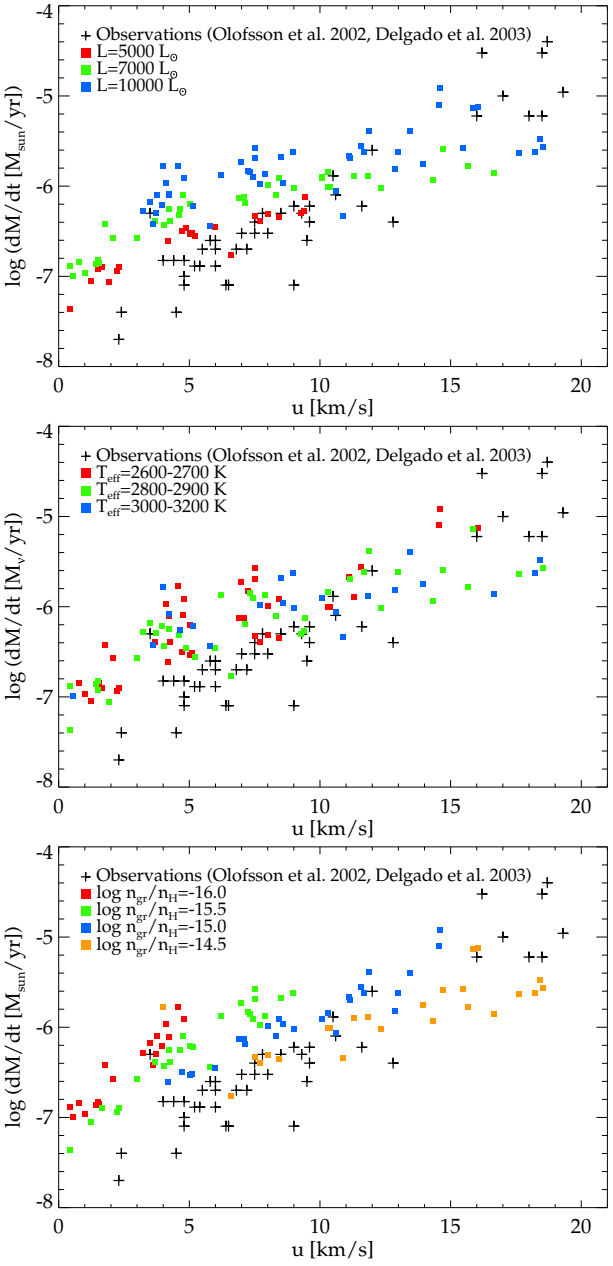

Fig. 18 Mass loss rates vs. wind velocities of PEDDRO-type wind models for M-type AGB stars by Bladh et al (2015, filled squares), compared to observations (plus signs). The three panels show the models with different colour-coding (see legend), according to stellar luminosity (top), effective temperature (middle) and seed particle abundance (bottom). The current stellar mass is 1 $M_{\odot}$ for all models. The plus signs represent observational data taken from Olofsson et al. (2002) and González Delgado et al. (2003b). Image reproduced with permission from Bladh et al. (2015), copyright by ESO

cess). This contradicts the conclusion of Elitzur and Ivezić (2001) that the observed correlation between mass-loss rate and wind velocity is proof of the importance of drift. In reality, probably, both mechanisms, i.e., a self-regulating feedback between grain growth and wind acceleration, as well as drift between gas and dust, will affect the efficiency of wind acceleration and, thereby, the relation between $\dot{M}$ and υ_∞.

5.2 Dependence of mass-loss rates on stellar properties

5.2.1 Trends derived from observations

Over the years, much effort has been spent on deriving the dependence of the mass-loss rate on stellar properties like mass, luminosity, effective temperature, radius, metallicity, etc., using observational studies. First attempts to determine empirical mass-loss laws for evolved stars date back several decades. Based on the observations of cool giant stars, Reimers (1975) introduced a relation describing the dependence of mass-loss rate on stellar characteristics as $\dot{M} \propto L_* R_* / M_*$. The constant of proportionality has been adjusted in later studies, attempting to obtain better fits to various results. Both, evolutionary models using this type of mass-loss formula and extensive observations of AGB stars, however, have shown that such a simple relation gives a far from adequate description of AGB mass loss.

Effective temperature The temperature in the stellar atmosphere is expected to affect dust condensation and, consequently, mass loss (see, e.g., Wachter et al. 2002), in particular near the threshold for dust-driven winds. The stellar effective temperature is a property that can be reasonably well determined for optically visible stars (Niedzielski et al. 2016), but often, in particular for the higher-mass-loss-rate objects, it is obtained as a by-product of SED fits, putting question marks on its reliability. The possibility to observationally find a dependence of mass-loss rate on effective temperature is also severely hampered by the limited range in magnitude of the latter combined with the spread in the mass-loss-rate estimates.

Only a few studies of the temperature dependence have been performed but the results are at least indicative. For low- and intermediate-mass-loss-rate stars (as determined from CO lines), there is no apparent mass-loss rate dependence on effective temperature (Schöier and Olofsson 2001; Olofsson et al. 2002), but a weak increase in mass-loss rate with decreasing temperature is seen for carbon stars when the higher-mass-loss-rate objects are included (Schöier and Olofsson 2001). Likewise, van Loon et al. (2005) found no clear dependence in a sample of LMC AGB stars when plotting $\dot{M}$ versus $T_{\rm eff}$, but a fit to the data performed in the (L_*,$T_{\rm eff}$)-plane suggests that such a dependence exists. Bergeat and Chevallier (2005) found that mass-loss rates increase with decreasing effective temperatures only at the lower temperatures, $\lesssim 2400$ K.

Luminosity The main problem in isolating a luminosity dependence of the mass-loss rate by observational means is caused by the influence of other parameters that also change together with the luminosity during AGB evolution, such as mass, effective temperature and pulsation properties. Furthermore, even though the mass-loss rate often shows a positive trend with L, the scatter in the data is (very) large.

A recent study of mass-loss rates by Danilovich et al. (2015), based on multi-line observations of CO towards solar neighbourhood stars, shows a strong scaling with luminosity, $\dot{M} \propto L_*^5$, i.e., substantially steeper than in Reimers' formula. This means that the range of typical mass-loss rates for nearby AGB stars (about 3 orders of magnitude, see Sect. 3.1) can be attributed to a range in luminosity corresponding to about a factor of 4, which is not unreasonable. It should be kept in mind that the luminosities of individual nearby stars may be more uncertain than (at least the relative) luminosities of stars in more distant samples.

Dust-emission-based studies of mainly extragalactic objects indicate a much weaker dependence of mass-loss rate on luminosity, but a unique scaling law is often difficult to identify due to the large scatter in the data (e.g., van Loon et al. 2005; Guandalini et al. 2006). Nevertheless, some results have been reported: $\dot{M} \propto L_*^{1.6}$ for a Galactic sample (Goldman et al. 2017), $\propto L_*^{0.9}$ for a Galactic Bulge, high-mass-loss-rate sample (Jiménez-Esteban and Engels 2015), and $\propto L_*^{1-1.6}$ for MCs samples of various types (Srinivasan et al. 2009; Groenewegen et al. 2009; Goldman et al. 2017). The best example of the complexity of this problem is provided by the work of Riebel et al. (2012). They use GRAMS models to determine $\dot{M}_\mathrm{d}$ and L_* for $\approx$30000 LMC objects, and plotted against each other a positive trend is there, but the scatter is so large that it is not meaningful to estimate a luminosity dependence. Interestingly, the results so far indicate that the mass-loss rates do not exceed an apparent (single scattering) upper limit of $\dot{M} = L_*/c\,\upsilon_\infty$, suggested by Eq. (8) for $\tau_\mathrm{F} = 1$ and $\Gamma \gg 1$, by more than a factor of a few (e.g., Jiménez-Esteban and Engels 2015). It should be noted though, that in many of the dust-related studies the estimates of luminosity and mass-loss rate are not entirely independent.

Metallicity A strong dependence of gas- and dust-mass-loss rates on metallicity is not necessarily expected for reasons discussed in Sect. 3.2. At least, from the similarity of the M_WD-distributions in open clusters of different metallicity, one may conclude that the total amount of mass lost does not depend (strongly) on the metallicity (Cummings et al. 2016). Detecting a weak metallicity effect may be a challenge for observational studies, due to the contamination with dependences on other stellar properties, combined with the scatter in the mass-loss-rate estimates.

In line with expectations, a comparison between samples from the Galaxy and the MCs shows that dust-mass-loss rates decrease with metallicity for O-rich stars, but carbon stars with similar pulsation properties produce similar quantities of dust regardless of their initial metallicity (Sloan et al. 2008; Groenewegen et al. 2009; Lagadec et al. 2012; Sloan et al. 2016). In contrast, however, van Loon et al. (2008) found that both O- and C-rich objects in the SMC have a lower dust content than similar objects in the LMC. Nevertheless, (highly) obscured, O-rich AGB stars exist in both the LMC and the SMC.

Extending these studies to additional galaxies, Sloan et al. (2012) found that eventually the dust production decreases also in C-rich objects at sufficiently low metallicities ($\approx 0.1\,Z_\odot$), but it is still operating at $\approx 0.01\,Z_\odot$ (Boyer et al. 2015a, b). In addition, the strength of the SiC feature, normalized to the continuum, also decreases with metallicity for these objects. The weakening of the dust-mass-loss rate with metallicity for the O-rich objects is supported by studies of lower-metallicity-galaxy objects

(Boyer et al. 2009), but the scarcity of O-rich evolved stars in such samples makes it difficult to draw firm conclusions. Some further information is obtained from studies of Galactic globular clusters, where a metallicity effect in the expected direction is found, although it is not very strong (Sloan et al. 2010).

Initial and current mass The fact that observed samples contain stars of different (initial and current) masses, and in different evolutionary stages, means that any dependences of mass loss rate on stellar mass and age are difficult to disentangle (Sect. 3.1.2). Furthermore, the current mass of an AGB star (which defines the gravitational potential, and therefore should have a strong effect on mass loss) is probably the fundamental parameter which is the most difficult to determine. In principle, it should be possible to derive the current mass from pulsation properties, if other stellar parameters can be pinned down. Considering the probably highly non-linear, non-adiabatic nature of AGB star pulsations and the simplifications used in present pulsation models (see Sect. 4.1), however, the results will be affected by considerable uncertainties. Nevertheless, Wood (2007) performed a study of this type, and found no obvious correlation between mass-loss rate and current mass.

Pulsation properties Finally, the mode, regularity, and amplitude of pulsation (regarding both radial motion and luminosity) may play important roles for the mass-loss process. In Fig. 19, showing mass-loss rates against periods, we summarize the results of a number of studies for different samples of M-, S-, and C-type AGB stars. There are some important points to note. A clear positive trend of mass-loss rate with period is visible in the range $\approx$ 300$^{\rm d}$ – 800$^{\rm d}$. The SRVs with periods of less than $\approx$ 200$^{\rm d}$ cover essentially the same mass-loss-rate range as the SRVs and Miras in the period range 300$^{\rm d}$ to 400$^{\rm d}$, suggesting that the mode of variability and the period play a little role in these period ranges. It appears that stars with periods longer than $\approx$ 800$^{\rm d}$ have

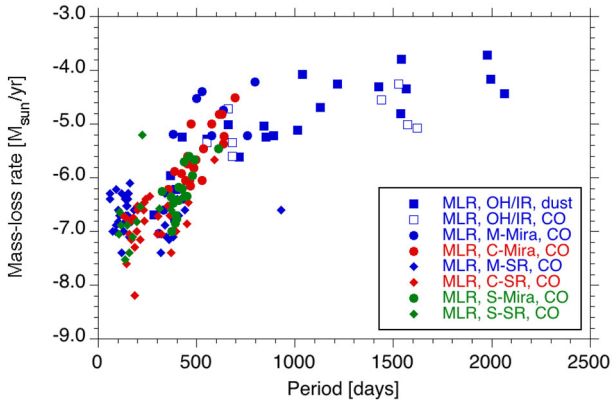

Fig. 19 Mass-loss rates estimated from CO line modelling (except some of the OH/IR stars data points where mass-loss rates are estimated from SED fits and assuming a gas-to-dust-mass ratio of 1000) versus period of pulsation for samples of AGB stars. O-, S-, and C-CSEs are blue, green and red, respectively. SRVs, Miras, and OH/IR-stars are diamonds, circles, and squares (open for the OH/IR stars with dust estimates), respectively. Data are taken from He and Chen (2001), Schöier and Olofsson (2001), Olofsson et al. (2002), González Delgado et al. (2003b), Ramstedt et al. (2009), De Beck et al. (2010)

reached their maximum mass-loss rate (except for possible brief periods of enhanced mass loss). This "saturation" effect is in line with the finding that the correlation of mass-loss rate with period is poor for samples of more extreme objects (Goldman et al. 2017). Other examples of $\dot{M}$–P relations are provided by Whitelock et al. (2006) and Sloan et al. (2016). In the former, the K–[12] colour increases monotonously with period in the range 250^{d} to 1000^{d} for a sample of Galactic carbon stars, and the latter obtained the same result for the [6.4]–[9.3] colour for Galactic and MCs samples of carbon stars.

Vassiliadis and Wood (1993) combined an empirical relation between mass-loss rate and period for Mira variables with a theoretical period–mass–radius relation to obtain a semi-empirical mass-loss-rate formula. The resulting dependence of mass-loss rate on luminosity is steep, roughly comparable to the results of Danilovich et al. (2015) discussed above. Interestingly, the recipe derived by Vassiliadis and Wood (1993) seems to give better results when applied to stellar evolution models than the Reimers formula with its moderate dependence on luminosity.

Summary of observed trends The primary conclusion is that an empirically derived dependence of the mass-loss rate on a specific stellar property is contaminated by dependences on other correlated stellar properties and by observational biases. Hence, any conclusions must be regarded with caution. The dependence on T_{eff} is expected to be strong, but the observational evidence for this is meager. Yet, the highest-mass-loss-rate objects are definitely of the cooler type. There is a positive luminosity dependence, but an exact scaling law is difficult to identify. In addition, the observational studies are expected to provide little information on the $\dot{M} - L_*$ relation of individual stars, unless the sample is narrow in stellar mass. There is good evidence that the dust-mass-loss rate and the terminal wind velocity both decrease with metallicity. In the case of the former more strongly for the O-rich objects, but eventually, for sufficiently low metallicity, also for the C-rich objects. On the other hand, objects with mass-loss rates of the order $10^{-5}\,M_{\odot}\,\mathrm{year}^{-1}$ (presumably C-rich) are found down to $0.1\,Z_{\odot}$, and dust production proceeds down to at least $0.01\,Z_{\odot}$, indicating a far from drastic dependence on metallicity. Finally, the mass-loss rates of typical Miras and SRVs increase with pulsational period, largely due to the combined effects of decreasing mass and increasing luminosity, with a saturation effect at periods longer than $\approx 800^{\mathrm{d}}$.

5.2.2 Theoretical mass-loss rates based on the PEDDRO scenario

Early examples of theoretical mass-loss formulas corresponding to the PEDDRO scenario are those by Blöcker (1995), inspired by the wind models of Bowen (1988), and by Arndt et al. (1997), derived from the models for C-rich TP-AGB stars by Fleischer et al. (1992) which featured a detailed description of dust formation (see Sect. 4.2) but still used gray radiative transfer. While these two power-law-style descriptions of mass loss gave some insights about the effects of superwinds on late stellar evolution (e.g., Schröder et al. 1998, 1999), both of them were based on a rather small number of individual wind models with a limited set of stellar parameter combinations. Regarding the latter point, the situation for C-rich stars improved through follow-up work by

Wachter et al. (2002, 2008), using a more appropriate selection of dust-driven wind models, and also exploring effects of metallicity.[7]

Several years later, Mattsson et al. (2010) presented a substantial grid of PEDDRO models for solar-metallicity C-rich stars, combining a detailed dust formation description and frequency-dependent radiative transfer. Comparing the mass-loss rates of the model grid to the formula of Wachter et al. (2002), Eriksson et al (2014, see their Fig. 7) found systematically lower mass-loss rates for given stellar parameters. This difference could be traced back to the different treatments of radiative transfer and opacities (frequency-dependent vs. grey), since the descriptions of dust formation in both types of models are comparable. Considering the rather good agreement of the model grid by Mattsson et al. (2010) and Eriksson et al. (2014) with observations (see Sect. 5.1), the values of mass-loss rates given by the Wachter et al. (2002) formula probably need to be revised downwards.

Regarding trends with stellar parameters, the mass-loss formula by Wachter et al. (2002) gives a strong dependence on luminosity i.e., $\dot{M} \propto L_*^{2.47}$ for fixed effective temperature and mass, and using the empirical $P - L_*$ relation by Groenewegen and Whitelock (1996). A simple visual inspection of the C-rich models by Eriksson et al. (2014, taking into account models which produce non-episodic winds) shows a comparable, but possibly somewhat less steep trend. However, we note again that the actual values of the mass-loss rates tend to be considerably lower than those resulting from the Wachter et al. formula for given stellar parameters. Furthermore, both the Wachter et al. (2002) formula and the Eriksson et al. (2014) grid predict a steep increase of mass-loss rate with decreasing effective temperature (i.e., an exponent of -6.81 in the formula, and, again, a possibly somewhat smaller, but still pronounced slope for the latter model grid).

In contrast, the M-model grid by Bladh et al. (2015) shows no clear correlation of mass-loss rate with stellar effective temperature (see Fig. 18, middle panel). One possible explanation for this difference between the C-type and M-type models is the dramatically different level of absorption by circumstellar dust, which may produce a significant back-warming effect in the C-rich models, affecting dust formation. The near-transparent envelopes of the M-type models have a much smaller thermal effect on the stellar atmosphere. Regarding the dependence of mass-loss rate on luminosity, on the other hand, the M-type models show a pronounced trend (see Fig. 18, top panel), comparable to both the C-rich models in Eriksson et al. (2014) and the Wachter et al. (2002) formula for C-stars. However, also in this case, the actual values of the mass-loss rates are significantly lower (about an order of magnitude, on average) than the results of the Wachter et al. (2002) formula for similar stellar parameters, and probably for the same reason (i.e., effects of frequency-dependent vs. grey radiative transfer on atmospheric densities).

The dependence of the wind properties on metallicity has, so far, only been explored with PEDDRO models for C-type AGB stars. Mattsson et al. (2008) argue that mass loss depends mostly on the carbon excess, C-O, and that no significant differences should be found for stars with comparable C-O, independent of metallicity. Since

[7] Note the typo in the mass loss formula from 2002 as given in the paper from 2008.

carbon is produced in AGB stars, it should be possible to reach typical solar C-O values also at lower metallicities. This seems to be consistent with observations, at least for metallicities down to typical values in the MCs (see Sects. 3.2 and 5.2.1). The formula by Wachter et al. (2008), in contrast, predicts a decrease in mass loss with metallicity, since it is based on models with constant C/O, corresponding to lower C-O for lower metallicity.

Finally, it should be mentioned that the pulsation properties (period, amplitude) are additional input parameters in current PEDDRO models since sub-photospheric dynamics is simulated by a variable inner boundary close to the photosphere (see Sect. 4.3). A dependence of mass-loss rate on the pulsation period is, indirectly, build into most models, since they tend to use observed relations between the period and the luminosity of the star, in order to reduce the number of independent input parameters.

5.2.3 What can we learn from discrepancies between observations and theory?

State-of-the-art PEDDRO models, in general, seem to predict a significantly steeper increase of mass-loss rate with luminosity than what is found in most observational studies, for both M- and C-type AGB stars. Regarding effective temperature, observations show no clear trend for M-type stars, which is consistent with current PEDDRO models, and a much weaker dependence for C-rich stars than what is predicted by the corresponding models.

While uncertainties in empirical mass-loss rates and stellar parameter determinations are probably considerable (see Sect. 5.2.1), they cannot reasonably be made responsible for all of the discrepancies. Neither is it likely that the PEDDRO models are fundamentally wrong, given their good agreement with observed wind properties ($\dot{M}$ and υ_∞), or spectra and photometric colours, as discussed in Sect. 5.1. So there should be a way to reconcile the seemingly major differences in dependence of mass-loss rate on luminosity or effective temperature.

To begin with, it should be noted that the trends derived from the models (e.g., expressed as exponents in a mass-loss formula) refer to the influence of individual stellar parameters, i.e., a situation where all other fundamental parameters are kept fixed, which will not be the case for observational samples. Taking the formula by Wachter et al. (2002) as an example, we can try to compensate for the offset in the theoretical trend with luminosity ($\dot{M} \propto L_*^{2.47}$) compared to typical observed relations ($\dot{M} \propto L_*^{0.9-1.6}$, see Sect. 5.2.1) by a correlation of luminosity with effective temperature (which affects the theoretical mass loss rate as $T_{\rm eff}^{-6.81}$) or current stellar mass (theoretical mass loss rate $\propto M^{-1.95}$). By simply looking at the signs of the exponents (positive for luminosity, negative for temperature and mass), it becomes clear that a simultaneous increase in temperature and/or mass with luminosity is needed to compensate for the strong theoretical luminosity trend.[8] The correlations of stellar parameters during the evolution of an individual star on the AGB, however, would lead

[8] To give an example, for a range of 0.5 dex in L_* (e.g., about 5000–15 000 $L_\odot$, which falls nicely within the typical regime of the PEDDRO scenario), the effective temperature of the stars would have to increase with increasing luminosity by about 10 % (typically 200–400 K), or the mass by 40–80 %, in order to reproduce the flatter L_*-dependence of typical observational relations.

to the opposite overall trends (i.e., decreasing effective temperature and mass as luminosity increases). This implies that observed mass-loss-rate relations probably reflect a diversity of evolutionary paths (corresponding to different initial stellar masses and compositions) and an age spread of the sample stars, in addition to the effects of stellar parameters during the evolution of individual stars along the AGB.

This idea was explored in detail in the review by Willson (2000). Defining a critical mass loss rate, $-\mathrm{d}\log(M)/\mathrm{d}t = \mathrm{d}\log(L)/\mathrm{d}t$ (referred to as "the cliff"), or $-\mathrm{d}M/\mathrm{d}t = (M/L)\ \mathrm{d}L/\mathrm{d}t$, where mass loss starts to dominate stellar evolution (with a value depending on initial mass and composition of the star), Willson (2000) argues that the observed mass-losing stars will fall mostly within the range of 1/10 to 10 times this critical mass-loss rate. The upper limit is caused by the scarcity of objects due to rapid evolution, driven by mass loss. The lower limit reflects that winds with low mass-loss rates are more difficult to detect or measure. This leads to a selection effect which favors the inclusion of stars near the critical mass-loss rate in the observed relations. "Thus, the empirical mass loss laws tell us the parameters of stars that are losing mass, and not the dependence of mass-loss rates on the parameters of any individual star.", Willson (2000) concludes.

Taking this argument to its extreme implies that a "mass loss formula", i.e., a quantitative description of how the mass-loss rate depends on individual stellar parameters (and, consequently, how it changes as stars evolve), can only be derived from wind models based on first principles, and not from observations. In reality, however, the situation is not as clear-cut.

Since the above interpretation of the discrepancies in observed and theoretical trends was proposed by Willson (2000), there has been significant progress with both modelling and empirical approaches. On the theoretical side, a new generation of improved PEDDRO models has been developed, which allows a direct comparison of synthetic spectra and photometric variations with observations. On the observational side, new space- and ground-based instrumentation has led to better sensitivity, permitting to probe a larger range of mass-loss rates, and large surveys have given better statistics and more possibilities to detect rare very-high-mass-loss-rate objects. Ironically, this progress, in general, has not made the perceived discrepancies smaller: on the contrary, the largest surveys seem to give the least clear trends, as discussed in Sect. 5.2.1. A notable exception is the study by Danilovich et al. (2015), based on multi-line CO observations of nearby stars, which indicates an increase of mass-loss rate with luminosity that is even steeper than in PEDDRO models. A possible explanation is that this particular sample of stars is narrow in initial mass and primarily shows the combined effects of simultaneous changes in luminosity, temperature and current mass along the AGB, which all favor an increase in mass-loss rate.

As mentioned in Sect. 5.2.1, the results of Danilovich et al. (2015) seem to be consistent with the semi-empirical mass-loss formula of Vassiliadis and Wood (1993) that includes the possibility of a superwind, i.e., a strong increase of mass loss towards the end of AGB evolution. When applied to stellar evolution models, this formula leads to significantly better results than Reimers-type mass loss laws with their more gentle dependence on stellar parameters (see, e.g., the discussion in Lattanzio and Karakas 2016). This is consistent with the interpretation of Willson (2000) that Reimers-type formulas, like most observational relations (in particular those based on large, diverse

samples of stars), describe the "cliff" (i.e., the critical mass loss rate for stars with different initial masses and compositions), rather than the dependence of mass-loss rate on stellar parameters during AGB evolution of individual stars. In the light of this interpretation, the apparently short duration of the superwind phase derived from observations (see Sect. 3.1.2) may be a natural consequence of a fast termination of AGB evolution by a run-away mass loss process.

A special case where the dependence of mass loss on stellar properties may be accessible to observations is individual nearby stars where the mass-loss history is imprinted on the structure of the CSE, in particular in the form of a so-called detached shell (believed to be caused by a He-shell flash, see Sect. 3.1.2). If the basic stellar parameters can be determined with sufficient accuracy, such stars can be used to test the interplay of mass loss and stellar evolution, i.e., the dependence of mass loss on the changing stellar parameter, and vice versa. However, uncertainties related to the dynamics of a CSE with varying wind velocity and mass-loss rate, or wind shaping by a close companion star, may complicate the comparison of model results and observations (see, e.g., Steffen and Schönberner 2000; Schöier et al. 2005; Mattsson et al. 2007; Maercker et al. 2012, 2016b).

6 Beyond the standard picture: challenges and opportunities

The standard CSE model (described in Sect. 2.2), on which every method for mass-loss-rate estimation rests, is based on the assumption that the mass-loss rate is constant with time (at least over a time scale much longer than that of the stellar pulsation). Apart from the brief episodes ($\geq$ few $\times 10^2$ year) of highly enhanced mass loss seen towards a minority of the observed stars (Sect. 3.1.2), and indications of a superwind at the end of the AGB, the evidence for temporal variations in the mass-loss rate on the AGB are scarce. Indeed, CO multi-line data are often well reproduced in radiative transfer models assuming a constant mass-loss rate (Danilovich et al. 2015). There are indications of variable mass loss in far-IR photometry data on non-Miras, but there are no quantitative estimates (Marengo et al. 2001). We conclude that the uncertainties in the estimated mass-loss rates due to any variability of the mass-loss rate with time are most likely limited, in particular for the regular long-period pulsators. Consequently, this aspect will not be further discussed here.

Another basic assumption in the standard CSE model is that of an isotropic mass loss, i.e., spherical symmetry. This is an assumption that it shares with the models which are currently used for making theoretical predictions about the dependence of mass-loss rates on stellar parameters (introduced in Sect. 4.3). As a first approximation, this is not entirely unreasonable: The dominant geometrical effects regarding temperatures, densities and velocities in the CSE can be expected to arise from the dependences of the radiative flux and gravitational force on the distance from the star (both scaling as $1/r^2$). From a modelling point of view, the assumption of spherical symmetry reduces the dynamical problem to one spatial dimension, focusing on the radial components of relevant forces, and the resulting gain in computational efficiency allows for detailed treatments of radiative transfer and micro-physics (Sects. 4.2 and 4.3).

The ongoing progress in high-angular-resolution observations, however, is revealing complex non-spherical structures on scales ranging from the stellar photospheres to the outer boundaries of the circumstellar envelopes. Some of these structures are probably caused by the highly dynamical nature of the star itself, or are intrinsic to the wind mechanism and may, therefore, have implications for the mass loss. Others are more likely due to shaping of the already established outflows by close companions (stars, maybe even planets), or to interaction with the surrounding interstellar medium, and they may have implications for empirical mass-loss-rate estimates.

In this section, we summarize the current understanding of the physical mechanisms behind the observed complex morphologies, and discuss their possible consequences for empirical mass-loss estimates based on the standard CSE model, the SCRA scenario. Regarding mass-loss theory, we look into aspects not covered by current PEDDRO models, including alternative mechanisms for atmospheric levitation or wind acceleration.

6.1 Complex morphology: causes and consequences for mass-loss rate estimates

6.1.1 Stellar surface patterns, dynamical atmospheres, dust clouds

High-angular resolution observations have made it increasingly apparent that the photospheres extended atmospheres and close environments of AGB stars are characterized by complex, variable, and non-spherical structures. Early indications came from speckle-interferometric observations, e.g., of the dust-enshrouded carbon star CW Leo (Weigelt et al. 1998) and the proto-type long-period variable star *o* Cet (Mira Ceti; Karovska et al. 1991). In the case of CW Leo, the observed variable intensity patterns were interpreted as the modulation of stellar light by inhomogeneous layers of circumstellar carbon dust. In the case of Mira, on the other hand, it is still unclear which observed features are intrinsically connected with the AGB star, and which are effects of its interaction with a companion star (e.g., Karovska et al. 1997; Ramstedt et al. 2014).

With increasing angular resolution, interferometric measurements at IR wavelengths have given indications of deviations from spherical symmetry in the extended atmospheres and wind formation regions of AGB stars. In the beginning, non-spherical structures were inferred from measurements using only a few baselines, e.g., taking non-zero closure phases as an indicator, but with the latest generation of instruments it has become possible to reconstruct resolved images of stellar surface intensities and molecular layers in the near-IR regime (e.g., Monnier et al. 2014; Haubois et al. 2015; Kamiński et al. 2016; Wittkowski et al. 2017). An interesting complement to ground-based IR interferometric studies are images of the extended atmospheres of CW Leo and Mira produced with the Cassini spacecraft by watching the stars pass behind Saturn's rings (Stewart et al. 2016a, b). Recently, direct imaging with extreme adaptive optics in the visual range has shown patchy dust clouds at about 2–3 R_* (e.g., Ohnaka et al. 2016) and changes of intensity patterns and grain sizes on time scales of months (e.g., Khouri et al. 2016a; Ohnaka et al. 2017) in the well-studied nearby AGB stars W Hya and R Dor.

The existence of non-spherical structures in the atmospheres of cool luminous giants was not unexpected. Both basic physical considerations (Schwarzschild 1975) and exploratory 3D radiation-hydrodynamical simulations of AGB stars (Freytag and Höfner 2008) predicted giant convection cells, on scales comparable to the stellar radius. These large-scale convective flows lead to complex, variable surface intensity patterns and propagating shock waves that leave their marks on atmospheric density structures, which, in turn should be reflected in the dust distribution, as indicated by the models of Freytag and Höfner (2008). It is, therefore, likely that the observed deviations from spherical symmetry on stellar scales are caused by direct or indirect effects of convection, as will be further discussed in Sect. 6.2.1.

6.1.2 Morphology of CSEs: from the wind acceleration region to global scales

There is ample evidence (mainly in qualitative terms) of the CSEs being inhomogeneous in density, i.e., they are clumpy. The detached CO shells discussed in Sect. 3.1.2 provide little line-of-sight confusion and their brightness distributions are clearly patchy suggesting considerable clumpiness (Olofsson et al. 2000; Maercker et al. 2012). The maser mechanism is sensitive to the physical conditions, and it is therefore a, at least qualitative, probe of clumpiness. In particular, H_2O maser line emission has been used in this context (Richards et al. 2012). The conclusions are that the H_2O maser clumps in AGB CSEs are typically 30 times denser than the average wind density, their volume filling factor is $< 1\%$, and their sizes scale with stellar radius (only apparent when RSGs are included). The clump masses reach a few $\times 10^{-7}\,M_\odot$, and in the lower-mass-loss-rate objects all the circumstellar mass lies in the clumps. These quantitative results have some considerable uncertainties though.

Inhomogeneities on a small scale (compared to the CSE size) are likely to develop early in the mass-loss process as discussed above, but they can also appear later, e.g., as a consequence of interaction between the circumstellar gas and dust (Simis et al. 2001; Simis and Woitke 2003). Whether the circumstellar medium is smooth or clumpy is important not only for our understanding of the mass-loss mechanism, but also for the reliability of the mass-loss-rate estimates as discussed in Sect. 6.1.4.

As larger regions of a CSE are studied, we may expect it to have a smoother and overall spherical appearance as a consequence of the larger number of clumps (presumably ejected isotropically) and the effect of contamination along the line of sight. This is essentially consistent with observations, as discussed in Sect. 3.1.3, but there are also interesting significant deviations from overall spherical symmetry. For instance, there is morphological evidence of the star (and the CSE) moving through the ISM in terms of bow shocks (Cox et al. 2012a; Matthews et al. 2013; Sahai and Mack-Crane 2014), Fig. 20, left panel. Fortunately, the bow shocks are fairly distant to the star (0.1–1 pc) and the amount of mass swept up is negligible (Cox et al. 2012b). Their emission is, therefore, not likely to affect mass-loss-rate estimates, but studying them can provide important information on the mass-loss-rate history. Another type of morphological structure is shown in Fig. 20, right panel. van Marle et al. (2014) provide an explanation for this in terms of the effect of an interstellar magnetic field on an expanding spherical envelope that sweeps up the interstellar medium. Also these structures lie at sufficiently large distances from the star to have little effect on mass-loss-rate

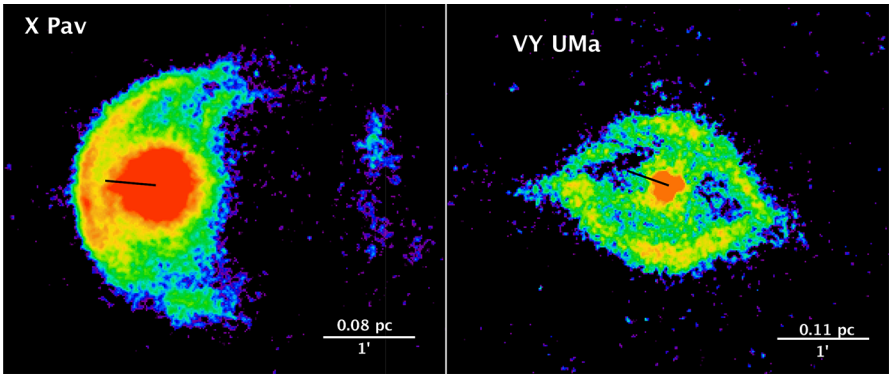

Fig. 20 Left: an Herschel/PACS 70 μm image of the circumstellar dust envelope around the M-star X Pav showing the effect of ISM-CSE interaction as the star moves through the ISM. Right: an Herschel/PACS 70 μm image of the circumstellar dust envelope around the carbon star VY UMa (see text for a possible explanation of this structure). Image reproduced with permission from Cox et al. (2012a), copyright by ESO

estimates. Of more concern in this context is the presence of complicated and bright structures closer to the star. The limited resolution of Herschel Space Observatory makes it difficult to answer this question conclusively.

6.1.3 Impacts of companions on CSE morphology

Another aspect of anisotropic CSEs are structures such as arcs and spiral patterns. The number of examples is steadily increasing, e.g., CW Leo (Cernicharo et al. 2015; Decin et al. 2015), RW LMi (Dinh-V-Trung 2009; Claussen et al. 2011; Kim et al. 2015), R Scl (Maercker et al. 2012), R Aqr and W Aql (Mayer et al. 2013), and π^1 Gru (Mayer et al. 2014). A prominent example is that of the dust and gas spiral towards AFGL3068 (Mauron and Huggins 2006; Kim et al. 2017), Fig. 21, left panel. Interpretations of such morphologies center around modulations in the density distribution as a consequence of multiplicity, i.e., at least one nearby companion.

The presence of a companion has primarily two effects on the CSE. The gravitational attraction of the companion focuses on the cirumstellar material to the orbital plane, leading to a flattening of the CSE (Mastrodemos and Morris 1999; Mohamed and Podsiadlowski 2007; Huggins et al. 2009), where also spirals can appear in its density distribution (Kim and Taam 2012b), and the reflex motion of the mass-losing star that leads to a modulation of the density structure of the CSE in the form of a spiral (in 3D) (Kim and Taam 2012a). The resulting observed morphology depends on the orientation of the orbital plane with respect to the line of sight in addition to the binary separation, the orbital eccentricity, and the mass ratio. As a consequence, spirals can often be seen instead as concentric arcs. Ways to derive properties of the binary system based on the CSE morphology are discussed in Huggins et al. (2009), Kim and Taam (2012c), and Kim et al. (2013), and interpretations of observed morphologies through hydrodynamical simulations can be found in, e.g., Maercker et al. (2012) and Kim et al. (2017), Fig. 21, right panel. Of interest in this context are the rings and arcs seen

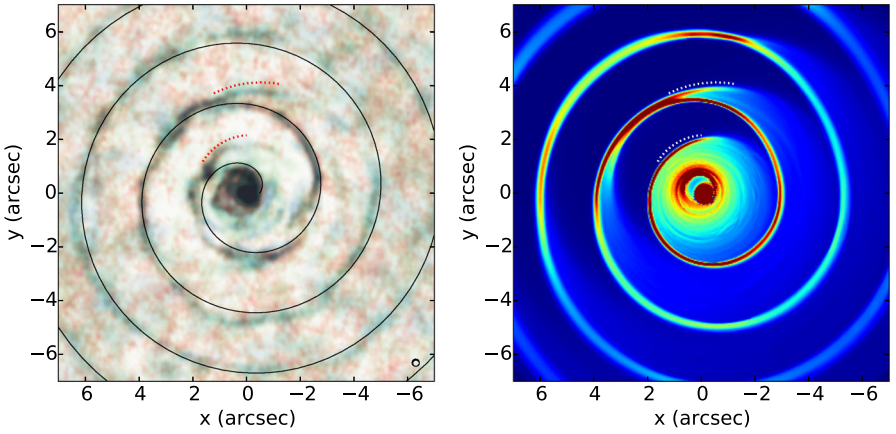

Fig. 21 Left panel: a combined ^{12}CO($J = 2-1$) (in blue), ^{13}CO($J = 2-1$) (in green), and HC_3N($J = 24-23$) (in red), after subtraction of an extended circumstellar component, image of the circumstellar environment of the carbon star AFGL3068 obtained with ALMA (3 km s^{-1} interval centered on the systemic velocity). Right panel: the gas mass distribution within the same velocity range in a hydrodynamic model of a mass-losing star and its companion with the masses of 3.5 $M_\odot$ and 3.1 $M_\odot$, respectively, a mean orbital separation of 166 au, an eccentricity of 0.8, and an inclination angle of 50^o for the orbital plane with respect to the plane of the sky. Image reproduced with permission from Kim et al. (2017), copyright by Macmillan

towards proto-PNe and PNe. The extensive study of Ramos-Larios et al. (2016) shows that such structures are present around 8 % of the objects. In the cases when multiple rings are seen, they correspond to time scales in the range 500–1200 year between the rings (for each source the time scale is constant), and the estimated time scale of the phenomenon is $\lesssim$ 4500 year. It is not clear what the cause of these rings and arcs is, but the effect of a companion is a possible explanation.

An active companion can also have profound non-gravitational effects on the CSE. Such an example is provided by Ramstedt et al. (2014), where it appears that the UV radiation, and possibly the high-velocity outflow, of Mira B are strongly affecting the CSE (at least the molecular component) formed through the mass loss of Mira A. In a case like this, the distortion of the CSE is so large that radiative transfer modelling of dust and line emission using the standard CSE model is a highly unreliable basis for deriving a mass-loss rate.

An interesting aspect in this context is whether the companion not only produces a modulation in the density, but also affects the actual mass loss of the primary. This is further discussed in Sect. 6.2.3. To give an example, Cernicharo et al. (2015) infer a substantial mass-loss-rate variation induced by the interaction with the companion in the case of CW Leo. To fit the data, they use a ten times higher mass-loss rate at perigee than at apogee.

Complicated morphologies of CSEs are a problem for the reliability of mass-loss-rate estimates, but they present an important way of studying binarity among AGB stars since direct detections of companions are difficult. This is also a complement, e.g., to searches for UV excesses as a binarity diagnostics (Sahai et al. 2008), since there may be other explanations of such an excess (Montez et al. 2017).

6.1.4 Effects of clumpiness and anisotropies on mass-loss rate estimates

As has been discussed in Sect. 3.1.3, there are numerous examples of largely spherical CSEs produced by a mass-loss rate that is constant in time, i.e., in this respect the CSEs are well described by a standard CSE model. However, the number of examples of departures from spherical symmetry and the evidence of clumpiness of the circumstellar medium also increases. As concerns the large-scale structure, the balance is still on the side of largely isotropic mass-loss, but a clumpy circumstellar medium is likely to be the rule rather than the exception and, hence, some aspects of the standard CSE model are not fulfilled.

A clumpy medium will affect the chemistry (including the ability of the molecules to survive dissociating radiation), the excitation of the atoms/molecules, and the radiative transfer of line as well as continuum emission. The primary problem is that the standard assumption of (smooth) CSE density/abundance distributions and kinetic and dust temperatures that fall off predictably with radius breaks down. It is very difficult to judge how profound an effect on mass-loss-rate estimates this has. It requires careful radiative transfer and chemistry modelling to assess, but presumably the mass-loss rates are underestimated. Work on the radiative effects of clumpy dust distributions has started (e.g., Scicluna and Siebenmorgen 2015).

Related to this are the modulations of the density structure due to binary interaction discussed above. Homan et al. (2015) investigated this problem from a radiative transfer point of view (i.e., effects on physics and chemistry were ignored) and concluded that the CO rotational line profiles are not particularly affected by this, hence they are not suited for identifying sources of this type. Imaging is required, and position–velocity diagrams appear particularly suited for diagnosing the 3D structure. Errors in mass-loss-rate estimates based on CO lines were also investigated with the conclusion that they are mainly of the order of a few, but can reach an order of magnitude.

Likewise, errors in mass-loss-rate estimates due to large-scale deviations from sphericity are difficult to estimate. It is possible that assuming a standard CSE model, an estimate based on radiative transfer modelling of CO line profiles from a non-spherical CSE, may lead to mass-loss rates that are significantly wrong, but the extent of it requires a detailed analysis that includes excitation and physics/chemistry.

6.2 Mass loss theory: beyond current wind models for AGB stars

6.2.1 Modifications of the basic PEDDRO scenario

As discussed in Sect. 4.2, dust formation is sensitive to both temperatures and gas densities in the circumstellar environment. Temperature, set by radiative processes, acts as a threshold and determines how close to the star dust grains can form and survive. Density defines the grain growth rates and, therefore, affects the amount of dust that will condense in an environment where grain growth is a race against time, with timescales set by dynamical processes. Together, they define lower and upper limits for the range of distances where efficient dust condensation may occur.

In the extended atmosphere of an AGB star with large-amplitude radial pulsations, a strong spherical shock wave is triggered once per period and propagates outwards (see Sect. 4.1). In addition, the temperatures in the close circumstellar environment vary with luminosity and, therefore, pulsation phase. Therefore, grain growth will be most efficient around the luminosity minimum (lowest temperatures), in the most dense parts of the atmosphere just beyond the condensation distance, usually in the wake of a shock wave (Fig. 14, right panel; see, e.g., Liljegren et al. 2016, for a detailed discussion). If dust grains with suitable properties form in sufficient amounts, radiation pressure may accelerate the gas-dust mixture beyond the local escape velocity. This is the basic PEDDRO scenario according to the current spherically symmetric wind models (cf. Sects. 4.3 and 5.1).

In a situation where there is a complex network of atmospheric shock waves (see Sect. 4.1, Fig. 12), triggered by large-scale convective flows, or possibly non-radial pulsations, dust condensation is expected to be patchy, in response to the local conditions (density, temperature). Grain formation and growth will still, mostly, occur in the dense wakes of the shocks, but will lead to partial shells, rather than complete spherical ones (see Fig. 2 and the paper by Freytag and Höfner 2008). This picture is qualitatively confirmed by recent spatially resolved observations of light scattered by dust clouds in the close vicinity of W Hya and R Dor (Khouri et al. 2016a; Ohnaka et al. 2016, 2017, see Fig. 22). In particular, Ohnaka et al. (2017) interpret changes in scattered light between pre-maximum and minimum light in W Hya as a change in dominant grain size. The corresponding particle radii, about 0.1 μm at minimum and 0.5 μm at maximum, fit well with current PEDDRO models for M-type AGB stars (Höfner 2008; Bladh et al. 2015; Höfner et al. 2016), implying grain growth between minimum and maximum light, and subsequent radiative acceleration by photon scattering.[9] An exploratory study by Aronson et al. (2017) which combines a range of pulsation phases from a spherical PEDDRO model into a non-spherical structure, mimicking the out-of-phase propagation of shocks in different radial directions, produces scattered light patterns that are comparable to the observations.

How such deviations from sphericity affect the dynamics of the extended atmosphere and inner wind region is still a matter of speculation, as no 3D models of dust-driven winds exist at present. The observational evidence for a clumpy structure of the CSE (Sect. 6.1.2) suggests that individual dust clouds may be accelerated away from the star, depending on the local grain properties. Matter in between these regions may either be dragged along, or fall back towards the star on ballistic trajectories. This could create turbulence in the outer atmosphere, or enhance the tendency towards dust-induced instabilities (Simis and Woitke 2003). It is difficult to guess which net effect such processes might have on the total time-averaged mass-loss rate.

While discussing mechanisms that may lead to deviations from spherical symmetry on stellar scales, rotation should also be mentioned. In principle, stellar rotation may directly affect the wind formation process by providing additional latitude-dependent

[9] It should be noted in this context that observations of scattered light at visual and near-IR wavelengths cannot distinguish between different grain materials. However, it seems likely that the small grains found around minimum light are mostly Al_2O_3 (forming first, closest to the star) which acquire silicate mantels during later phases, before being accelerated away from the star (see discussion in Sect. 4.2).

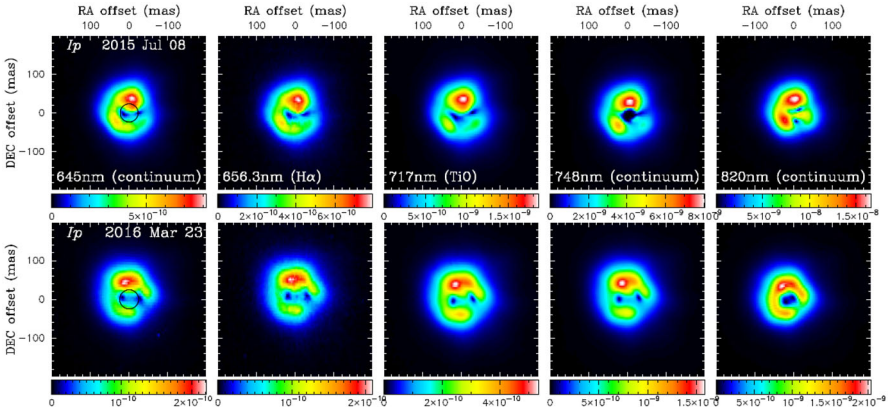

Fig. 22 Polarized intensity maps of W Hya observed with SPHERE-ZIMPOL at 2 different epochs (top row: July 8, 2015, phase 0.92; bottom row: March 23, 2016, phase 0.54). The polarized light is interpreted as stellar light scattered by circumstellar dust grains. The images show clear changes in morphology between the two epochs. The circles in the leftmost panels represent the size of the star measured in the continuum near 2.3 μm. Image reproduced with permission from Ohnaka et al. (2017), copyright by ESO

levitation, resulting in stronger mass loss near the equator (Dorfi and Höfner 1996), or indirectly, through effects on the large-scale convective flows (Freytag et al. 2017). In view of their large radii and the related high moment of inertia, typical AGB stars are expected to rotate slowly, both in terms of surface velocities, and regarding angular momentum, compared to gravity. This is supported by observational studies of stellar surface rotation which find only a small fraction of fast rotators among red giant stars (see, e.g., Ceillier et al. 2017, and references therein). Based on the present knowledge, it seems unlikely that stellar rotation will create significant anisotropies in the wind, unless the outer layers of an AGB star experience a spin-up due to redistribution of angular momentum inside the star, or angular momentum transfer from a (sub-) stellar companion.

In summary, we expect that the 2-step scenario for wind-driving (illustrated in Fig. 2), qualitatively, also holds when convection, non-radial pulsation, or rotation introduces deviations from spherical symmetry which are not covered by current PEDDRO models. However, it seems more appropriate to refer to this, more generally, as a Shock-Enhanced Dust-DRiven Outflow, i.e., SEDDRO, considering that the shock waves which provide atmospheric levitation may not exclusively be caused by (radial) pulsation. At present, it is difficult to guess how non-radial dynamical processes will affect the total mass-loss rate, quantitatively speaking. Global dynamical 3D models, reaching from the stellar interior to the wind formation region, will be required to answer this question.

6.2.2 Other wind-driving mechanisms in cool stars

A pre-requisite of the PEDDRO scenario, with or without the modifications discussed above, is the formation of sufficient amounts of suitable dust grains, within a distance of a few stellar radii and on time-scales shorter than ballistic movements in the outer

atmosphere. This, clearly, puts limits on the stellar parameter space where dust-driven outflows will occur. The effective temperature and luminosity of the star are obvious limiting factors, as they will affect the distance at which grains can form and survive. Furthermore, the ratio of the stellar luminosity to the current mass of the star defines the relative strengths of radiative acceleration and gravitational deceleration and, therefore, the critical opacity required for driving a wind (see Eq. 2). Last but not least, the abundances of condensible chemical elements set an upper limit for the total dust opacity.

Large grids of wind models are starting to reveal the theoretical boundaries in stellar parameter space for PEDDRO-type mass loss. However, one should not expect simple dividing lines in terms of individual parameters, e.g., effective temperature, or luminosity, as these are linked in complex ways during AGB evolution, and collectively affect the conditions for wind formation (see Sect. 5 for a discussion of these issues). While there are strong indications that radiation pressure on dust is responsible for the most massive outflows of matter towards the end of AGB evolution, there is direct and indirect evidence of mass loss before the stars enter this regime, and also on the red giant branch, prior to the AGB phase (see Sect. 3.3). These winds are probably driven by other mechanisms.

Direct momentum input from Alvén waves seems to be a promising mechanism for driving the winds of red giants and possibly red supergiants (Airapetian et al. 2000, 2010; Cranmer and Saar 2011), but there is doubt if it extends to the typical stellar parameter regime of AGB stars, and especially to the cooler part of the effective temperature range, where the highest mass-loss rates are found. A lack of free charges (low degree of ionization) may prevent the gas from coupling to the magnetic field, as the photospheric UV flux decreases dramatically with a lower effective temperature of the star. Occasionally, the existence of emission lines, or bright spots in the atmospheres of certain AGB stars, is taken as an indication of small regions of high gas temperature. The origin of these phenomena, and if they affect the mass loss, is however still a matter of debate. While it seems unlikely that dust-forming AGB stars have chromospheres in the classical sense, a complex network of atmospheric shocks might intermittently produce small pockets of gas that are substantially warmer than their surroundings, presumably with a much lower spatial filling factor than in warmer giants (e.g., Harper et al. 2013; Wedemeyer et al. 2017).

A few years ago, Cranmer and Saar (2011) presented a predictive description of mass loss, based on Alvén-wave-driven winds, spanning from the MS phase to the RGB. Stars of the former type lose mass at low rates, supposedly due to outflows driven by thermal pressure in a hot corona. In this case, the Alvén waves (i.e., incompressible, transverse magneto-hydrodynamic waves) are assumed to provide a source of heating by dissipation. When the stars develop into cool giants and cross a well-known dividing line in the HR-diagram (Linsky and Haisch 1979), a transition occurs from a hot corona to a cool chromosphere. A common assumption in wave-driven wind models for cool giant stars is direct momentum input (wave pressure), in contrast to dissipative heating and high gas pressure. While early linear models of winds driven by Alvén waves had to invoke a dissipation mechanism in order to avoid too high flow velocities (e.g., Hartmann and MacGregor 1980), more recent non-linear numerical simulations of red giant star winds do not suffer from this problem (Airapetian et al. 2000, 2010). The

assumptions about the thermal structure of the atmosphere in these models, however, tend to be simplistic (e.g., isothermal), and the actual wave-generation mechanisms are not part of the wind models, introducing free parameters. A recent study by Wedemeyer et al. (2017) addresses the origin of waves in red giant atmospheres with detailed numerical models.

It should be noted that Alvén-wave-driven winds require open flux tubes, radially directed away from the star, in order for the gas to be accelerated and escape. The present knowledge of magnetic field strengths and geometries in cool giants is very limited. To measure directly the magnetic field of an AGB star has turned out to be difficult, but a recent result on the S-star χ Cyg, indicating a field strength of a few Gauss (Lèbre et al. 2014), suggests that major progress may be done in this area in the future. Magnetic field strength estimates in CSEs are based on maser lines of SiO, H_2O, and OH, and on "normal" line emission from CN through the Zeeman effect (Duthu et al. 2017) and from CO through the Goldreich-Kylafis effect (Vlemmings et al. 2012). The maser results are notoriously difficult to interpret, but they suggest (when extrapolated) magnetic field strengths in the range 10^{0-2} G and a radial dependence in between r^{-2} (solar-type) and r^{-1} (toroidal) for M-stars (Vlemmings 2014). The CN results on C-rich objects are consistent with a stellar magnetic field strength of a few Gauss and a toroidal field (Duthu et al. 2017). The large-scale structure remains uncertain, but future observations of, e.g., the polarization of CO line emission with ALMA may make good progress here for AGB stars of all chemical types. The origin of the magnetic field of AGB stars is not known, but various possible mechanisms have been put forward (see, e.g., Vlemmings 2014). If magnetic fields play a role in the mass-loss process, one may expect a correlation between the wind properties (mass-loss rate, wind velocity) and the magnetic field strength, but such a correlation remains to be shown.

A question sometimes raised in the literature is whether the presence of dust in the CSEs of AGB stars implies that the wind is initiated by radiation pressure, or if the observed grains can form as a by-product in an existing outflow, triggered by a different mechanism, with or without further accelerating the flow. Considering observed correlations of mass-loss indicators with pulsation properties, it is sometimes discussed if pulsation-induced shock waves alone can drive the winds of Miras and other long-period variables.

Willson (2000) argues that current PEDDRO models may overestimate the radiative cooling rates behind shocks in the critical region where the wind is initiated.[10] If radiative cooling between the passage of successive shocks through the gas is sufficiently slow, a warm extended atmosphere (referred to as "calorisphere", i.e., a continuous spherical region of warm gas, not to be confused with small intermittent "hot spots") may result, instead of a cool one. Bowen (1988) presented simulations of winds driven by high gas pressure in a calorisphere, i.e., a thermal wind instead of a radiation-driven

[10] It should be noted in this context that Schirrmacher et al. (2003) arrived at a different conclusion. Extending the cooling function to include a variety of molecular species, they found a high, LTE-like cooling rate down to very low densities for temperatures in the range of 2000-3000 K. However, this study is based on chemical equilibrium for the molecular species which may lead to an overestimation of molecular abundances in the post-shock region.

outflow, more similar to the classical Parker-wind scenario for the Sun. However, there are several problems with this scenario. The higher atmospheric temperatures required to drive a wind with thermal pressure should produce observable effects on the spectra, and they would inhibit dust formation close to the star. In contrast, observed spectra for AGB stars with pronounced outflows are in good agreement with cool dynamically extended atmospheres (e.g., Bessell et al. 1989; Bladh et al. 2013), and mid-IR interferometry as well as scattered light observations at visible and near-IR wavelengths place the inner edge of the dust shell at about 2 stellar radii (e.g., Wittkowski et al. 2007; Karovicova et al. 2013; Norris et al. 2012; Ohnaka et al. 2017). This suggests that post-shock cooling is rather efficient, and that pulsation-induced shocks contribute to atmospheric levitation, but not directly to wind driving.

6.2.3 Interaction with companions

In Sect. 6.1.3, we briefly discussed how a companion may put its marks on the large-scale structure of the CSE (shaping the wind of the AGB star with its gravity and radiation), and thereby affect empirical mass-loss estimates. Depending on the distance and the properties of the companion (mass, radiative flux, evolution stage), it may also directly affect the physics of the mass-loss process. Simply speaking, the companion can modify the gravitational potential of the AGB star, or add angular momentum to its outer layers, in such a way as to enhance the outflow. On the other hand, a hot radiation field may affect dust formation negatively, or a strong wind originating from the companion could modify the conditions in the wind acceleration region of the AGB star. 3D hydrodynamical models of a cool giant interacting with a close stellar companion are still in an exploratory phase, focusing on wind shaping (see Sec. 6.1.3) or mass transfer and common envelope formation (e.g., Passy et al. 2012; Staff et al. 2016; Iaconi et al. 2017). Compared to models that aim at predicting the dependence of the mass-loss rate of AGB stars on their fundamental parameters (see Sects. 4.3 and 5.1), binary interaction models often use a simplified description of the underlying physics, e.g., regarding atmospheric structure, radiative transfer, or dust formation.

Mass transfer and binary evolution The transfer of mass and angular momentum in binary systems and the resulting effects on stellar evolution are topics in their own right, well beyond the scope of this review. We refer the reader to the recent review by De Marco and Izzard (2017) for a comprehensive overview and an in-depth discussion of the subject. Here, we can only give a flavour of aspects that are being discussed in the AGB literature. An extreme scenario of mass transfer is that of the AGB star filling its Roche lobe. The rotation of such binaries around their common center of mass may produce periodic light variability caused by the distortion of the cool giant due to the gravity of its companion (so-called sequence E stars, e.g., Wood et al. 1999; Nicholls and Wood 2012; Nie et al. 2012, 2017). Mass transfer by Roche-lobe overflow is very efficient; it has strong effects on stellar evolution, and, most likely, on the formation of PNe (see below). A less dramatic, but efficient mode of mass transfer, is wind Roche-lobe overflow (Mohamed and Podsiadlowski 2007, 2012), which results from a situation where the slow wind of the AGB star is filling the Roche-lobe, instead of

the star itself expanding to this size. In wide binaries, this mechanism may drastically increase the mass transfer rate to the companion, compared to classical Bondi-Hoyle-Lyttleton accretion, with implications for stellar and galactic chemical evolution, e.g., the origin of carbon-enhanced metal-poor stars (Abate et al. 2013).

Shaping of planetary nebulae Although the fascinating phenomenon of the shaping of PNe, often into very complex geometrical patterns (e.g., Balick 2004), is beyond the scope of this review, it is clear that it is related to the mass loss on the AGB. The large majority of the proto-PNe and PNe are axially symmetric rather than spherical, a phenomenon that is more common among the younger objects (e.g., Sahai et al. 2007, 2011). Based on the extensive studies of AGB CSEs, it is clear that the change in morphology must take place at the end of the AGB or shortly after that. It may be due to a change in the mass-loss-rate characteristics of the star, but evidence is mounting that the origin is rather related to the presence of a companion. Observational indications in the form of spirals and arcs in AGB CSEs and concentric shells around proto-PNe are well explained by interaction within a binary system, although the details remain to be worked out, Sect. 6.1.3. In this way, the shaping of PNe becomes a natural step in the evolution of mass loss on the AGB.

It is often assumed that the formation of an equatorial density enhancement, e.g., a disk, is an important step in this context. Indeed, the presence of a disk has been inferred in a number of post-AGB objects (Bujarrabal et al. 2013), while disks around AGB stars have remained elusive. However, clear evidence of a dust disk with an inner and outer edge lying at $\approx$ 6 and $\approx$ 13 au, respectively, has recently been found towards the M-star L_2 Pup (Kervella et al. 2015; Lykou et al. 2015; Ohnaka et al. 2015). This could be the first evidence of disk formation around a star at the end of its evolution on the AGB.

7 Current understanding and future perspectives

From its humble beginnings about half a century ago, the topic of stellar mass loss on the AGB has developed into a major research field in stellar astrophysics, driven by a fruitful interaction of observations and theory. Milestones on the observational side are the opening-up of the IR and radio/sub-mm domains, critical for determining the physical conditions in the circumstellar envelopes (including dust properties and kinematics of outflows), and the recent progress in high-angular resolution techniques, spanning from the visual to radio regime, which is crucial for direct insights into the extended dynamical atmospheres of AGB stars where the winds are triggered. On the theoretical side, significant progress has been made in understanding essential ingredients of the mass-loss process, in particular stellar pulsation and convection, dust formation and the onset of dust-driven winds, as well as in modeling these phenomena quantitatively, from first principles.

The picture that has emerged can be summarized as follows: The slow, massive winds of AGB stars, with typical mass loss rates of 10^{-7}–$10^{-5}\,M_\odot$/year, and above (see Sect. 3), are most likely triggered by a combination of pulsation-induced shock waves, creating favorable conditions for dust formation in the outer atmospheric layers, and the subsequent radiative acceleration of these newly-formed dust grains, which

collide with the surrounding gas and drag it along (Sect. 4). Mid-IR spectroscopy and spectro-interferometry have made it possible to identify the chemical composition of circumstellar dust, and where different species originate. Combining these observations with results of dynamical atmosphere and winds models suggests that the winds of typical M-type AGB stars are driven by scattering of stellar photons on Fe-poor, Mg-rich silicate grains which start forming at around 2 stellar radii and grow to sizes in the range of 0.1–1 μm, possibly on top of Al_2O_3 cores which condense even closer to the star (Sect. 4.2). The winds of C-type AGB stars, on the other hand, are generally assumed to be driven by radiation pressure on opaque amorphous carbon grains which produce significant circumstellar reddening but otherwise featureless IR spectra.

A more or less pronounced clumpiness of the circumstellar gas and dust—first indicated by observations of maser emission in the CSE and CO rotational-line data, but recently also confirmed by direct imaging of the close stellar environment—may be a consequence of giant convection cells inside the star which introduce significant deviations from spherical symmetry in the dynamical atmosphere (Sects. 6.1.1, 6.1.2 and 6.2.1). On larger scales, however, these effects seem to average out, and no significant deviations from spherical symmetry are detected on global scales in the CSEs, except where the effects of close companions or interaction with the surrounding ISM are concerned (Sect. 6.1.3). In contrast, the large-scale radial structure of the CSE may show signs of changing mass-loss rates and wind velocities on evolutionary timescales, e.g., in the form of so-called detached shells (Sect. 3.1.2).

A major motivation for studying the mass loss of AGB stars is its impact on stellar and galactic chemical evolution, in particular regarding the final fate of low- and intermediate mass stars, the potential progenitor systems of type Ia supernovae, and the origin of the building blocks of our own solar system. Understanding these phenomena requires a quantitative description of how mass-loss rates and chemical yields depend on fundamental stellar parameters. As discussed in Sect. 5, neither a purely empirical approach, nor current wind models, can provide a satisfactory answer to this question, and further work in both areas is needed. Therefore, we round off this review with a discussion of what will be required to make significant progress in estimating and predicting the characteristics of stellar mass loss on the AGB.

7.1 Empirical mass loss rates: updates to the standard CSE model

Except for detailed studies of individual objects at high spatial resolution, the concept of a standard CSE seems indispensable for estimating the mass-loss rates of larger samples of AGB stars. We discuss here improvements of the standard CSE model, divided into the gas and dust components that are well within reach in the near future.

The gas CSE Rotational lines of CO will remain the best probe of the gas, and the standard CSE model will be tailored to fit an accurate radiative transfer treatment of this molecule. The physical model presently used dates back to the work of Goldreich and Scoville (1976) to a large extent. In particular, the treatment of the thermodynamics of the gas, and the chemistry of CO, its formation and subsequent photodissociation, needs to be updated, as well as observationally constrained. The initial abundance of

CO with respect to H_2, determined by the chemistry in the extended stellar atmosphere, can possibly be directly estimated in some cases using UV absorption lines. The treatment of CO photodissociation has been updated since the work of Mamon et al. (1988), but it remains to be adapted to the special case of AGB CSEs. An inherent uncertainty in this context is the local interstellar radiation field, but observations with, e.g., ALMA will put constraints on the CO line brightness distributions. Another problem in this context is that other molecules may affect the thermodynamics of the gas through line cooling/heating of the gas, e.g., H_2O in O-CSEs and HCN in C-CSEs. This requires that both the chemistry and the radiative transfer of these molecules must be solved self-consistently together with the CO modelling. The physical conditions in the inner CSE, e.g., the acceleration zone, are expected to have only a small influence on the CO mass-loss-rate estimates as long as they are not dependent solely on higher-energy lines. Observations of the 21 cm line of HI can be used to firmly establish to what extent the estimated CO mass-loss rates must be corrected for the loss of also atomic gas.

The circumstellar medium is in all likelihood inhomogeneous, but the characteristics of this "clumpiness" are unknown, and they will be difficult to estimate. A reasonable way forward is to develop radiative line transfer codes for clumpy media in order to get at least an understanding of the magnitude of the uncertainties of mass-loss rates estimated using a standard CSE. The same applies to large-scale asymmetries in the CSEs, where 3D radiative transfer codes can be used in the analysis. High-angular resolution observations will put constraints on the occurrence and the nature of any asymmetries on larger scales.

The dust CSE In the case of the dust, the challenges are considerable if the uncertainties in the dust-mass-loss-rate estimates, not to mention the conversion to the total mass-loss rate, are to be lowered well below the present order-of-magnitude level. The dust velocity cannot be measured, but possibly estimated with a good enough model for the dust acceleration. The dust composition must be determined, as well as the grain size distribution, and the structure of the grains (shape, coated, porous, etc.). This is a monumental task. As a reasonable step forward it would be of significant interest to study in detail the dust characteristics of the nearby sources that are well-studied in circumstellar CO. The estimated gas-mass-loss rates and gas terminal expansion velocities will provide important constraints on the dust modelling. This can serve as a very useful comparison sample for studies of mass loss in, e.g., extragalactic sources.

7.2 Improving theoretical predictions of mass loss rates

The simplistic descriptions of AGB mass loss in current stellar evolution models are regularly pointed out as a major shortcoming (see, e.g., Karakas and Lattanzio 2014; Lattanzio and Karakas 2016), and the related uncertainties propagate into our understanding of galactic evolution and the origin of chemical elements, as well as of cosmic dust. As discussed in Sect. 5, it is unlikely that the dependence of mass loss rates on individual stellar parameters can be derived with empirical methods alone; a theoretical approach, based on predictive dynamical models, is required to construct a more realistic description of AGB mass loss for stellar evolution. The

present wind models will have to be improved in several respects to achieve this goal, as discussed below. In this context, it should also be noted that future descriptions of AGB mass-loss rates will probably not take the form of simple power laws, but rather of multi-dimensional look-up tables (see Mattsson et al. 2010).

Input data and basic physical processes As mentioned in Sect. 4.2, PEDDRO models need a wide range of micro-physical input data, in order to describe the formation, composition and optical properties of the wind-driving dust grains. At present, critical data are uncertain or missing, e.g., reliable optical constants in the near-IR regime (where the stellar flux peaks) for near-transparent condensates which are most likely to form close to the star, due to low radiative heating. The optical properties of such materials may depend critically on structural defects or a contamination with trace elements (e.g., Zeidler et al. 2011), with potential consequences for wind driving. New measurement or ab-initio calculations of optical properties, taking into account such effects for materials expected to form in the close stellar vicinity, are needed. Furthermore, there are many open questions regarding the formation of the first seed nuclei from the gas phase (see, e.g., Gobrecht et al. 2016; Gail et al. 2016), and more work is needed in that area to arrive at a consistent, comprehensive description of the nucleation process. Further possible sources of uncertainty are non-equilibrium effects in the gas-phase chemistry, introduced by strong atmospheric shock waves (e.g., Cherchneff 2006, 2011, 2012), or non-LTE radiative cooling of the shocked gas (e.g., Willson 2000; Schirrmacher et al. 2003).

Gas dynamics and morphology In the current generation of PEDDRO models, the effects of sub-photospheric dynamical processes (pulsation, convection) are introduced by variable inner boundary conditions, just below the photosphere ("piston models"). Improvements, based on dynamical models of pulsation and convection, are in progress, in order to eliminate free parameters and discrepancies in time-dependent behavior between wind models and observations (e.g., Liljegren et al. 2016, 2017). Effects of purely radial pulsations (leading to spherical shock waves), as well as local effects of dust formation and radial radiative acceleration, can be described reasonably well with 1D (spherically symmetric) dynamical models, as demonstrated by a comparison of the resulting wind properties and photometry with observations (see Sect. 5.1). In the long run, however, it will be necessary to construct global 3D dynamical models, reaching from the convective/pulsating stellar interior to the wind acceleration zone, in order to take intrinsically 3-dimensional effects properly into account, and to study the emergence of morphological structures in the outflows. At present, it is unclear if magnetic fields play a dynamical role in AGB stars, and further work, both observational and theoretical, will be required to answer this question.

7.3 Observational perspectives

The prospects for gathering observational information crucial to our understanding of stellar mass loss on the AGB must be considered excellent. High-resolution spectrometers, high-angular-resolution instrumentation, often combined, and high-sensitivity telescopes are now available over a broad wavelength range; in principle, only obser-

vational capabilities in the far-IR will be limited for quite some time. To be able to actually resolve the stellar surfaces and simultaneously determine the kinematics of their extended atmospheres is now possible. Combination of data obtained at different wavelengths will probe different parts of the atmosphere. Characteristics of inhomogeneities in density and temperature, shock-wave velocities, dust components, magnetic fields, etc., will be in reach. Such detailed observations are essential, but probably restricted to a limited sample of stars. In particular, since a full understanding will require observations at different epochs, in the best case in a coordinated way between different observing facilities. Hence, a substantial amount of observing time will be needed. In this context, one should not forget traditional photometry time-series observations that provide additional constraints on, e.g., wind models.

A better understanding of the physics/chemistry of CSEs is of importance for the reliability of mass-loss-rate estimates based on CO rotational lines as discussed above. The relevant information in this context will come through detailed imaging of the CO brightness distributions for a moderate-sized sample of stars. It should preferably be done in several rotational transitions since they are, at least partly, sensitive to different radial regimes. This study should be complemented with a detailed study of the dust characteristics of the same objects. In this way, we will have a sample of AGB stars where both the gas and the dust in the CSEs are observed in the best possible way. Only in this way will we be able to identify the shortcomings of our present methods for estimating stellar mass-loss rates on the AGB. Single-dish observations of larger samples of objects, well-controlled in terms of completeness, etc., will add understanding on how the mass-loss rate depends on various stellar characteristics, but we iterate the words of caution associated with observational biases in this context. It appears particularly important to investigate objects in their final high-mass-loss-rate phase, because these are the objects that dominate the mass return of AGB stars. Finally, we have to accept that mass-loss rates estimated from CO rotational lines will inevitably be very limited in their coverage of environmental characteristics. The initial results show that it will be very difficult to go beyond the MCs even with such a powerful instrument as ALMA.

We need to understand the dependence of stellar mass-loss rate, and also dust production, on metallicity in order to assess the importance of AGB stars in the gas/dust cycle over cosmic time. This will require observations of dust emission in the near- to far-IR. Observationally, it is important to find effective discriminators between different types of objects, not the least eliminating the RSGs that contaminate in increasing portion the samples of more distant objects. Unfortunately, the filters of the major instruments are often not tailored for this specific purpose. Finally, the methods for estimating the dust-mass-loss rate, and the scaling to the total mass-loss rate, must be refined, but this will not be an easy task.

Acknowledgements We thank K. Eriksson, S. Bladh, S. Ramstedt, R. Lombaert, B. Freytag, L.A. Willson, B. Gustafsson and M. André for numerous discussions and comments on earlier versions of the manuscript, and S. Liljegren for providing custom-made figures.

References

Abate C, Pols OR, Izzard RG, Mohamed SS, de Mink SE (2013) Wind Roche-lobe overflow: application to carbon-enhanced metal-poor stars. A&A 552:A26. https://doi.org/10.1051/0004-6361/201220007. arXiv:1302.4441

Airapetian V, Carpenter KG, Ofman L (2010) Winds from luminous late-type stars. II. Broadband frequency distribution of Alfvén waves. ApJ 723:1210–1218. https://doi.org/10.1088/0004-637X/723/2/1210. arXiv:1008.3955

Airapetian VS, Ofman L, Robinson RD, Carpenter K, Davila J (2000) Winds from luminous late-type stars. I. The effects of nonlinear Alfvén waves. ApJ 528:965–971. https://doi.org/10.1086/308198

Alvarez R, Jorissen A, Plez B, Gillet D, Fokin A (2000) Envelope tomography of long-period variable stars. I. The Schwarzschild mechanism and the Balmer emission lines. A&A 362:655–665 arXiv:astro-ph/0010132

Arimatsu K, Izumiura H, Ueta T, Yamamura I, Onaka T (2011) Detection of the Detached dust shell of U antliae at mid-infrared wavelengths with AKARI/IRC. ApJL 729:L19. https://doi.org/10.1088/2041-8205/729/2/L19. arXiv:1102.0339

Aringer B, Girardi L, Nowotny W, Marigo P, Lederer MT (2009) Synthetic photometry for carbon rich giants. I. Hydrostatic dust-free models. A&A 503:913–928. https://doi.org/10.1051/0004-6361/200911703. arXiv:0905.4415

Arndt TU, Fleischer AJ, Sedlmayr E (1997) Circumstellar dust shells around long-period variables. VI. an approximative formula for the mass loss rate of C-rich stars. A&A 327:614–619

Aronson E, Bladh S, Höfner S (2017) Modelling polarized light from dust shells surrounding asymptotic giant branch stars. A&A 603:A116, https://doi.org/10.1051/0004-6361/201730495. arXiv:1705.08703

Auer LH, Woolf NJ (1965) Mass loss and the formation of White-dwarf stars. ApJ 142:182

Balick B (2004) NGC 6543. I. Understanding the anatomy of the Cat's Eye. AJ 127:2262–2268. https://doi.org/10.1086/382518

Baud B, Habing HJ (1983) The maser strength of OH/IR stars, evolution of mass loss and the creation of a superwind. A&A 127:73–83

Bedijn PJ (1987) Dust shells around Miras and OH/IR stars—interpretation of IRAS and other infrared measurements. A&A 186:136–152

Bedijn PJ (1988) Pulsation, mass loss, and evolution of upper asymptotic giant branch stars. A&A 205:105–124

Bergeat J, Chevallier L (2005) The mass loss of C-rich giants. A&A 429:235–246. https://doi.org/10.1051/0004-6361:20041280. arXiv:astro-ph/0601366

Bergeat J, Knapik A, Rutily B (2001) The effective temperatures of carbon-rich stars. A&A 369:178–209. https://doi.org/10.1051/0004-6361:20010106

Bessell MS, Brett JM, Wood PR, Scholz M (1989) The effects of photospheric extension upon the spectra of M-type Mira variables. A&A 213:209–225

Bessell MS, Scholz M, Wood PR (1996) Phase and cycle dependence of the photospheric structure and observable properties of Mira variables. A&A 307:481–499

Bladh S, Höfner S (2012) Exploring wind-driving dust species in cool luminous giants. I. Basic criteria and dynamical models of M-type AGB stars. A&A 546:A76. https://doi.org/10.1051/0004-6361/201219138

Bladh S, Höfner S, Nowotny W, Aringer B, Eriksson K (2013) Exploring wind-driving dust species in cool luminous giants. II. Constraints from photometry of M-type AGB stars. A&A 553:A20. https://doi.org/10.1051/0004-6361/201220590

Bladh S, Höfner S, Aringer B, Eriksson K (2015) Exploring wind-driving dust species in cool luminous giants. III. Wind models for M-type AGB stars: dynamic and photometric properties. A&A 575:A105. https://doi.org/10.1051/0004-6361/201424917 arXiv:1502.00032

Bladh S, Paladini C, Höfner S, Aringer B (2017) Tomography of silicate dust around M-type AGB stars I. Diagnostics based on dynamical models. arXiv:1709.09797

Blasius TD, Monnier JD, Tuthill PG, Danchi WC, Anderson M (2012) The Keck Aperture masking experiment: dust-enshrouded red giants. MNRAS 426:2652–2667. https://doi.org/10.1111/j.1365-2966.2012.21543.x. arXiv:1208.0958

Blöcker T (1995) Stellar evolution of low and intermediate-mass stars. I. Mass loss on the AGB and its consequences for stellar evolution. A&A 297:727

Blommaert JADL, Groenewegen MAT, Okumura K, Ganesh S, Omont A, Cami J, Glass IS, Habing HJ, Schultheis M, Simon G, van Loon JT (2006) ISO mid-infrared spectroscopy of Galactic Bulge AGB stars. A&A 460:555–563. https://doi.org/10.1051/0004-6361:20066145. arXiv:astro-ph/0609230

Blommaert JADL, de Vries BL, Waters LBFM, Waelkens C, Min M, Van Winckel H, Molster F, Decin L, Groenewegen MAT, Barlow M, García-Lario P, Kerschbaum F, Posch T, Royer P, Ueta T, Vandenbussche B, Van de Steene G, van Hoof P (2014) Herschel/PACS observations of the 69 μm band of crystalline olivine around evolved stars. A&A 565:A109. https://doi.org/10.1051/0004-6361/201322554. arXiv:1403.6335

Bowen GH (1988) Dynamical modeling of long-period variable star atmospheres. ApJ 329:299–317

Boyer ML, Skillman ED, van Loon JT, Gehrz RD, Woodward CE (2009) A Spitzer study of asymptotic giant branch stars. III. Dust production and gas return in local group Dwarf irregular galaxies. ApJ 697:1993–2014. https://doi.org/10.1088/0004-637X/697/2/1993. arXiv:0903.3871

Boyer ML, Srinivasan S, Riebel D, McDonald I, van Loon JT, Clayton GC, Gordon KD, Meixner M, Sargent BA, Sloan GC (2012) The dust budget of the small magellanic cloud: are asymptotic giant branch stars the primary dust source at low metallicity? ApJ 748:40. https://doi.org/10.1088/0004-637X/748/1/40. arXiv:1201.5384

Boyer ML, McDonald I, Srinivasan S, Zijlstra A, van Loon JT, Olsen KAG, Sonneborn G (2015) Identification of a class of low-mass asymptotic giant branch stars struggling to become carbon stars in the magellanic clouds. ApJ 810:116. https://doi.org/10.1088/0004-637X/810/2/116 arXiv:1507.07003

Boyer ML, McQuinn KBW, Barmby P, Bonanos AZ, Gehrz RD, Gordon KD, Groenewegen MAT, Lagadec E, Lennon D, Marengo M, McDonald I, Meixner M, Skillman E, Sloan GC, Sonneborn G, van Loon JT, Zijlstra A (2015) An infrared census of DUST in nearby galaxies with spitzer (DUSTiNGS). II. Discovery of metal-poor dusty AGB stars. ApJ 800:51. https://doi.org/10.1088/0004-637X/800/1/51 arXiv:1412.0695

Bujarrabal V, Alcolea J, Van Winckel H, Santander-García M, Castro-Carrizo A (2013) Extended rotating disks around post-AGB stars. A&A 557:A104. https://doi.org/10.1051/0004-6361/201322015. arXiv:1307.1975

Burns D, Baldwin JE, Boysen RC, Haniff CA, Lawson PR, Mackay CD, Rogers J, Scott TR, St-Jacques D, Warner PJ, Wilson DMA, Young JS (1998) Large-amplitude periodic variations in the angular diameter of R Leonis. MNRAS 297:462–466. https://doi.org/10.1046/j.1365-8711.1998.01527.x

Buss RH Jr, Tielens AGGM, Cohen M, Werner MW, Bregman JD, Witteborn FC (1993) Infrared spectra of transition objects and the composition and evolution of carbon dust. ApJ 415:250–257. https://doi.org/10.1086/173160

Cami J, Bernard-Salas J, Peeters E, Malek SE (2010) Detection of C_{60} and C_{70} in a young planetary Nebula. Science 329:1180. https://doi.org/10.1126/science.1192035

Castro-Carrizo A, Quintana-Lacaci G, Neri R, Bujarrabal V, Schöier FL, Winters JM, Olofsson H, Lindqvist M, Alcolea J, Lucas R, Grewing M (2010) Mapping the ^{12}CO J = 1-0 and J = 2-1 emission in AGB and early post-AGB circumstellar envelopes. I. The COSAS program, first sample. A&A 523:A59. https://doi.org/10.1051/0004-6361/201014755

Ceillier T, Tayar J, Mathur S, Salabert D, García RA, Stello D, Pinsonneault MH, van Saders J, Beck PG, Bloemen S (2017) Surface rotation of Kepler red giant stars. A&A 605:A111. https://doi.org/10.1051/0004-6361/201629884 arXiv:1707.05989

Cernicharo J, Guélin M, Kahane C (2000) A lambda 2 mm molecular line survey of the C-star envelope IRC+10216. A&AS 142:181–215

Cernicharo J, Teyssier D, Quintana-Lacaci G, Daniel F, Agúndez M, Velilla-Prieto L, Decin L, Guélin M, Encrenaz P, García-Lario P, de Beck E, Barlow MJ, Groenewegen MAT, Neufeld D, Pearson J (2014) Discovery of time variation of the intensity of molecular lines in IRC+10216 in the submillimeter and far-infrared domains. ApJL 796:L21. https://doi.org/10.1088/2041-8205/796/1/L21. arXiv:1410.5852

Cernicharo J, Marcelino N, Agúndez M, Guélin M (2015) Molecular shells in IRC+10216: tracing the mass loss history. A&A 575:A91. https://doi.org/10.1051/0004-6361/201424565. arXiv:1412.1948

Cherchneff I (2006) A chemical study of the inner winds of asymptotic giant branch stars. A&A 456:1001–1012. https://doi.org/10.1051/0004-6361:20064827

Cherchneff I (2011) Water in IRC+10216: a genuine formation process by shock-induced chemistry in the inner wind. A&A 526:L11. https://doi.org/10.1051/0004-6361/201016035. arXiv:1012.5076

Cherchneff I (2012) The inner wind of IRC+10216 revisited: new exotic chemistry and diagnostic for dust condensation in carbon stars. A&A 545:A12. https://doi.org/10.1051/0004-6361/201118542. arXiv:1111.6809

Cherchneff I, Barker JR, Tielens AGGM (1991) Polycyclic aromatic hydrocarbon optical properties and contribution to the acceleration of stellar outflows. ApJ 377:541–552. https://doi.org/10.1086/170383

Claussen MJ, Sjouwerman LO, Rupen MP, Olofsson H, Schöier FL, Bergman P, Knapp GR (2011) A pilot imaging line survey of RW LMi and IK tau using the expanded very large array. ApJL 739:L5. https://doi.org/10.1088/2041-8205/739/1/L5. arXiv:1106.6064

Cox NLJ, Kerschbaum F, van Marle AJ, Decin L, Ladjal D, Mayer A, Groenewegen MAT, van Eck S, Royer P, Ottensamer R, Ueta T, Jorissen A, Mecina M, Meliani Z, Luntzer A, Blommaert JADL, Posch T, Vandenbussche B, Waelkens C (2012) A far-infrared survey of bow shocks and detached shells around AGB stars and red supergiants. A&A 537:A35. https://doi.org/10.1051/0004-6361/201117910. arXiv:1110.5486

Cox NLJ, Kerschbaum F, van Marle AJ, Decin L, Ladjal D, Mayer A, Groenewegen MAT, van Eck S, Royer P, Ottensamer R, Ueta T, Jorissen A, Mecina M, Meliani Z, Luntzer A, Blommaert JADL, Posch T, Vandenbussche B, Waelkens C (2012) A far-infrared survey of bow shocks and detached shells around AGB stars and red supergiants (Corrigendum). A&A 543:C1. https://doi.org/10.1051/0004-6361/201117910e

Cranmer SR, Saar SH (2011) Testing a predictive theoretical model for the mass loss rates of cool stars. ApJ 741:54. https://doi.org/10.1088/0004-637X/741/1/54. arXiv:1108.4369

Cummings JD, Kalirai JS, Tremblay PE, Ramirez-Ruiz E (2015) Initial-final mass relation for 3 to 4 $M_{\odot}$ progenitors of white dwarfs from the single cluster NGC 2099. ApJ 807:90. https://doi.org/10.1088/0004-637X/807/1/90 arXiv:1505.06737

Cummings JD, Kalirai JS, Tremblay PE, Ramirez-Ruiz E (2016) Two massive White Dwarfs from NGC 2323 and the initial–final mass relation for progenitors of 4 to 6.5 M. ApJ 818:84. https://doi.org/10.3847/0004-637X/818/1/84 arXiv:1601.03053

Danilovich T, Bergman P, Justtanont K, Lombaert R, Maercker M, Olofsson H, Ramstedt S, Royer P (2014) Detailed modelling of the circumstellar molecular line emission of the S-type AGB star W Aquilae. A&A 569:A76. https://doi.org/10.1051/0004-6361/201322807. arXiv:1408.1825

Danilovich T, Teyssier D, Justtanont K, Olofsson H, Cerrigone L, Bujarrabal V, Alcolea J, Cernicharo J, Castro-Carrizo A, Garcia-Lario P, Marston A (2015) New observations and models of circumstellar CO line emission of AGB stars in the Herschel SUCCESS programme. A&A 581:A60

De Beck E, Decin L, de Koter A, Justtanont K, Verhoelst T, Kemper F, Menten KM (2010) Probing the mass-loss history of AGB and red supergiant stars from CO rotational line profiles. II. CO line survey of evolved stars: derivation of mass-loss rate formulae. A&A 523:A18. https://doi.org/10.1051/0004-6361/200913771 arXiv:1008.1083

De Marco O, Izzard RG (2017) Dawes review 6: the impact of companions on stellar evolution. PASA 34:e001. https://doi.org/10.1017/pasa.2016.52 arXiv:1611.03542

de Vries BL, Min M, Waters LBFM, Blommaert JADL, Kemper F (2010) Determining the forsterite abundance of the dust around asymptotic giant branch stars. A&A 516:A86. https://doi.org/10.1051/0004-6361/200913588. arXiv:1003.3100

de Vries BL, Blommaert JADL, Waters LBFM, Waelkens C, Min M, Lombaert R, Van Winckel H (2014) The problematically short superwind of OH/IR stars. Probing the outflow with the 69 μm spectral band of forsterite. A&A 561:A75. https://doi.org/10.1051/0004-6361/201322546. arXiv:1311.6908

Decin L, Hony S, de Koter A, Justtanont K, Tielens AGGM, Waters LBFM (2006) Probing the mass-loss history of AGB and red supergiant stars from CO rotational line profiles. I. Theoretical model—mass-loss history unravelled in VY CMa. A&A 456:549–563. https://doi.org/10.1051/0004-6361:20065230. arXiv:astro-ph/0606299

Decin L, Justtanont K, De Beck E, Lombaert R, de Koter A, Waters LBFM, Marston AP, Teyssier D, Schöier FL, Bujarrabal V, Alcolea J, Cernicharo J, Dominik C, Melnick G, Menten K, Neufeld DA, Olofsson H, Planesas P, Schmidt M, Szczerba R, de Graauw T, Helmich F, Roelfsema P, Dieleman P, Morris P, Gallego JD, Díez-González MC, Caux E (2010) Water content and wind acceleration in the envelope

around the oxygen-rich AGB star IK Tauri as seen by Herschel/HIFI. A&A 521:L4. https://doi.org/10.1051/0004-6361/201015069. arXiv:1007.1102

Decin L, Richards AMS, Neufeld D, Steffen W, Melnick G, Lombaert R (2015) ALMA data suggest the presence of spiral structure in the inner wind of CW Leonis. A&A 574:A5. https://doi.org/10.1051/0004-6361/201424593. arXiv:1410.2060

Dell'Agli F, García-Hernández DA, Ventura P, Schneider R, Di Criscienzo M, Rossi C (2015) AGB stars in the SMC: evolution and dust properties based on Spitzer observations. MNRAS 454:4235–4249. https://doi.org/10.1093/mnras/stv2298. arXiv:1510.01230

Dell'Agli F, Di Criscienzo M, Boyer ML, García-Hernández DA (2016) Evolved stars in the local group galaxies - I. AGB evolution and dust production in IC 1613. MNRAS 460:4230–4241. https://doi.org/10.1093/mnras/stw1276. arXiv:1605.08090

Deutsch AJ (1956) The circumstellar envelope of alpha herculis. ApJ 123:210

Dinh-V-Trung Lim J (2009) Tracing the asymmetry in the envelope around the carbon star CIT 6. ApJ 701:292–297. https://doi.org/10.1088/0004-637X/701/1/292. arXiv:0812.3372

Dorfi EA, Höfner S (1996) Non-spherical dust driven winds of slowly rotating AGB stars. A&A 313:605–610

Dorschner J (2010) From dust astrophysics towards dust mineralogy—a historical review. In: Henning T (ed) Astromineralogy, Lecture Notes in Physics, vol 815. Springer, Berlin, pp 1–60. https://doi.org/10.1007/978-3-642-13259-9_1

Dreyer C, Hegmann M, Sedlmayr E (2011) Circumstellar dust shells around long-period variables. X. Dynamics of envelopes around standard luminous. C-rich AGB stars. A&A 525:A135. https://doi.org/10.1051/0004-6361/201015651. arXiv:1010.4183

Duthu A, Herpin F, Wiesemeyer H, Baudry A, Lèbre A, Paubert G (2017) Magnetic field in IRC+10216 and other C-rich evolved stars. A&A 604:A12. https://doi.org/10.1051/0004-6361/201730485. arXiv:1705.04588

Elitzur M, Ivezić Ž (2001) Dusty winds - I. Self-similar solutions. MNRAS 327:403

Elitzur M, Brown JA, Johnson HR (1989) On the onset of mass loss in late-type stars. ApJL 341:L95–L98. https://doi.org/10.1086/185466

Engels D, Bunzel F (2015) A database of circumstellar OH masers. A&A 582:A68. https://doi.org/10.1051/0004-6361/201322589. arXiv:1508.06200

Engels D, Jiménez-Esteban F (2007) Lifetime of OH masers at the tip of the asymptotic giant branch. A&A 475:941–948. https://doi.org/10.1051/0004-6361:20078250. arXiv:0710.1697

Engels D, Kreysa E, Schultz GV, Sherwood WA (1983) The nature of OH/IR stars. I. Infrared Mira variables. A&A 124:123

Engels D, Etoka S, Gérard E, Richards A (2015) Phase-lag distances of OH Masing AGB stars. In: Kerschbaum F, Wing RF, Hron J (eds) Why Galaxies care about AGB Stars III: a closer look in space and time, astronomical society of the Pacific, ASP conference series, vol 497, p 473. arXiv:1503.04674

Epchtein N, Le Bertre T, Lepine JRD (1990) Carbon star envelopes—near-IR photometry, mass loss and evolutionary status of a sample of IRAS stars. A&A 227:82–104

Eriksson K, Nowotny W, Höfner S, Aringer B, Wachter A (2014) Synthetic photometry for carbon-rich giants. IV. An extensive grid of dynamic atmosphere and wind models. A&A 566:A95. https://doi.org/10.1051/0004-6361/201323241. arXiv:1404.7515

Ferrarotti AS, Gail HP (2006) Composition and quantities of dust produced by AGB-stars and returned to the interstellar medium. A&A 447:553–576. https://doi.org/10.1051/0004-6361:20041198

Fleischer AJ, Gauger A, Sedlmayr E (1992) Circumstellar dust shells around long-period variables. I. Dynamical models of C-stars including dust formation, growth and evaporation. A&A 266:321–339

Fonfría JP, Cernicharo J, Richter MJ, Fernández-López M, Velilla Prieto L, Lacy JH (2015) The abundance of ^{28}Si^{32}S, ^{29}Si^{32}S, ^{28}Si^{34}S, and ^{30}Si^{32}S in the inner layers of the envelope of IRC+10216. MNRAS 453:439–449. https://doi.org/10.1093/mnras/stv1634. arXiv:1507.06037

Fong D, Justtanont K, Meixner M, Campbell MT (2002) Imaging the circumstellar envelope of OH 26.5+0.6. A&A 396:581–587

Freytag B, Höfner S (2008) Three-dimensional simulations of the atmosphere of an AGB star. A&A 483:571–583

Freytag B, Liljegren S, Höfner S (2017) Global 3D radiation-hydrodynamics models of AGB stars. Effects of convection and radial pulsations on atmospheric structures. A&A 600:A137. https://doi.org/10.1051/0004-6361/201629594. arXiv:1702.05433

Gail HP, Sedlmayr E (1988) Dust formation in stellar winds. IV–heteromolecular carbon grain formation and growth. A&A 206:153–168
Gail HP, Sedlmayr E (1999) Mineral formation in stellar winds. I. Condensation sequence of silicate and iron grains in stationary oxygen rich outflows. A&A 347:594–616
Gail HP, Sedlmayr E (2014) Physics and chemistry of circumstellar dust shells. Cambridge University Press, Cambridge
Gail HP, Scholz M, Pucci A (2016) Silicate condensation in Mira variables. A&A 591:A17. https://doi.org/10.1051/0004-6361/201628113. arXiv:1604.04636
Gauger A, Gail HP, Sedlmayr E (1990) Dust formation, growth and evaporation in a cool pulsating circumstellar shell. A&A 235:345–361
Gehrz RD, Woolf NJ (1971) Mass loss from M stars. ApJ 165:285
Gillett FC, Low FJ, Stein WA (1968) Stellar spectra from 2.8 to 14 microns. ApJ 154:677
Gilman RC (1969) On the composition of circumstellar grains. ApJL 155:L185
Girardi L, Marigo P (2007) The TP-AGB phase. Lifetimes from C and M star counts in magellanic cloud clusters. A&A 462:237–243. https://doi.org/10.1051/0004-6361:20065249. arXiv:astro-ph/0609626
Girardi L, Williams BF, Gilbert KM, Rosenfield P, Dalcanton JJ, Marigo P, Boyer ML, Dolphin A, Weisz DR, Melbourne J, Olsen KAG, Seth AC, Skillman E (2010) The ACS nearby galaxy survey treasury. IX. Constraining asymptotic giant branch evolution with old metal-poor galaxies. ApJ 724:1030–1043. https://doi.org/10.1088/0004-637X/724/2/1030. arXiv:1009.4618
Glass IS, Schultheis M, Blommaert JADL, Sahai R, Stute M, Uttenthaler S (2009) Mid-infrared period-magnitude relations for AGB stars. MNRAS 395:L11–L15. https://doi.org/10.1111/j.1745-3933.2009.00628.x. arXiv:0901.3032
Glassgold AE, Huggins PJ (1983) Atomic and molecular hydrogen in the circumstellar envelopes of late-type stars. MNRAS 203:517–532
Gobrecht D, Cherchneff I, Sarangi A, Plane JMC, Bromley ST (2016) Dust formation in the oxygen-rich AGB star IK Tauri. A&A 585:A6. https://doi.org/10.1051/0004-6361/201425363. arXiv:1509.07613
Goldman SR, van Loon JT, Zijlstra AA, Green JA, Wood PR, Nanni A, Imai H, Whitelock PA, Matsuura M, Groenewegen MAT, Gómez JF (2017) The wind speeds, dust content, and mass-loss rates of evolved AGB and RSG stars at varying metallicity. MNRAS 465:403–433. https://doi.org/10.1093/mnras/stw2708. arXiv:1610.05761
Goldreich P, Scoville N (1976) OH-IR stars. I—physical properties of circumstellar envelopes. ApJ 205:144–154
Golriz SS, Blommaert JADL, Vanhollebeke E, Groenewegen MAT, Habing HJ, Kemper F, Schultheis M, Tielens AGGM, Waters LBFM, Wood PR, Cami J (2014) Infrared spectroscopy of asymptotic giant branch stars in the Galactic bulge. MNRAS 443:3402–3434. https://doi.org/10.1093/mnras/stu1317
González Delgado D, Olofsson H, Schwarz HE, Eriksson K, Gustafsson B, Gledhill T (2003) Imaging polarimetry of stellar light scattered in detached shells around the carbon stars R Scl and U Ant. A&A 399:1021–1035
González Delgado D, Olofsson H, Kerschbaum F, Schöier FL, Lindqvist M, Groenewegen MAT (2003) Thermal SiO radio line emission towards M-type AGB stars: a probe of circumstellar dust formation and dynamics. A&A 411:123–147. https://doi.org/10.1051/0004-6361:20031068. arXiv:astro-ph/0302179
Groenewegen MAT (1994) A revised model for circumstellar molecular emission. A&A 290:531–543
Groenewegen MAT (1994) The mass loss rates of OH/IR 32.8-0.3 and OH/IR 44.8-2.3. A&A 290:544–552
Groenewegen MAT, Blommaert JADL (2005) Mira variables in the OGLE bulge fields. A&A 443:143–156. https://doi.org/10.1051/0004-6361:20053131. arXiv:astro-ph/0506338
Groenewegen MAT, Whitelock PA (1996) A revised period-luminosity relation for carbon Miras. MNRAS 281:1347–1351
Groenewegen MAT, Whitelock PA, Smith CH, Kerschbaum F (1998) Dust shells around carbon Mira variables. MNRAS 293:18
Groenewegen MAT, Wood PR, Sloan GC, Blommaert JADL, Cioni MRL, Feast MW, Hony S, Matsuura M, Menzies JW, Olivier EA, Vanhollebeke E, van Loon JT, Whitelock PA, Zijlstra AA, Habing HJ, Lagadec E (2007) Luminosities and mass-loss rates of carbon stars in the magellanic clouds. MNRAS 376:313–337. https://doi.org/10.1111/j.1365-2966.2007.11428.x
Groenewegen MAT, Sloan GC, Soszyński I, Petersen EA (2009) Luminosities and mass-loss rates of SMC and LMC AGB stars and red supergiants. A&A 506:1277–1296. https://doi.org/10.1051/0004-6361/200912678. arXiv:0908.3087

Groenewegen MAT, Vlemmings WHT, Marigo P, Sloan GC, Decin L, Feast MW, Goldman SR, Justtanont K, Kerschbaum F, Matsuura M, McDonald I, Olofsson H, Sahai R, van Loon JT, Wood PR, Zijlstra AA, Bernard-Salas J, Boyer ML, Guzman-Ramirez L, Jones OC, Lagadec E, Meixner M, Rawlings MG, Srinivasan S (2016) The ALMA detection of CO rotational line emission in AGB stars in the large magellanic cloud. A&A 596:A50. https://doi.org/10.1051/0004-6361/201629590. arXiv:1609.09647

Gruendl RA, Chu YH, Seale JP, Matsuura M, Speck AK, Sloan GC, Looney LW (2008) Discovery of extreme carbon stars in the large magellanic cloud. ApJL 688:L9. https://doi.org/10.1086/593979. arXiv:0809.5107

Guandalini R, Busso M, Ciprini S, Silvestro G, Persi P (2006) Infrared photometry and evolution of mass-losing AGB stars. I. Carbon stars revisited. A&A 445:1069–1080. https://doi.org/10.1051/0004-6361:20053208. arXiv:astro-ph/0509739

Gullieuszik M, Groenewegen MAT, Cioni MRL, de Grijs R, van Loon JT, Girardi L, Ivanov VD, Oliveira JM, Emerson JP, Guandalini R (2012) The VMC survey. III. Mass-loss rates and luminosities of LMC AGB stars. A&A 537:A105. https://doi.org/10.1051/0004-6361/201117493. arXiv:1110.4497

Habing HJ (1996) Circumstellar envelopes and asymptotic giant branch stars. A&ARv 7:97–207

Habing HJ, Olofsson H (eds) (2003) Asymptotic giant branch stars, Astronomy and Astrophysics Library. Springer, New York. https://doi.org/10.1007/978-1-4757-3876-6

Harper GM, O'Riain N, Ayres TR (2013) Chromospheric thermal continuum millimetre emission from non-dusty K and M red giants. MNRAS 428:2064–2073. https://doi.org/10.1093/mnras/sts170. arXiv:1210.2627

Hartmann L, MacGregor KB (1980) Momentum and energy deposition in late-type stellar atmospheres and winds. ApJ 242:260–282. https://doi.org/10.1086/158461

Haubois X, Wittkowski M, Perrin G, Kervella P, Mérand A, Thiébaut E, Ridgway ST, Ireland M, Scholz M (2015) Resolving asymmetries along the pulsation cycle of the Mira star X Hydrae. A&A 582:A71. https://doi.org/10.1051/0004-6361/201526482. arXiv:1508.03180

He JH, Chen PS (2001) On the Difference between Type E and Type A OH/IR stars. AJ 121:2752–2757. https://doi.org/10.1086/320380. arXiv:astro-ph/0503558

Herwig F (2005) Evolution of asymptotic giant branch stars. ARA&A 43:435–479. https://doi.org/10.1146/annurev.astro.43.072103.150600

Heske A, Habing HJ, Forveille T, Omont A, van der Veen WECJ (1990) Deficiency of CO emission from massive envelopes around cool OH/IR stars. A&A 239:173–185

Hill SJ, Willson LA (1979) Theoretical velocity structure of long-period variable star photospheres. ApJ 229:1029–1045. https://doi.org/10.1086/157038

Hinkle KH, Hall DNB, Ridgway ST (1982) Time series infrared spectroscopy of the Mira variable Chi Cygni. ApJ 252:697–714. https://doi.org/10.1086/159596

Hinkle KH, Lebzelter T, Scharlach WWG (1997) Infrared velocities of long period variables: CO delta(upsilon)=3 in four miras and five SR variables. AJ 114:2686. https://doi.org/10.1086/118679

Hoai DT, Nhung PT, Gérard E, Matthews LD, Villaver E, Le Bertre T (2015) Modelling the H I 21-cm line profile from circumstellar shells around red giants. MNRAS 449:2386–2395. https://doi.org/10.1093/mnras/stv486

Höfner S (2008) Winds of M-type AGB stars driven by micron-sized grains. A&A 491:L1–L4

Höfner S (2016) (Re)Solving mysteries of convection and mass loss of agb stars: what new models and observations tell us about long-standing problems. In: 19th Cambridge workshop on cool stars, stellar systems, and the sun (CS19), p 19. https://doi.org/10.5281/zenodo.154673. arXiv:1610.08937

Höfner S, Dorfi EA (1997) Dust formation in winds of long-period variables. IV. Atmospheric dynamics and mass loss. A&A 319:648–654

Höfner S, Gautschy-Loidl R, Aringer B, Jørgensen UG (2003) Dynamic model atmospheres of AGB stars III. Effects of frequency-dependent radiative transfer. A&A 399:589–601

Höfner S, Bladh S, Aringer B, Ahuja R (2016) Dynamic atmospheres and winds of cool luminous giants. I. Al_2O_3 and silicate dust in the close vicinity of M-type AGB stars. A&A 594:A108. https://doi.org/10.1051/0004-6361/201628424. arXiv:1605.09730

Homan W, Decin L, de Koter A, van Marle AJ, Lombaert R, Vlemmings W (2015) Simplified models of stellar wind anatomy for interpreting high-resolution data. Analytical approach to embedded spiral geometries. A&A 579:A118. https://doi.org/10.1051/0004-6361/201525933. arXiv:1504.04996

Huggins PJ, Mauron N, Wirth EA (2009) The shapes of asymptotic giant branch envelopes as probes of binary companions. MNRAS 396:1805–1814. https://doi.org/10.1111/j.1365-2966.2009.14874.x. arXiv:0904.1884

Iaconi R, Reichardt T, Staff J, De Marco O, Passy JC, Price D, Wurster J, Herwig F (2017) The effect of a wider initial separation on common envelope binary interaction simulations. MNRAS 464:4028–4044. https://doi.org/10.1093/mnras/stw2377. arXiv:1603.01953

Ireland MJ, Scholz M, Wood PR (2004) On the observability of geometric pulsation of M-type Mira variables. MNRAS 352:318–324. https://doi.org/10.1111/j.1365-2966.2004.07928.x

Ireland MJ, Tuthill PG, Bedding TR, Robertson JG, Jacob AP (2004) Multiwavelength diameters of nearby Miras and semiregular variables. MNRAS 350:365–374. https://doi.org/10.1111/j.1365-2966.2004.07651.x. arXiv:astro-ph/0402326

Ireland MJ, Tuthill PG, Davis J, Tango W (2005) Dust scattering in the Miras R Car and RR Sco resolved by optical interferometric polarimetry. MNRAS 361:337–344. https://doi.org/10.1111/j.1365-2966.2005.09181.x. arXiv:astro-ph/0505112

Ireland MJ, Scholz M, Wood PR (2008) Dynamical opacity-sampling models of Mira variables—I. Modelling description and analysis of approximations. MNRAS 391:1994–2002. https://doi.org/10.1111/j.1365-2966.2008.14037.x

Ireland MJ, Scholz M, Wood PR (2011) Dynamical opacity-sampling models of Mira variables—II. Time-dependent atmospheric structure and observable properties of four M-type model series. MNRAS 418:114–128. https://doi.org/10.1111/j.1365-2966.2011.19469.x. arXiv:1107.3619

Ita Y, Onaka T, Kato D, Tanabé T, Sakon I, Kaneda H, Kawamura A, Shimonishi T, Wada T, Usui F, Koo BC, Matsuura M, Takahashi H, Nakada Y, Hasegawa T, Tamura M (2008) AKARI IRC survey of the large magellanic cloud: outline of the survey and initial results. PASJ 60:S435–S451 arXiv:0808.3022

Ivezić Ž, Elitzur M (1995) Infrared emission and dynamics of outlfows in late-type stars. ApJ 445:415–432

Ivezić Ž, Elitzur M (2010) Dusty winds—II. Observational implications. MNRAS 404:1415–1424. https://doi.org/10.1111/j.1365-2966.2010.16348.x. arXiv:1001.4579

Izumiura H, Ueta T, Yamamura I, Matsunaga N, Ita Y, Matsuura M, Nakada Y, Fukushi H, Mito H, Tanabé T, Hashimoto O (2011) Extended dust shell of the carbon star U Hydrae observed with AKARI. A&A 528:A29. https://doi.org/10.1051/0004-6361/201015163

Jeong KS, Winters JM, Le Bertre T, Sedlmayr E (2003) Self-consistent modeling of the outflow from the O-rich Mira IRC -20197. A&A 407:191–206. https://doi.org/10.1051/0004-6361:20030693

Jiménez-Esteban FM, Engels D (2015) Study of extremely reddened AGB stars in the Galactic bulge. A&A 579:A76. https://doi.org/10.1051/0004-6361/201424609. arXiv:1504.05712

Jones OC, McDonald I, Rich RM, Kemper F, Boyer ML, Zijlstra AA, Bendo GJ (2015) A Spitzer Space Telescope survey of extreme asymptotic giant branch stars in M32. MNRAS 446:1584–1596. https://doi.org/10.1093/mnras/stu2169. arXiv:1410.4504

Jorgensen UG, Johnson HR (1992) Radiative force on molecules and its possible role for mass loss in evolved AGB stars. A&A 265:168–176

Jura M (1988) Mass loss from S stars. ApJS 66:33–41

Justtanont K, Skinner CJ, Tielens AGGM, Meixner M, Baas F (1996) Modeling of the dust and gas outflows from OH 26.5 + 0.6: the superwind. ApJ 456:337

Justtanont K, Teyssier D, Barlow MJ, Matsuura M, Swinyard B, Waters LBFM, Yates J (2013) OH/IR stars and their superwinds as observed by the Herschel Space Observatory. A&A 556:A101. https://doi.org/10.1051/0004-6361/201321812. arXiv:1306.1777

Justtanont K, Barlow MJ, Blommaert J, Decin L, Kerschbaum F, Matsuura M, Olofsson H, Owen P, Royer P, Swinyard B, Teyssier D, Waters LBFM, Yates J (2015) Herschel observations of extreme OH/IR stars. The isotopic ratios of oxygen as a sign-post for the stellar mass. A&A 578:A115. https://doi.org/10.1051/0004-6361/201526270. arXiv:1505.05750

Kalirai JS, Marigo P, Tremblay PE (2014) The core mass growth and stellar lifetime of thermally pulsing asymptotic giant branch stars. ApJ 782:17. https://doi.org/10.1088/0004-637X/782/1/17. arXiv:1312.4544

Kamiński T, Wong KT, Schmidt MR, Müller HSP, Gottlieb CA, Cherchneff I, Menten KM, Keller D, Brünken S, Winters JM, Patel NA (2016) An observational study of dust nucleation in Mira (o Ceti). I. Variable features of AlO and other Al-bearing species. A&A 592:A42. https://doi.org/10.1051/0004-6361/201628664. arXiv:1604.05641

Karakas AI, Lattanzio JC (2014) The Dawes review 2: nucleosynthesis and stellar yields of low- and intermediate-mass single stars. PASA 31:e030. https://doi.org/10.1017/pasa.2014.21. arXiv:1405.0062

Karovicova I, Wittkowski M, Ohnaka K, Boboltz DA, Fossat E, Scholz M (2013) New insights into the dust formation of oxygen-rich AGB stars. A&A 560:A75. https://doi.org/10.1051/0004-6361/201322376

Karovska M, Nisenson P, Papaliolios C, Boyle RP (1991) Asymmetries in the atmosphere of Mira. ApJL 374:L51–L54. https://doi.org/10.1086/186069

Karovska M, Hack W, Raymond J, Guinan E (1997) First hubble space telescope observations of Mira AB wind-accreting binary systems. ApJL 482:L175–L178. https://doi.org/10.1086/310704

Kerschbaum F, Olofsson H (1999) Oxygen-rich semiregular and irregular variables. A catalogue of circumstellar CO observations. A&AS 138:299–322

Kerschbaum F, Maercker M, Brunner M, Lindqvist M, Olofsson H, Mecina M, De Beck E, Groenewegen MAT, Lagadec E, Mohamed S, Paladini C, Ramstedt S, Vlemmings WHT, Wittkowski M (2017) Rings and filaments: the remarkable detached CO shell of U Antliae. A&A 605:A116. https://doi.org/10.1051/0004-6361/201730665. arXiv:1708.02915

Kervella P, Montargès M, Lagadec E, Ridgway ST, Haubois X, Girard JH, Ohnaka K, Perrin G, Gallenne A (2015) The dust disk and companion of the nearby AGB star L_2 Puppis. SPHERE/ZIMPOL polarimetric imaging at visible wavelengths. A&A 578:A77. https://doi.org/10.1051/0004-6361/201526194. arXiv:1511.04448

Khouri T, de Koter A, Decin L, Waters LBFM, Lombaert R, Royer P, Swinyard B, Barlow MJ, Alcolea J, Blommaert JADL, Bujarrabal V, Cernicharo J, Groenewegen MAT, Justtanont K, Kerschbaum F, Maercker M, Marston A, Matsuura M, Melnick G, Menten KM, Olofsson H, Planesas P, Polehampton E, Posch T, Schmidt M, Szczerba R, Vandenbussche B, Yates J (2014) The wind of W Hydrae as seen by Herschel. I. The CO envelope. A&A 561:A5. https://doi.org/10.1051/0004-6361/201322578. arXiv:1403.2892

Khouri T, de Koter A, Decin L, Waters LBFM, Maercker M, Lombaert R, Alcolea J, Blommaert JADL, Bujarrabal V, Groenewegen MAT, Justtanont K, Kerschbaum F, Matsuura M, Menten KM, Olofsson H, Planesas P, Royer P, Schmidt MR, Szczerba R, Teyssier D, Yates J (2014) The wind of W Hydrae as seen by Herschel. II. The molecular envelope of W Hydrae. A&A 570:A67. https://doi.org/10.1051/0004-6361/201424298. arXiv:1409.0396

Khouri T, Waters LBFM, de Koter A, Decin L, Min M, de Vries BL, Lombaert R, Cox NLJ (2015) Dusty wind of W Hydrae. Multi-wavelength modelling of the present-day and recent mass loss. A&A 577:A114. https://doi.org/10.1051/0004-6361/201425092. arXiv:1503.04765

Khouri T, Maercker M, Waters LBFM, Vlemmings WHT, Kervella P, de Koter A, Ginski C, De Beck E, Decin L, Min M, Dominik C, O'Gorman E, Schmid HM, Lombaert R, Lagadec E (2016) Study of the inner dust envelope and stellar photosphere of the AGB star R Doradus using SPHERE/ZIMPOL. A&A 591:A70. https://doi.org/10.1051/0004-6361/201628435. arXiv:1605.05504

Khouri T, Vlemmings WHT, Ramstedt S, Lombaert R, Maercker M, De Beck E (2016) ALMA observations of the vibrationally excited rotational CO transition $v = 1, J = 3 - -2$ towards five AGB stars. MNRAS 463:L74–L78. https://doi.org/10.1093/mnrasl/slw161. arXiv:1608.03271

Kim H, Taam RE (2012) A new method of determining the characteristics of evolved binary systems revealed in the observed circumstellar patterns: application to AFGL 3068. ApJL 759:L22. https://doi.org/10.1088/2041-8205/759/1/L22. arXiv:1209.6360

Kim H, Taam RE (2012) Probing substellar companions of asymptotic giant branch stars through spirals and arcs. ApJ 744:136. https://doi.org/10.1088/0004-637X/744/2/136. arXiv:1110.1288

Kim H, Taam RE (2012) Wide binary effects on asymmetries in asymptotic giant branch circumstellar envelopes. ApJ 759:59. https://doi.org/10.1088/0004-637X/759/1/59. arXiv:1209.2128

Kim H, Hsieh IT, Liu SY, Taam RE (2013) Evidence of a binary-induced spiral from an incomplete ring pattern of CIT 6. ApJ 776:86. https://doi.org/10.1088/0004-637X/776/2/86. arXiv:1308.4140

Kim H, Liu SY, Hirano N, Zhao-Geisler R, Trejo A, Yen HW, Taam RE, Kemper F, Kim J, Byun DY, Liu T (2015) High-resolution CO observation of the carbon star CIT 6 revealing the spiral structure and a nascent bipolar outflow. ApJ 814:61. https://doi.org/10.1088/0004-637X/814/1/61. arXiv:1510.03916

Kim H, Trejo A, Liu SY, Sahai R, Taam RE, Morris MR, Hirano N, Hsieh IT (2017) The large-scale nebular pattern of a superwind binary in an eccentric orbit. Nat Astron 1:0060. https://doi.org/10.1038/s41550-017-0060. arXiv:1704.00449

Kozasa T, Sogawa H (1997) Formation of Al_2O_3 grains and the 13μM feature in circumstellar envelopes of oxygen-rich AGB stars. Ap&SS 255:437–443. https://doi.org/10.1023/A:1001570111811

Kozasa T, Sogawa H (1997) Formation of dust grains in circumstellar envelopes of oxygen-rich AGB stars. Ap&SS 251:165–170. https://doi.org/10.1023/A:1000780505203

Krüger D, Sedlmayr E (1997) Two-fluid models for stationary dust driven winds. II. The grain size distribution in consideration of drift. A&A 321:557–567

Krüger D, Gauger A, Sedlmayr E (1994) Two-fluid models for stationary dust-driven winds. I. Momentum and energy balance. A&A 290:573–589

Lacour S, Thiébaut E, Perrin G, Meimon S, Haubois X, Pedretti E, Ridgway ST, Monnier JD, Berger JP, Schuller PA, Woodruff H, Poncelet A, Le Coroller H, Millan-Gabet R, Lacasse M, Traub W (2009) The pulsation of χ Cygni imaged by optical interferometry: a novel technique to derive distance and mass of Mira stars. ApJ 707:632–643. https://doi.org/10.1088/0004-637X/707/1/632. arXiv:0910.3869

Lagadec E, Zijlstra AA, Matsuura M, Menzies JW, van Loon JT, Whitelock PA (2008) Dust mass-loss rates from asymptotic giant branch stars in the Fornax and Sagittarius dwarf spheroidal galaxies. MNRAS 383:399–410. https://doi.org/10.1111/j.1365-2966.2007.12561.x. arXiv:0710.4468

Lagadec E, Zijlstra AA, Sloan GC, Wood PR, Matsuura M, Bernard-Salas J, Blommaert JADL, Cioni MRL, Feast MW, Groenewegen MAT, Hony S, Menzies JW, van Loon JT, Whitelock PA (2009) Metal-rich carbon stars in the Sagittarius dwarf spheroidal galaxy. MNRAS 396:598–608. https://doi.org/10.1111/j.1365-2966.2009.14736.x. arXiv:0903.1045

Lagadec E, Zijlstra AA, Mauron N, Fuller G, Josselin E, Sloan GC, Riggs AJE (2010) The low wind expansion velocity of metal-poor carbon stars in the Halo and the Sagittarius stream. MNRAS 403:1331–1338. https://doi.org/10.1111/j.1365-2966.2009.16088.x. arXiv:0911.4376

Lagadec E, Sloan GC, Zijlstra AA, Mauron N, Houck JR (2012) Dust and gas in carbon stars towards the Galactic halo. MNRAS 427:2588–2596. https://doi.org/10.1111/j.1365-2966.2012.21874.x. arXiv:1208.1306

Lamers HJGLM, Cassinelli JP (1999) Introduction to stellar winds. Cambridge University Press, Cambridge

Lattanzio J, Karakas A (2016) Uncertainties in AGB evolution and nucleosynthesis. J Phys Conf Ser 728(2):022002. https://doi.org/10.1088/1742-6596/728/2/022002. arXiv:1605.06163

Le Bertre T, Gérard E (2004) The circumstellar environments of EP Aqr and Y CVn probed by the H I emission at 21 cm. A&A 419:549–561. https://doi.org/10.1051/0004-6361:20035797

Lèbre A, Aurière M, Fabas N, Gillet D, Herpin F, Konstantinova-Antova R, Petit P (2014) Search for surface magnetic fields in Mira stars. First detection in χ Cygni. A&A 561:A85. https://doi.org/10.1051/0004-6361/201322826. arXiv:1310.4379

Lebzelter T, Wood PR (2011) Long period variables and mass loss in the globular clusters NGC 362 and NGC 2808. A&A 529:A137. https://doi.org/10.1051/0004-6361/201016319. arXiv:1103.5299

Lebzelter T, Hinkle KH, Wood PR, Joyce RR, Fekel FC (2005) A study of bright Southern long period variables. A&A 431:623–634. https://doi.org/10.1051/0004-6361:20041575. arXiv:astro-ph/0411599

Lebzelter T, Wood PR, Hinkle KH, Joyce RR, Fekel FC (2005) Long period variables in the globular cluster 47 Tuc: radial velocity variations. A&A 432:207–217. https://doi.org/10.1051/0004-6361:20047164. arXiv:astro-ph/0501336

Li X, Millar TJ, Walsh C, Heays AN, van Dishoeck EF (2014) Photodissociation and chemistry of N_2 in the circumstellar envelope of carbon-rich AGB stars. A&A 568:A111. https://doi.org/10.1051/0004-6361/201424076. arXiv:1406.7354

Li X, Millar TJ, Heays AN, Walsh C, van Dishoeck EF, Cherchneff I (2016) Chemistry and distribution of daughter species in the circumstellar envelopes of O-rich AGB stars. A&A 588:A4. https://doi.org/10.1051/0004-6361/201525739

Liljegren S, Höfner S, Nowotny W, Eriksson K (2016) Dust-driven winds of AGB stars: the critical interplay of atmospheric shocks and luminosity variations. A&A 589:A130. https://doi.org/10.1051/0004-6361/201527885. arXiv:1603.06735

Liljegren S, Höfner S, Eriksson K, Nowotny W (2017) Pulsation-induced atmospheric dynamics in M-type AGB stars. Effects on wind properties, photometric variations and near-IR CO line profiles. A&A 606:A6. https://doi.org/10.1051/0004-6361/201731137. arXiv:1706.08332

Lindqvist M, Olofsson H, Lucas R, Schöier FL, Neri R, Bujarrabal V, Kahane C (1999) The young detached CO shell around U Camelopardalis. A&A 351:L1–L4

Linsky JL, Haisch BM (1979) Outer atmospheres of cool stars. I—the sharp division into solar-type and non-solar-type stars. ApJL 229:L27–L32. https://doi.org/10.1086/182924

Liu J, Jiang BW, Li A, Gao J (2017) On the silicate crystallinities of oxygen-rich evolved stars and their mass-loss rates. MNRAS 466:1963–1986. https://doi.org/10.1093/mnras/stw3165. arXiv:1612.02115

Lombaert R, de Vries BL, de Koter A, Decin L, Min M, Smolders K, Mutschke H, Waters LBFM (2012) Observational evidence for composite grains in an AGB outflow. MgS in the extreme carbon star LL Pegasi. A&A 544:L18. https://doi.org/10.1051/0004-6361/201219782. arXiv:1207.1606

Lombaert R, Decin L, de Koter A, Blommaert JADL, Royer P, De Beck E, de Vries BL, Khouri T, Min M (2013) H_2O vapor excitation in dusty AGB envelopes. A PACS view of OH 127.8+0.0. A&A 554:A142. https://doi.org/10.1051/0004-6361/201218974. arXiv:1505.07696

Lombaert R, Decin L, Royer P, de Koter A, Cox NLJ, González-Alfonso E, Neufeld D, De Ridder J, Agúndez M, Blommaert JADL, Khouri T, Groenewegen MAT, Kerschbaum F, Cernicharo J, Vandenbussche B, Waelkens C (2016) Constraints on the H_2O formation mechanism in the wind of carbon-rich AGB stars. A&A 588:A124. https://doi.org/10.1051/0004-6361/201527049. arXiv:1601.07017

Lykou F, Klotz D, Paladini C, Hron J, Zijlstra AA, Kluska J, Norris BRM, Tuthill PG, Ramstedt S, Lagadec E, Wittkowski M, Maercker M, Mayer A (2015) Dissecting the AGB star L_2 Puppis: a torus in the making. A&A 576:A46. https://doi.org/10.1051/0004-6361/201322828. arXiv:1503.05031

Maercker M, Olofsson H, Eriksson K, Gustafsson B, Schöier FL (2010) The detached dust and gas shells around the carbon star U Antliae. A&A 511:A37. https://doi.org/10.1051/0004-6361/200913376. arXiv:0912.2673

Maercker M, Mohamed S, Vlemmings WHT, Ramstedt S, Groenewegen MAT, Humphreys E, Kerschbaum F, Lindqvist M, Olofsson H, Paladini C, Wittkowski M, de Gregorio-Monsalvo I, Nyman LA (2012) Unexpectedly large mass loss during the thermal pulse cycle of the red giant star R Sculptoris. Nature 490:232–234. https://doi.org/10.1038/nature11511. arXiv:1210.3030

Maercker M, Ramstedt S, Leal-Ferreira ML, Olofsson G, Floren HG (2014) The detached dust shells around the carbon AGB stars R Sculptoris and V644 Scorpii. A&A 570:A101. https://doi.org/10.1051/0004-6361/201424892. arXiv:1409.4410

Maercker M, Danilovich T, Olofsson H, De Beck E, Justtanont K, Lombaert R, Royer P (2016) A HIFI view on circumstellar H_2O in M-type AGB stars: radiative transfer, velocity profiles, and H_2O line cooling. A&A 591:A44. https://doi.org/10.1051/0004-6361/201628310. arXiv:1605.00504

Maercker M, Vlemmings WHT, Brunner M, De Beck E, Humphreys EM, Kerschbaum F, Lindqvist M, Olofsson H, Ramstedt S (2016) A detailed view of the gas shell around R Sculptoris with ALMA. A&A 586:A5. https://doi.org/10.1051/0004-6361/201527128. arXiv:1512.01350

Males JR, Close LM, Skemer AJ, Hinz PM, Hoffmann WF, Marengo M (2012) Four decades of IRC +10216: evolution of a carbon-rich dust shell resolved at 10 μm with MMT adaptive optics and MIRAC4. ApJ 744:133. https://doi.org/10.1088/0004-637X/744/2/133. arXiv:1111.4687

Mamon GA, Glassgold AE, Huggins PJ (1988) The photodissociation of CO in circumstellar envelopes. ApJ 328:797–808

Marengo M, Ivezić Ž, Knapp GR (2001) 100-yr mass-loss modulations on the asymptotic giant branch. MNRAS 324:1117–1130

Mastrodemos N, Morris M (1999) Bipolar pre-planetary nebulae: hydrodynamics of dusty winds in binary systems. II. Morphology of the circumstellar envelopes. ApJ 523:357–380

Matsuura M, Zijlstra AA, Bernard-Salas J, Menzies JW, Sloan GC, Whitelock PA, Wood PR, Cioni MRL, Feast MW, Lagadec E, van Loon JT, Groenewegen MAT, Harris GJ (2007) Spitzer space telescope spectral observations of AGB stars in the Fornax dwarf spheroidal galaxy. MNRAS 382:1889–1900. https://doi.org/10.1111/j.1365-2966.2007.12501.x. arXiv:0709.3199

Matsuura M, Barlow MJ, Zijlstra AA, Whitelock PA, Cioni MRL, Groenewegen MAT, Volk K, Kemper F, Kodama T, Lagadec E, Meixner M, Sloan GC, Srinivasan S (2009) The global gas and dust budget of the large magellanic cloud: AGB stars and supernovae, and the impact on the ISM evolution. MNRAS 396:918–934. https://doi.org/10.1111/j.1365-2966.2009.14743.x. arXiv:0903.1123

Matsuura M, Woods PM, Owen PJ (2013) The global gas and dust budget of the small magellanic cloud. MNRAS 429:2527–2536. https://doi.org/10.1093/mnras/sts521. arXiv:1212.1468

Matthews LD, Le Bertre T, Gérard E, Johnson MC (2013) A H I imaging survey of asymptotic giant branch stars. AJ 145:97. https://doi.org/10.1088/0004-6256/145/4/97. arXiv:1301.7429

Matthews LD, Gérard E, Le Bertre T (2015) Discovery of a shell of neutral atomic hydrogen surrounding the carbon star IRC+10216. MNRAS 449:220–233. https://doi.org/10.1093/mnras/stv263. arXiv:1502.02050

Mattsson L, Höfner S, Herwig F (2007) Mass loss evolution and the formation of detached shells around TP-AGB stars. A&A 470:339–352. https://doi.org/10.1051/0004-6361:20066368. arXiv:0705.2232

Mattsson L, Wahlin R, Höfner S, Eriksson K (2008) Intense mass loss from C-rich AGB stars at low metallicity? A&A 484:L5–L8. https://doi.org/10.1051/0004-6361:200809689. arXiv:0804.2482

Mattsson L, Wahlin R, Höfner S (2010) Dust driven mass loss from carbon stars as a function of stellar parameters. I. A grid of solar-metallicity wind models. A&A 509:A14

Mauron N, Huggins PJ (2006) Imaging the circumstellar envelopes of AGB stars. A&A 452:257–268. https://doi.org/10.1051/0004-6361:20054739. arXiv:astro-ph/0602623

Mauron N, Huggins PJ, Cheung CL (2013) Deep optical imaging of asymptotic giant branch circumstellar envelopes. A&A 551:A110. https://doi.org/10.1051/0004-6361/201219517. arXiv:1302.4263

Mayer A, Jorissen A, Kerschbaum F, Ottensamer R, Nowotny W, Cox NLJ, Aringer B, Blommaert JADL, Decin L, van Eck S, Gail HP, Groenewegen MAT, Kornfeld K, Mecina M, Posch T, Vandenbussche B, Waelkens C (2013) Large-scale environments of binary AGB stars probed by Herschel. I. Morphology statistics and case studies of R Aquarii and W Aquilae. A&A 549:A69. https://doi.org/10.1051/0004-6361/201219259. arXiv:1211.3595

Mayer A, Jorissen A, Paladini C, Kerschbaum F, Pourbaix D, Siopis C, Ottensamer R, Mečina M, Cox NLJ, Groenewegen MAT, Klotz D, Sadowski G, Spang A, Cruzalèbes P, Waelkens C (2014) Large-scale environments of binary AGB stars probed by Herschel. II. Two companions interacting with the wind of π^1 Gruis. A&A 570:A113. https://doi.org/10.1051/0004-6361/201424465. arXiv:1408.3965

McDonald I, Zijlstra AA (2016) Pulsation-triggered mass loss from AGB stars: the 60 day critical period. ApJL 823:L38. https://doi.org/10.3847/2041-8205/823/2/L38. arXiv:1605.02622

McDonald I, van Loon JT, Decin L, Boyer ML, Dupree AK, Evans A, Gehrz RD, Woodward CE (2009) Giants in the globular cluster ω Centauri: dust production, mass-loss and distance. MNRAS 394:831–856. https://doi.org/10.1111/j.1365-2966.2008.14370.x. arXiv:0812.0326

McDonald I, Johnson CI, Zijlstra AA (2011) Empirical determination of the integrated red giant and horizontal branch stellar mass-loss in ω Centauri. MNRAS 416:L6–L10. https://doi.org/10.1111/j.1745-3933.2011.01086.x. arXiv:1106.1016

McDonald I, Zijlstra AA, Lagadec E, Sloan GC, Boyer ML, Matsuura M, Smith RJ, Smith CL, Yates JA, van Loon JT, Jones OC, Ramstedt S, Avison A, Justtanont K, Olofsson H, Blommaert JADL, Goldman SR, Groenewegen MAT (2015) ALMA reveals sunburn: CO dissociation around AGB stars in the globular cluster 47 Tucanae. MNRAS 453:4324–4336. https://doi.org/10.1093/mnras/stv1968. arXiv:1508.05240

Meixner M, Gordon KD, Indebetouw R, Hora JL, Whitney B, Blum R, Reach W, Bernard JP, Meade M, Babler B, Engelbracht CW, For BQ, Misselt K, Vijh U, Leitherer C, Cohen M, Churchwell EB, Boulanger F, Frogel JA, Fukui Y, Gallagher J, Gorjian V, Harris J, Kelly D, Kawamura A, Kim S, Latter WB, Madden S, Markwick-Kemper C, Mizuno A, Mizuno N, Mould J, Nota A, Oey MS, Olsen K, Onishi T, Paladini R, Panagia N, Perez-Gonzalez P, Shibai H, Sato S, Smith L, Staveley-Smith L, Tielens AGGM, Ueta T, van Dyk S, Volk K, Werner M, Zaritsky D (2006) Spitzer survey of the large magellanic cloud: surveying the agents of a galaxy's evolution (SAGE). I. Overview and initial results. AJ 132:2268–2288. https://doi.org/10.1086/508185. arXiv:astro-ph/0606356

Mendoza EE (1967) Multicolor photometry of long period variables. Boletin de los Observatorios Tonantzintla y Tacubaya 4:114–148

Messenger SJ, Speck A, Volk K (2013) Probing the 30 μm feature: lessons from extreme carbon stars. ApJ 764:142. https://doi.org/10.1088/0004-637X/764/2/142

Michałowski MJ (2015) Dust production 680–850 million years after the Big Bang. A&A 577:A80. https://doi.org/10.1051/0004-6361/201525644. arXiv:1503.08210

Millar TJ (2016) Chemistry in AGB stars: successes and challenges. J Phys: Conf Ser 728(5):052001. https://doi.org/10.1088/1742-6596/728/5/052001. arXiv:1605.03365

Miller Bertolami MM (2016) New models for the evolution of post-asymptotic giant branch stars and central stars of planetary nebulae. A&A 588:A25. https://doi.org/10.1051/0004-6361/201526577. arXiv:1512.04129

Mohamed S, Podsiadlowski P (2007) Wind Roche-Lobe Overflow: a new mass-transfer mode for wide binaries. In: Napiwotzki R, Burleigh MR (eds) 15th European workshop on white dwarfs, astronomical society of the Pacific, ASP conference series, vol 372, p 397

Mohamed S, Podsiadlowski P (2012) Mass transfer in Mira-type binaries. Baltic Astron 21:88–96

Molster FJ, Waters LBFM, Kemper F (2010) The mineralogy of interstellar and circumstellar dust in galaxies. In: Henning T (ed) Astromineralogy, Lecture Notes in Physics, vol 815. Springer, Berlin, pp 143–201. https://doi.org/10.1007/978-3-642-13259-9_3

Monnier JD, Berger JP, Le Bouquin JB, Tuthill PG, Wittkowski M, Grellmann R, Müller A, Renganswany S, Hummel C, Hofmann KH, Schertl D, Weigelt G, Young J, Buscher D, Sanchez-Bermudez J, Alberdi A, Schoedel R, Köhler R, Soulez F, Thiébaut É, Kluska J, Malbet F, Duvert G, Kraus S, Kloppenborg BK, Baron F, de Wit WJ, Rivinius T, Merand A (2014) The 2014 interferometric imaging beauty contest. Optical Infrared Interferom IV 9146:91461Q. https://doi.org/10.1117/12.2057312

Montez R Jr, Ramstedt S, Kastner JH, Vlemmings W, Sanchez E (2017) A catalog of GALEX ultraviolet emission from asymptotic giant branch stars. ApJ 841:33. https://doi.org/10.3847/1538-4357/aa704d. arXiv:1705.05371

Mosser B, Dziembowski WA, Belkacem K, Goupil MJ, Michel E, Samadi R, Soszyński I, Vrard M, Elsworth Y, Hekker S, Mathur S (2013) Period-luminosity relations in evolved red giants explained by solar-like oscillations. A&A 559:A137. https://doi.org/10.1051/0004-6361/201322243. arXiv:1310.0839

Nanni A, Bressan A, Marigo P, Girardi L (2013) Evolution of thermally pulsing asymptotic giant branch stars—II. Dust production at varying metallicity. MNRAS 434:2390–2417. https://doi.org/10.1093/mnras/stt1175. arXiv:1306.6183

Nanni A, Bressan A, Marigo P, Girardi L (2014) Evolution of thermally pulsing asymptotic giant branch stars—III. Dust production at supersolar metallicities. MNRAS 438:2328–2340. https://doi.org/10.1093/mnras/stt2348. arXiv:1312.0875

Netzer N, Elitzur M (1993) The dynamics of stellar outflows dominated by interaction of dust and radiation. ApJ 410:701–713

Neugebauer G, Leighton RB (1969) Two-micron sky survey. A preliminary catalogue. NASA SP-3047, Washington

Nicholls CP, Wood PR (2012) Eccentric ellipsoidal red giant binaries in the LMC: complete orbital solutions and comments on interaction at periastron. MNRAS 421:2616–2628. https://doi.org/10.1111/j.1365-2966.2012.20492.x. arXiv:1201.1043

Nie JD, Wood PR, Nicholls CP (2012) Predicting the fate of binary red giants using the observed sequence E star population: binary planetary nebula nuclei and post-RGB stars. MNRAS 423:2764–2780. https://doi.org/10.1111/j.1365-2966.2012.21087.x. arXiv:1204.2648

Nie JD, Wood PR, Nicholls CP (2017) The orbital nature of 81 ellipsoidal red giant binaries in the large magellanic cloud. ApJ 835:209. https://doi.org/10.3847/1538-4357/835/2/209. arXiv:1702.02376

Niedzielski A, Deka-Szymankiewicz B, Adamczyk M, Adamów M, Nowak G, Wolszczan A (2016) The Penn State—Toruń centre for astronomy planet search stars. A&A 585:A73. https://doi.org/10.1051/0004-6361/201527362

Nittler LR, Ciesla F (2016) Astrophysics with extraterrestrial materials. ARA&A 54:53–93. https://doi.org/10.1146/annurev-astro-082214-122505

Norris BRM, Tuthill PG, Ireland MJ, Lacour S, Zijlstra AA, Lykou F, Evans TM, Stewart P, Bedding TR (2012) A close halo of large transparent grains around extreme red giant stars. Nature 484:220–222. https://doi.org/10.1038/nature10935

Nowotny W, Höfner S, Aringer B (2010) Line formation in AGB atmospheres including velocity effects. Molecular line profile variations of long period variables. A&A 514:A35. https://doi.org/10.1051/0004-6361/200911899. arXiv:1002.1849

Nowotny W, Aringer B, Höfner S, Lederer MT (2011) Synthetic photometry for carbon-rich giants. II. The effects of pulsation and circumstellar dust. A&A 529:A129. https://doi.org/10.1051/0004-6361/201016272. arXiv:1103.5005

Nowotny W, Aringer B, Höfner S, Eriksson K (2013) Synthetic photometry for carbon-rich giants. III. Tracing the sequence of mass-losing galactic C-type Miras. A&A 552:A20. https://doi.org/10.1051/0004-6361/201220335. arXiv:1302.3715

Nyman LÅ, Booth RS, Carlstrom U, Habing HJ, Heske A, Sahai R, Stark R, van der Veen WEJC, Winnberg A (1992) A survey of circumstellar CO emission from a sample of IRAS point sources. A&AS 93:121–150

Ohnaka K, Schertl D, Hofmann KH, Weigelt G (2015) AMBER-NACO aperture-synthesis imaging of the half-obscured central star and the edge-on disk of the red giant L_2 Puppis. A&A 581:A127. https://doi.org/10.1051/0004-6361/201526338. arXiv:1507.06668

Ohnaka K, Weigelt G, Hofmann KH (2016) Clumpy dust clouds and extended atmosphere of the AGB star W Hydrae revealed with VLT/SPHERE-ZIMPOL and VLTI/AMBER. A&A 589:A91. https://doi.org/10.1051/0004-6361/201628229. arXiv:1603.01197

Ohnaka K, Weigelt G, Hofmann KH (2017) Clumpy dust clouds and extended atmosphere of the AGB star W Hydrae revealed with VLT/SPHERE-ZIMPOL and VLTI/AMBER. II. Time variations between pre-maximum and minimum light. A&A 597:A20. https://doi.org/10.1051/0004-6361/201629761. arXiv:1611.04622

Olofsson H (2003) Asymptotic giant branch stars. In: Habing HJ, Olofsson H (eds) Asymptotic giant branch stars, Astronomy and Astrophysics Library. Springer, New York, pp 325–410. https://doi.org/10.1007/978-1-4757-3876-6_7

Olofsson H, Carlström U, Eriksson K, Gustafsson B, Willson LA (1990) Bright carbon stars with detached circumstellar envelopes—a natural consequence of helium shell flashes? A&A 230:L13–L16
Olofsson H, Eriksson K, Gustafsson B, Carlström U (1993) A study of circumstellar envelopes around bright carbon stars. I—structure, kinematics, and mass-loss rate. ApJS 87:267–304
Olofsson H, Bergman P, Eriksson K, Gustafsson B (1996) Carbon stars with episodic mass loss: observations and models of molecular emission from detached circumstellar shells. A&A 311:587–615
Olofsson H, Bergman P, Lucas R, Eriksson K, Gustafsson B, Bieging JH (2000) A high-resolution study of episodic mass loss from the carbon star TT Cygni. A&A 353:583–597
Olofsson H, González Delgado D, Kerschbaum F, Schöier F (2002) Mass loss rates of a sample of irregularly and semiregularly variable AGB-stars of M-type. A&A 391:1053–1067
Olofsson H, Maercker M, Eriksson K, Gustafsson B, Schöier F (2010) High-resolution HST/ACS images of detached shells around carbon stars. A&A 515:A27. https://doi.org/10.1051/0004-6361/200913929. arXiv:1003.0362
Olofsson H, Vlemmings WHT, Maercker M, Humphreys EML, Lindqvist M, Nyman L, Ramstedt S (2015) ALMA view of the circumstellar environment of the post-common-envelope-evolution binary system HD 101584. A&A 576:L15. https://doi.org/10.1051/0004-6361/201526026. arXiv:1503.08609
Owocki S (2010) Hot-star mass-loss mechanisms: winds and outbursts. In: Leitherer C, Bennett PD, Morris PW, Van Loon JT (eds) Hot and cool: bridging gaps in massive star evolution, Astronomical Society of the Pacific Conference Series, vol 425, p 199
Papoular R (2008) On the formation and abundance of CO in envelopes of asymptotic giant branch stars. MNRAS 390:1727–1732. https://doi.org/10.1111/j.1365-2966.2008.13865.x. arXiv:0808.2790
Passy JC, De Marco O, Fryer CL, Herwig F, Diehl S, Oishi JS, Mac Low MM, Bryan GL, Rockefeller G (2012) Simulating the common envelope phase of a red giant using smoothed-particle hydrodynamics and uniform-grid codes. ApJ 744:52. https://doi.org/10.1088/0004-637X/744/1/52. arXiv:1107.5072
Price SD, Walker RG (1976) The AFGL four color infrared sky survey: Catalog of observations at 4.2, 11.0, 19.8 and 27.4 micrometers. AFGL-TR-0208 environmental research papers
Puls J, Sundqvist JO, Markova N (2015) Physics of mass loss in massive stars. In: Meynet G, Georgy C, Groh J, Stee P (eds) New windows on massive stars, IAU symposium, vol 307, pp 25–36. https://doi.org/10.1017/S174392131400622X. arXiv:1409.3582
Ramos-Larios G, Santamaría E, Guerrero MA, Marquez-Lugo RA, Sabin L, Toalá JA (2016) Rings and arcs around evolved stars—I. Fingerprints of the last gasps in the formation process of planetary nebulae. MNRAS 462:610–635. https://doi.org/10.1093/mnras/stw1572
Ramstedt S, Olofsson H (2014) The $^{12}CO/^{13}CO$ ratio in AGB stars of different chemical type. Connection to the $^{12}C/^{13}C$ ratio and the evolution along the AGB. A&A 566:A145. https://doi.org/10.1051/0004-6361/201423721. arXiv:1405.6404
Ramstedt S, Schöier FL, Olofsson H, Lundgren AA (2008) On the reliability of mass-loss-rate estimates for AGB stars. A&A 487:645–657. https://doi.org/10.1051/0004-6361:20078876. arXiv:0806.0517
Ramstedt S, Schöier FL, Olofsson H (2009) Circumstellar molecular line emission from S-type AGB stars: mass-loss rates and SiO abundances. A&A 499:515–527. https://doi.org/10.1051/0004-6361/200911730. arXiv:0903.1672
Ramstedt S, Maercker M, Olofsson G, Olofsson H, Schöier FL (2011) Imaging the circumstellar dust around AGB stars with PolCor. A&A 531:A148. https://doi.org/10.1051/0004-6361/201015964. arXiv:1105.5405
Ramstedt S, Mohamed S, Vlemmings WHT, Maercker M, Montez R, Baudry A, De Beck E, Lindqvist M, Olofsson H, Humphreys EML, Jorissen A, Kerschbaum F, Mayer A, Wittkowski M, Cox NLJ, Lagadec E, Leal-Ferreira ML, Paladini C, Pérez-Sánchez A, Sacuto S (2014) The wonderful complexity of the Mira AB system. A&A 570:L14. https://doi.org/10.1051/0004-6361/201425029. arXiv:1410.1529
Reimers D (1975) Circumstellar absorption lines and mass loss from red giants. Memoires of the Societe Royale des Sciences de Liege 8:369–382
Reiter M, Marengo M, Hora JL, Fazio GG (2015) A Spitzer/IRAC characterization of Galactic AGB and RSG stars. MNRAS 447:3909–3923. https://doi.org/10.1093/mnras/stu2725. arXiv:1501.02749
Renzini A, Voli M (1981) Advanced evolutionary stages of intermediate-mass stars. I—evolution of surface compositions. A&A 94:175
Richards AMS, Etoka S, Gray MD, Lekht EE, Mendoza-Torres JE, Murakawa K, Rudnitskij G, Yates JA (2012) Evolved star water maser cloud size determined by star size. A&A 546:A16. https://doi.org/10.1051/0004-6361/201219514. arXiv:1207.2583

Riebel D, Srinivasan S, Sargent B, Meixner M (2012) The mass-loss return from evolved stars to the large magellanic cloud. VI. Luminosities and mass-loss rates on population scales. ApJ 753:71. https://doi.org/10.1088/0004-637X/753/1/71. arXiv:1205.0280

Sacuto S, Ramstedt S, Höfner S, Olofsson H, Bladh S, Eriksson K, Aringer B, Klotz D, Maercker M (2013) The wind of the M-type AGB star RT virginis probed by VLTI/MIDI. A&A 551:A72. https://doi.org/10.1051/0004-6361/201220524. arXiv:1301.5872

Sahai R, Mack-Crane GP (2014) The astrosphere of the asymptotic giant branch star CIT 6. AJ 148:74. https://doi.org/10.1088/0004-6256/148/4/74. arXiv:1408.1050

Sahai R, Morris M, Sánchez Contreras C, Claussen M (2007) Preplanetary Nebulae: a hubble space telescope imaging survey and a new morphological classification system. AJ 134:2200–2225. https://doi.org/10.1086/522944. arXiv:0707.4662

Sahai R, Findeisen K, Gil de Paz A, Sánchez Contreras C (2008) Binarity in cool asymptotic giant branch stars: a GALEX search for ultraviolet excesses. ApJ 689:1274–1278. https://doi.org/10.1086/592559. arXiv:0807.1944

Sahai R, Morris MR, Villar GG (2011) Young planetary nebulae: hubble space telescope imaging and a new morphological classification system. AJ 141:134. https://doi.org/10.1088/0004-6256/141/4/134. arXiv:1101.2214

Saio H, Wood PR, Takayama M, Ita Y (2015) Oscillatory convective modes in red giants: a possible explanation of the long secondary periods. MNRAS 452:3863–3868. https://doi.org/10.1093/mnras/stv1587. arXiv:1507.03430

Sanchez E, Montez R Jr, Ramstedt S, Stassun KG (2015) First detection of ultraviolet emission from a detached dust shell: galaxy evolution explorer observations of the carbon asymptotic giant branch star u hya. ApJL 798:L39. https://doi.org/10.1088/2041-8205/798/2/L39

Sandin C, Höfner S (2003) Three-component modeling of C-rich AGB star winds. II. The effects of drift in long-period variables. A&A 404:789–807. https://doi.org/10.1051/0004-6361:20030515. arXiv:astro-ph/0304278

Sandin C, Höfner S (2004) Three-component modeling of C-rich AGB star winds. III. Micro-physics of drift-dependent dust formation. A&A 413:789–798. https://doi.org/10.1051/0004-6361:20031530. arXiv:astro-ph/0309822

Sargent BA, Srinivasan S, Meixner M (2011) The mass-loss return from evolved stars to the large magellanic cloud. IV. Construction and validation of a grid of models for oxygen-rich AGB stars, red supergiants, and extreme AGB stars. ApJ 728:93. https://doi.org/10.1088/0004-637X/728/2/93. arXiv:1407.8452

Sargent BA, Patel NA, Meixner M, Otsuka M, Riebel D, Srinivasan S (2013) CO $J = 2 - -1$ emission from evolved stars in the galactic bulge. ApJ 765:20. https://doi.org/10.1088/0004-637X/765/1/20. arXiv:1407.8453

Schöier FL, Olofsson H (2001) Models of circumstellar molecular radio line emission. Mass loss rates for a sample of bright carbon stars. A&A 368:969–993

Schirrmacher V, Woitke P, Sedlmayr E (2003) On the gas temperature in the shocked circumstellar envelopes of pulsating stars. III. Dynamical models for AGB star winds including time-dependent dust formation and non-LTE cooling. A&A 404:267–282. https://doi.org/10.1051/0004-6361:20030444

Schneider R, Valiante R, Ventura P, dell'Agli F, Di Criscienzo M, Hirashita H, Kemper F (2014) Dust production rate of asymptotic giant branch stars in the magellanic clouds. MNRAS 442:1440–1450. https://doi.org/10.1093/mnras/stu861. arXiv:1404.7132

Schöier FL, Lindqvist M, Olofsson H (2005) Properties of detached shells around carbon stars. Evidence of interacting winds. A&A 436:633–646. https://doi.org/10.1051/0004-6361:20042510. arXiv:astro-ph/0503245

Schöier FL, Maercker M, Justtanont K, Olofsson H, Black JH, Decin L, de Koter A, Waters R (2011) A chemical inventory of the S-type AGB star χ Cygni based on Herschel/HIFI observations of circumstellar line emission. The importance of non-LTE chemical processes in a dynamical region. A&A 530:A83. https://doi.org/10.1051/0004-6361/201116597

Scholz M, Wood PR (2000) The derivation of pulsation velocities from Doppler line profiles in M-type Mira variables. A&A 362:1065–1071

Schröder KP, Winters JM, Arndt TU, Sedlmayr E (1998) A theoretical model for episodic mass-loss producing detached shells around bright carbon stars. A&A 335:L9–L12

Schröder KP, Winters JM, Sedlmayr E (1999) Tip-AGB stellar evolution in the presence of a pulsating, dust-induced superwind. A&A 349:898–906

Schwarzschild M (1975) On the scale of photospheric convection in red giants and supergiants. ApJ 195:137–144. https://doi.org/10.1086/153313

Scicluna P, Siebenmorgen R (2015) Extinction and dust properties in a clumpy medium. A&A 584:A108. https://doi.org/10.1051/0004-6361/201323149. arXiv:1510.06149

Simis Y, Woitke P (2003) Dynamics and instabilities in dusty winds. In: Habing HJ, Olofsson H (eds) Asymptotic giant branch stars, Astronomy and Astrophysics Library. Springer, New York, pp 291–323. https://doi.org/10.1007/978-1-4757-3876-6_6

Simis YJW, Icke V, Dominik C (2001) Origin of quasi-periodic shells in dust forming AGB winds. A&A 371:205–221

Skrutskie MF, Cutri RM, Stiening R, Weinberg MD, Schneider S, Carpenter JM, Beichman C, Capps R, Chester T, Elias J, Huchra J, Liebert J, Lonsdale C, Monet DG, Price S, Seitzer P, Jarrett T, Kirkpatrick JD, Gizis JE, Howard E, Evans T, Fowler J, Fullmer L, Hurt R, Light R, Kopan EL, Marsh KA, McCallon HL, Tam R, Van Dyk S, Wheelock S (2006) The two micron all sky survey (2MASS). AJ 131:1163–1183. https://doi.org/10.1086/498708

Sloan GC, Kraemer KE, Wood PR, Zijlstra AA, Bernard-Salas J, Devost D, Houck JR (2008) The magellanic zoo: mid-infrared spitzer spectroscopy of evolved stars and circumstellar dust in the magellanic clouds. ApJ 686:1056–1081. https://doi.org/10.1086/591437. arXiv:0807.2998

Sloan GC, Matsuura M, Zijlstra AA, Lagadec E, Groenewegen MAT, Wood PR, Szyszka C, Bernard-Salas J, van Loon JT (2009) Dust formation in a galaxy with primitive abundances. Science 323:353. https://doi.org/10.1126/science.1165626

Sloan GC, Matsunaga N, Matsuura M, Zijlstra AA, Kraemer KE, Wood PR, Nieusma J, Bernard-Salas J, Devost D, Houck JR (2010) Spitzer spectroscopy of mass-loss and dust production by evolved stars in globular clusters. ApJ 719:1274–1292. https://doi.org/10.1088/0004-637X/719/2/1274. arXiv:1006.5016

Sloan GC, Matsuura M, Lagadec E, van Loon JT, Kraemer KE, McDonald I, Groenewegen MAT, Wood PR, Bernard-Salas J, Zijlstra AA (2012) Carbon-rich dust production in metal-poor galaxies in the local group. ApJ 752:140. https://doi.org/10.1088/0004-637X/752/2/140. arXiv:1204.5754

Sloan GC, Lagadec E, Zijlstra AA, Kraemer KE, Weis AP, Matsuura M, Volk K, Peeters E, Duley WW, Cami J, Bernard-Salas J, Kemper F, Sahai R (2014) Carbon-rich dust past the asymptotic giant branch: aliphatics, aromatics, and fullerenes in the magellanic clouds. ApJ 791:28. https://doi.org/10.1088/0004-637X/791/1/28. arXiv:1406.7034

Sloan GC, Kraemer KE, McDonald I, Groenewegen MAT, Wood PR, Zijlstra AA, Lagadec E, Boyer ML, Kemper F, Matsuura M, Sahai R, Sargent BA, Srinivasan S, van Loon JT, Volk K (2016) The infrared spectral properties of magellanic carbon stars. ApJ 826:44. https://doi.org/10.3847/0004-637X/826/1/44. arXiv:1604.06464

Smith N (2014) Mass loss: its effect on the evolution and fate of high-mass stars. ARA&A 52:487–528. https://doi.org/10.1146/annurev-astro-081913-040025. arXiv:1402.1237

Solomon P, Jefferts KB, Penzias AA, Wilson RW (1971) Observation of CO emission at 2.6 millimeters from IRC+10216. ApJL 163:L53

Soszyński I, Wood PR (2013) Semiregular variables with periods lying between the period-luminosity sequences C', C, and D. ApJ 763:103. https://doi.org/10.1088/0004-637X/763/2/103. arXiv:1212.0549

Soszynski I, Dziembowski WA, Udalski A, Kubiak M, Szymanski MK, Pietrzynski G, Wyrzykowski L, Szewczyk O, Ulaczyk K (2007) The optical gravitational lensing experiment. Period-luminosity relations of variable red giant stars. AcA 57:201–225 arXiv:0710.2780

Srinivasan S, Meixner M, Leitherer C, Vijh U, Volk K, Blum RD, Babler BL, Block M, Bracker S, Cohen M, Engelbracht CW, For BQ, Gordon KD, Harris J, Hora JL, Indebetouw R, Markwick-Kemper F, Meade M, Misselt KA, Sewilo M, Whitney B (2009) The mass loss return from evolved stars to the large magellanic cloud: empirical relations for excess emission at 8 and 24 μm. AJ 137:4810–4823. https://doi.org/10.1088/0004-6256/137/6/4810. arXiv:0903.1661

Srinivasan S, Sargent BA, Meixner M (2011) The mass-loss return from evolved stars to the large magellanic cloud. V. The GRAMS carbon-star model grid. A&A 532:A54. https://doi.org/10.1051/0004-6361/201117033. arXiv:1106.3256

Staff JE, De Marco O, Macdonald D, Galaviz P, Passy JC, Iaconi R, Low MMM (2016) Hydrodynamic simulations of the interaction between an AGB star and a main-sequence companion in eccentric orbits. MNRAS 455:3511–3525. https://doi.org/10.1093/mnras/stv2548. arXiv:1510.08429

Steffen M, Schönberner D (2000) On the origin of thin detached gas shells around AGB stars. Insights from time-dependent hydrodynamical simulations. A&A 357:180–196

Stewart PN, Tuthill PG, Monnier JD, Ireland MJ, Hedman MM, Nicholson PD, Lacour S (2016) The weather report from IRC+10216: evolving irregular clouds envelop carbon star. MNRAS 455:3102–3109. https://doi.org/10.1093/mnras/stv2454. arXiv:1510.05929

Stewart PN, Tuthill PG, Nicholson PD, Hedman MM (2016) High-angular-resolution stellar imaging with occultations from the Cassini spacecraft-III. Mira. MNRAS 457:1410–1418. https://doi.org/10.1093/mnras/stw045

Takayama M, Saio H, Ita Y (2013) On the pulsation modes of OGLE small amplitude red giant variables in the LMC. MNRAS 431:3189–3195. https://doi.org/10.1093/mnras/stt398. arXiv:1303.7059

Tej A, Lançon A, Scholz M (2003) The structure of H_2O shells in Mira atmospheres. Correlation with disk brightness distributions and a spectrophotometric signature. A&A 401:347–355. https://doi.org/10.1051/0004-6361:20030123. arXiv:astro-ph/0301500

Teyssier D, Hernandez R, Bujarrabal V, Yoshida H, Phillips TG (2006) CO line emission from circumstellar envelopes. A&A 450:167–179. https://doi.org/10.1051/0004-6361:20053759

Tielens AGGM (2005) The physics and chemistry of the interstellar medium. Cambridge University Press, Cambridge

Trabucchi M, Wood PR, Montalbán J, Marigo P, Pastorelli G, Girardi L (2017) A new interpretation of the period-luminosity sequences of long-period variables. ApJ 847:139. https://doi.org/10.3847/1538-4357/aa8998. arXiv:1708.09350

Ueta T, Meixner M (2003) 2-DUST: a dust radiative transfer code for an axisymmetric system. ApJ 586:1338–1355. https://doi.org/10.1086/367818. arXiv:astro-ph/0212523

van der Veen WECJ (1989) The mass-loss evolution of oxygen-rich AGB stars and its consequences for stellar evolution. A&A 210:127–146

van Loon JT, Cioni MRL, Zijlstra AA, Loup C (2005) An empirical formula for the mass-loss rates of dust-enshrouded red supergiants and oxygen-rich asymptotic giant branch stars. A&A 438:273–289. https://doi.org/10.1051/0004-6361:20042555. arXiv:astro-ph/0504379

van Loon JT, Cohen M, Oliveira JM, Matsuura M, McDonald I, Sloan GC, Wood PR, Zijlstra AA (2008) Molecules and dust production in the magellanic clouds. A&A 487:1055–1073. https://doi.org/10.1051/0004-6361:200810036. arXiv:0806.3557

van Marle AJ, Cox NLJ, Decin L (2014) Eyes in the sky. Interactions between asymptotic giant branch star winds and the interstellar magnetic field. A&A 570:A131. https://doi.org/10.1051/0004-6361/201424452. arXiv:1408.1510

Vassiliadis E, Wood PR (1993) Evolution of low- and intermediate-mass stars to the end of the asymptotic giant branch with mass loss. ApJ 413:641–657

Velilla Prieto L, Sánchez Contreras C, Cernicharo J, Agúndez M, Quintana-Lacaci G, Bujarrabal V, Alcolea J, Balança C, Herpin F, Menten KM, Wyrowski F (2017) The millimeter IRAM-30 m line survey toward IK Tauri. A&A 597:A25. https://doi.org/10.1051/0004-6361/201628776. arXiv:1609.01904

Villaume A, Conroy C, Johnson BD (2015) Circumstellar dust around AGB stars and implications for infrared emission from galaxies. ApJ 806:82. https://doi.org/10.1088/0004-637X/806/1/82. arXiv:1504.00900

Vlemmings WHT (2014) Magnetic fields around AGB stars and Planetary Nebulae. In: Petit P, Jardine M, Spruit HC (eds) Magnetic fields throughout stellar evolution, IAU Symposium, vol 302, pp 389–397. https://doi.org/10.1017/S1743921314002580

Vlemmings WHT, Ramstedt S, Rao R, Maercker M (2012) Polarization of thermal molecular lines in the envelope of IK Tauri. A&A 540:L3. https://doi.org/10.1051/0004-6361/201218897. arXiv:1203.2922

Wachter A, Schröder KP, Winters JM, Arndt TU, Sedlmayr E (2002) An improved mass-loss description for dust-driven superwinds and tip-AGB evolution models. A&A 384:452–459

Wachter A, Winters JM, Schröder KP, Sedlmayr E (2008) Dust-driven winds and mass loss of C-rich AGB stars with subsolar metallicities. A&A 486:497–504. https://doi.org/10.1051/0004-6361:200809893. arXiv:0805.3656

Waters LBFM, Loup C, Kester DJM, Bontekoe TR, de Jong T (1994) Resolution of a fossil dust shell around U Hydrae using maximum entropy image reconstruction. A&A 281:L1–L4

Wedemeyer S, Kučinskas A, Klevas J, Ludwig HG (2017) Three-dimensional hydrodynamical CO^5BOLD model atmospheres of red giant stars. VI. First chromosphere model of a late-type giant. A&A 606:A26. https://doi.org/10.1051/0004-6361/201730405. arXiv:1705.09641

Weigelt G, Balega Y, Bloecker T, Fleischer AJ, Osterbart R, Winters JM (1998) 76mas speckle-masking interferometry of IRC+10216 with the SAO 6m telescope: evidence for a clumpy shell structure. A&A 333:L51–L54 arXiv:astro-ph/9805022

Whitelock P, Feast M, Catchpole R (1991) IRAS sources and the nature of the galactic bulge. MNRAS 248:276–312. https://doi.org/10.1093/mnras/248.2.276

Whitelock PA, Feast MW, van Loon JT, Zijlstra AA (2003) Obscured asymptotic giant branch variables in the large magellanic cloud and the period-luminosity relation. MNRAS 342:86–104. https://doi.org/10.1046/j.1365-8711.2003.06514.x. arXiv:astro-ph/0302246

Whitelock PA, Feast MW, Marang F, Groenewegen MAT (2006) Near-infrared photometry of carbon stars. MNRAS 369:751–782. https://doi.org/10.1111/j.1365-2966.2006.10322.x. arXiv:astro-ph/0603504

Whitelock PA, Menzies JW, Feast MW, Matsunaga N, Tanabé T, Ita Y (2009) Asymptotic giant branch stars in the Fornax dwarf spheroidal galaxy. MNRAS 394:795–809. https://doi.org/10.1111/j.1365-2966.2008.14365.x. arXiv:0812.0903

Wickramasinghe NC, Donn BD, Stecher TP (1966) A mechanism for mass ejection in red giants. ApJ 146:590

Willems FJ, de Jong T (1988) IRAS low resolution spectra of cool carbon stars. IV—a scenario for carbon star evolution. A&A 196:173–184

Willson LA (2000) Mass loss from cool stars: impact on the evolution of stars and stellar populations. ARA&A 38:573–611

Willson LA, Hill SJ (1979) Shock wave interpretation of emission lines in long period variable stars. II—periodicity and mass loss. ApJ 228:854–869. https://doi.org/10.1086/156911

Willson LA, Wallerstein G, Pilachowski CA (1982) Atmospheric kinematics of high velocity long period variables. MNRAS 198:483–516

Wilson WJ, Barrett AH (1968) Discovery of hydroxyl radio emission from infrared stars. Science 161:778–779. https://doi.org/10.1126/science.161.3843.778

Winnberg A, Deguchi S, Reid MJ, Nakashima J, Olofsson H, Habing HJ (2009) CO in OH/IR stars close to the Galactic centre. A&A 497:177–181. https://doi.org/10.1051/0004-6361/200911655. arXiv:0902.2347

Winters JM, Le Bertre T, Jeong KS, Helling C, Sedlmayr E (2000) A systematic investigation of the mass loss mechanism in dust forming long-period variable stars. A&A 361:641–659

Wittkowski M, Boboltz DA, Ohnaka K, Driebe T, Scholz M (2007) The Mira variable S Orionis: relationships between the photosphere, molecular layer, dust shell, and SiO maser shell at 4 epochs. A&A 470:191–210. https://doi.org/10.1051/0004-6361:20077168. arXiv:0705.4614

Wittkowski M, Chiavassa A, Freytag B, Scholz M, Höfner S, Karovicova I, Whitelock PA (2016) Near-infrared spectro-interferometry of Mira variables and comparisons to 1D dynamic model atmospheres and 3D convection simulations. A&A 587:A12. https://doi.org/10.1051/0004-6361/201527614. arXiv:1601.02368

Wittkowski M, Hofmann KH, Höfner S, Le Bouquin JB, Nowotny W, Paladini C, Young J, Berger JP, Brunner M, de Gregorio-Monsalvo I, Eriksson K, Hron J, Humphreys EML, Lindqvist M, Maercker M, Mohamed S, Olofsson H, Ramstedt S, Weigelt G (2017) Aperture synthesis imaging of the carbon AGB star R Sculptoris. Detection of a complex structure and a dominating spot on the stellar disk. A&A 601:A3. https://doi.org/10.1051/0004-6361/201630214. arXiv:1702.02574

Woitke P (2006) Too little radiation pressure on dust in the winds of oxygen-rich AGB stars. ApJ 460:L9

Wood PR (1979) Pulsation and mass loss in Mira variables. ApJ 227:220–231

Wood PR (2007) Pulsation and Mass Loss in Red Giant Stars. In: Vallenari A, Tantalo R, Portinari L, Moretti A (eds) From stars to galaxies: building the pieces to build up the universe, Astronomical Society of the Pacific Conference Series, vol 374, p 47

Wood PR (2015) The pulsation modes, masses and evolution of luminous red giants. MNRAS 448:3829–3843. https://doi.org/10.1093/mnras/stv289. arXiv:1502.03137

Wood PR, Alcock C, Allsman RA, Alves D, Axelrod TS, Becker AC, Bennett DP, Cook KH, Drake AJ, Freeman KC, Griest K, King LJ, Lehner MJ, Marshall SL, Minniti D, Peterson BA, Pratt MR, Quinn PJ, Stubbs CW, Sutherland W, Tomaney A, Vandehei T, Welch DL (1999) MACHO observations of LMC red giants: Mira and semi-regular pulsators, and contact and semi-detached binaries. In: Le Bertre T, Lebre A, Waelkens C (eds) Asymptotic Giant Branch Stars, IAU Symposium, vol 191, p 151

Woodruff HC, Tuthill PG, Monnier JD, Ireland MJ, Bedding TR, Lacour S, Danchi WC, Scholz M (2008) The Keck aperture masking experiment: multiwavelength observations of six mira variables. ApJ 673:418–433. https://doi.org/10.1086/523936. arXiv:0709.3878

Woods PM, Walsh C, Cordiner MA, Kemper F (2012) The chemistry of extragalactic carbon stars. MNRAS 426:2689–2702. https://doi.org/10.1111/j.1365-2966.2012.21771.x. arXiv:1207.5519

Woolf NJ, Ney EP (1969) Circumstellar infrared emission from cool stars. ApJL 155:L181

Young K (1995) A CO(3–2) survey of nearby mira variables. ApJ 445:872–888

Zaritsky D, Harris J, Thompson IB, Grebel EK (2004) The magellanic clouds photometric survey: the large magellanic cloud stellar catalog and extinction map. AJ 128:1606–1614. https://doi.org/10.1086/423910. arXiv:astro-ph/0407006

Zeidler S, Posch T, Mutschke H, Richter H, Wehrhan O (2011) Near-infrared absorption properties of oxygen-rich stardust analogs. The influence of coloring metal ions. A&A 526:A68. https://doi.org/10.1051/0004-6361/201015219. arXiv:1101.0695

Zhao JK, Oswalt TD, Willson LA, Wang Q, Zhao G (2012) The initial–final mass relation among white dwarfs in wide binaries. ApJ 746:144. https://doi.org/10.1088/0004-637X/746/2/144. arXiv:1112.0281

Zhao-Geisler R, Quirrenbach A, Köhler R, Lopez B (2012) Dust and molecular shells in asymptotic giant branch stars. A&A 545:A56. https://doi.org/10.1051/0004-6361/201118150

Zhukovska S, Henning T (2013) Dust input from AGB stars in the large magellanic cloud. A&A 555:A99. https://doi.org/10.1051/0004-6361/201321368. arXiv:1305.3521

Zijlstra AA, Loup C, Waters LBFM, de Jong T (1992) Interrupted mass loss on the asymptotic giant branch. A&A 265:L5–L8